Ion acoustic solitons in the ionosphere

Jonas Ekeberg
jonase@irf.se

Swedish Institute of Space Physics

Acoustic solitons

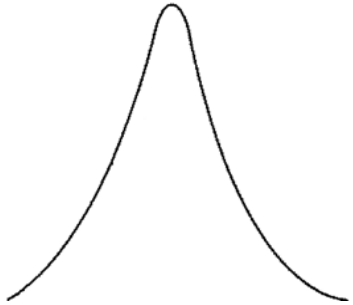

- nonlinear vs. dispersive effects
  $\leftrightarrow$ steepening vs. spreading out
- fluid theory $\Rightarrow$ *KdV* equation (non-linear PDF)

  $B = 0$: dispersion fr. charge separation
  scale ~ λ_{De}
  $B \neq 0$: dispersion fr. perp. propagation
  scale ~ c_s/Ω_i

- existence in the F-region?
- detectable with radar?

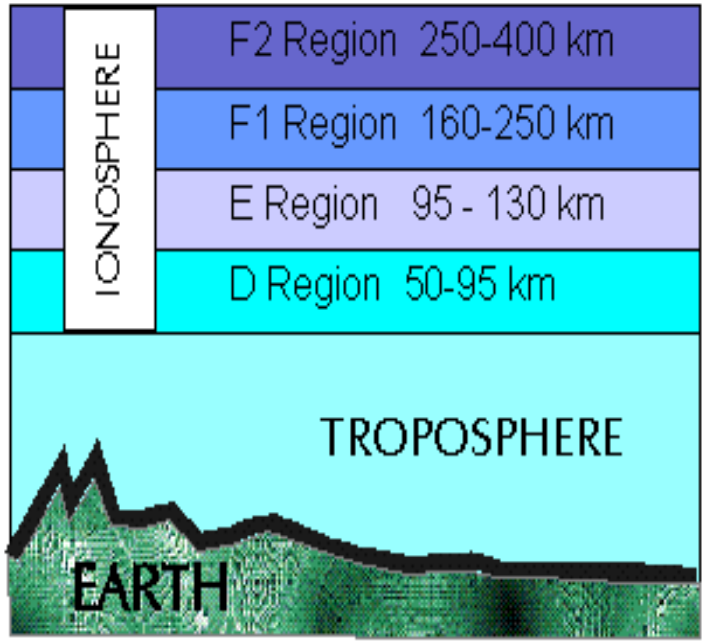

Spectral signature?

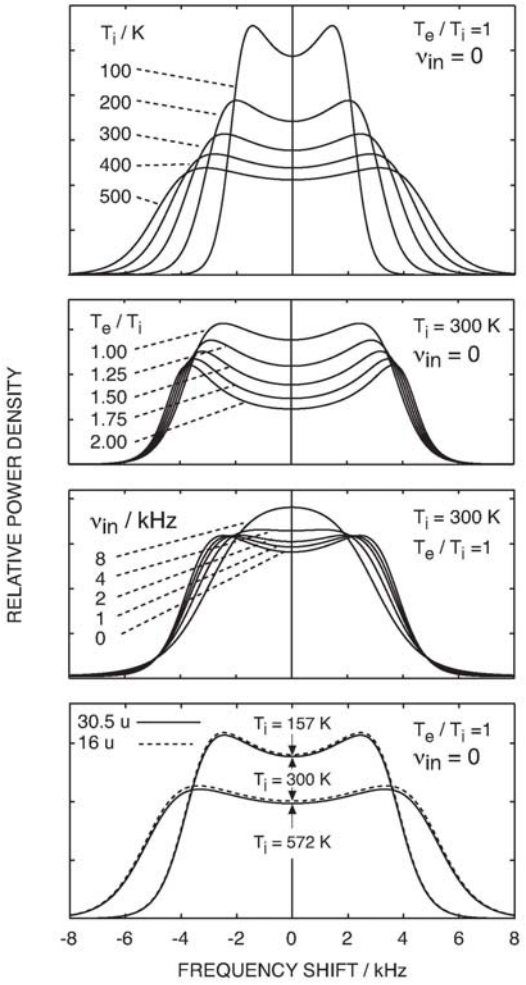

Nygrén 1996

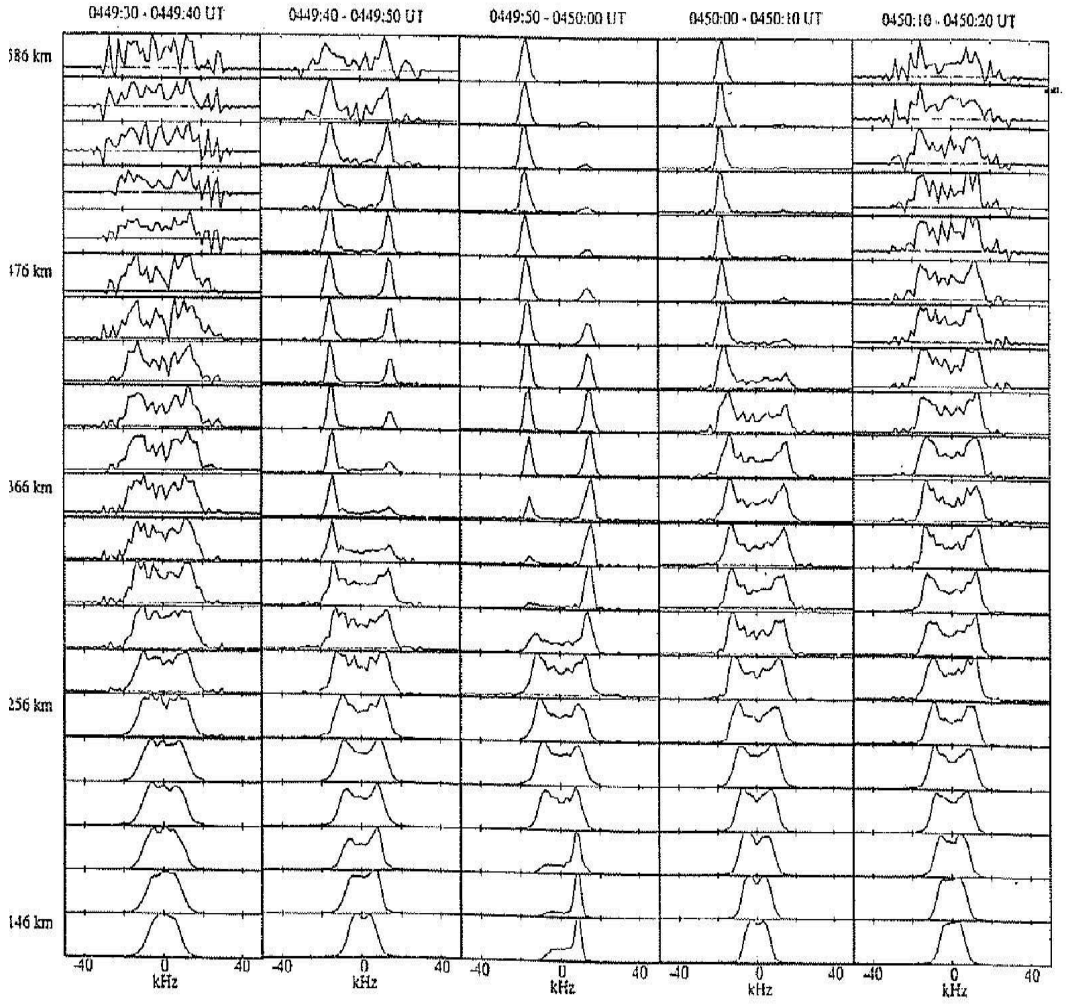

Rietveld *et al.* 1991

Oxygen-proton difference of the sub-keV ring current ion drift

Tony T. Giang
tony@irf.se
IRF, Kiruna

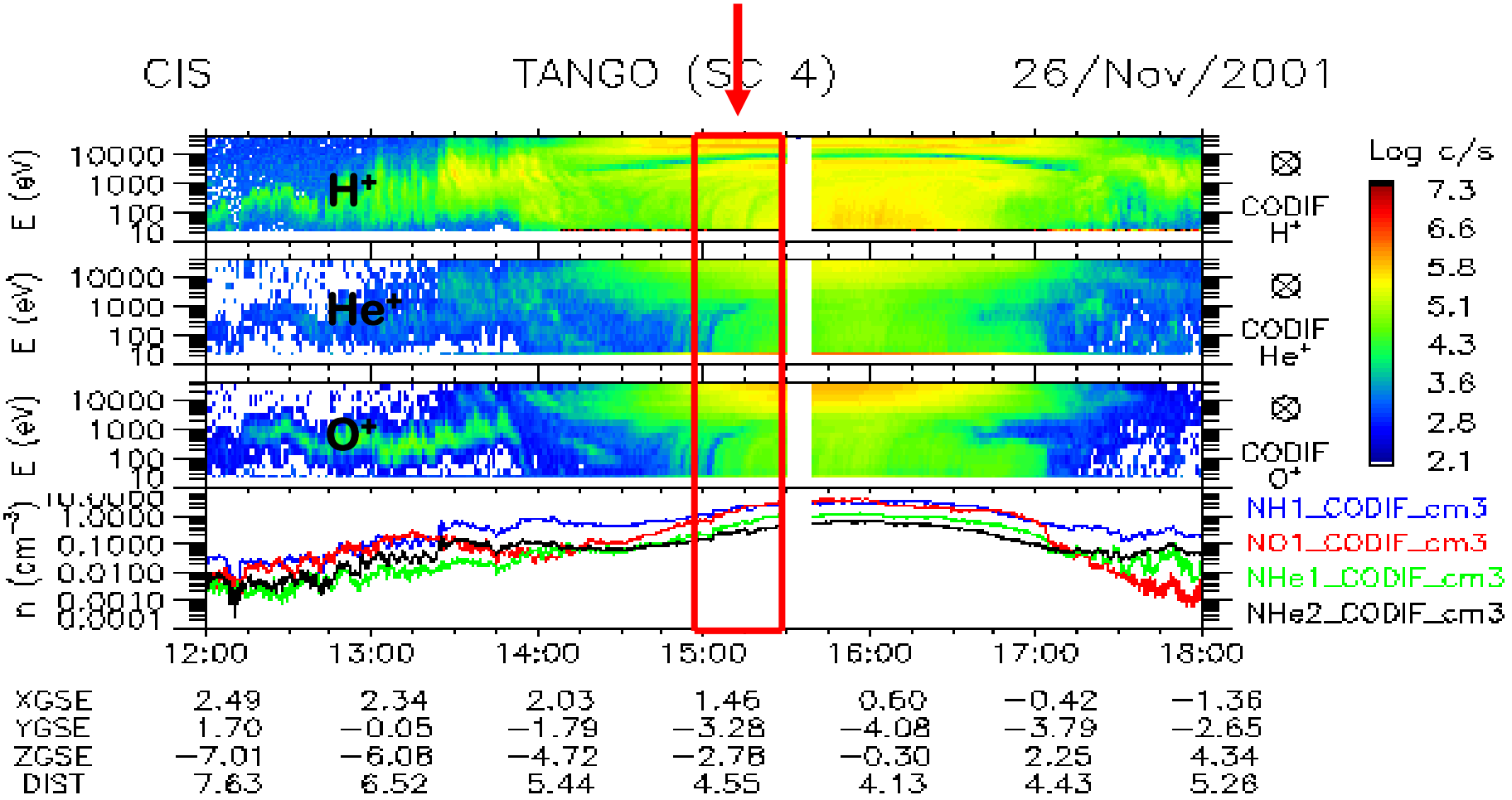

2001-11-26

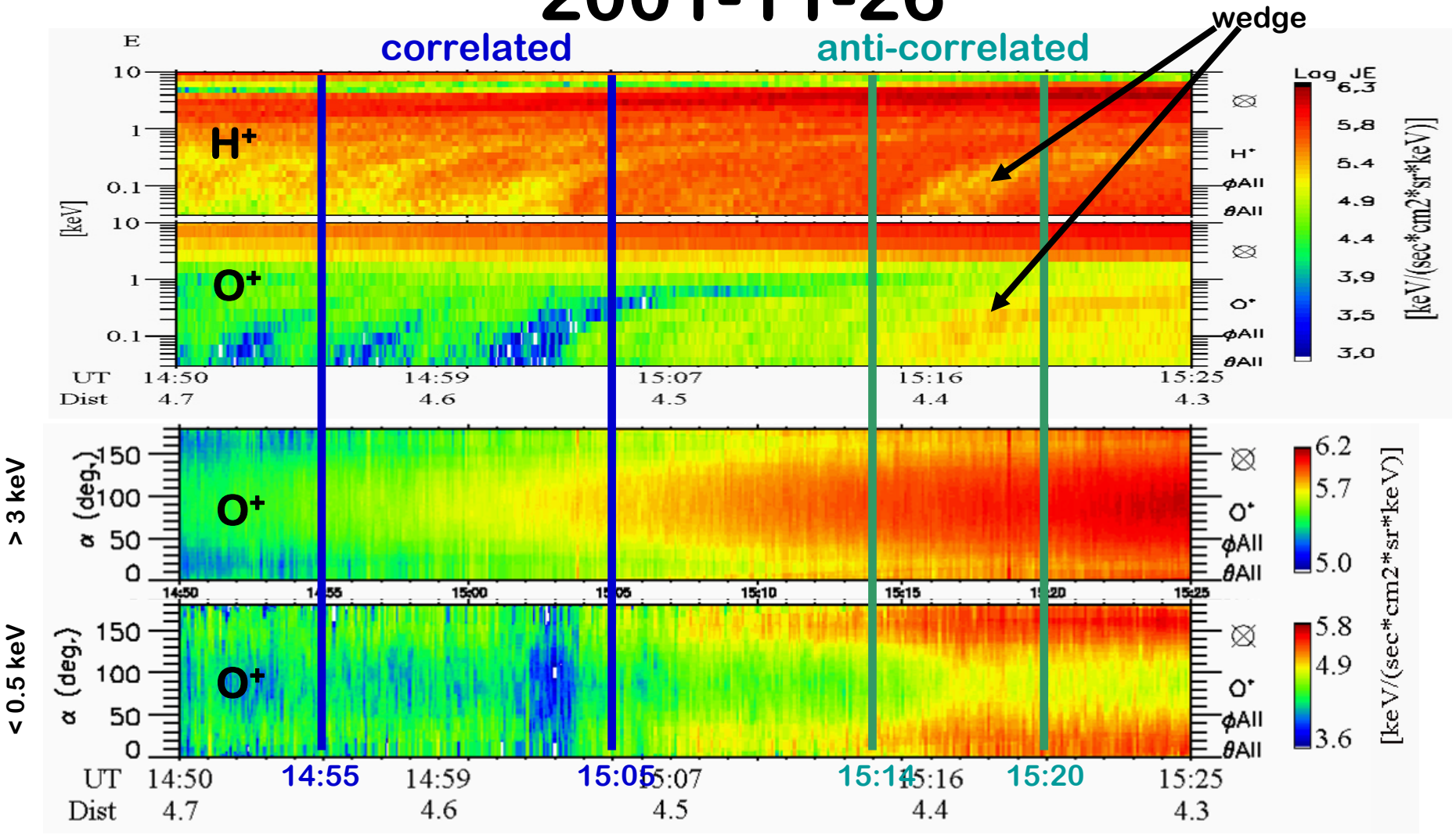

- Both O+ and H+ have wedge-like structures between 14:55-15:05 UT and 15:14-15:20 UT.
- In the sub-keV range both O+ and H+ have energy-latitude dispersed structures of similar shape.
- In the anti-correlated region the wedge shape in H+ is a reduction in flux where there is an increase in O+.
- O+ are trapped inside the ordinary ring current.
- The pitch-angle distribution inside the wedge has a conic-like feature at nearly 0 and 180 degrees pitch-angles for O+.

2001-11-26

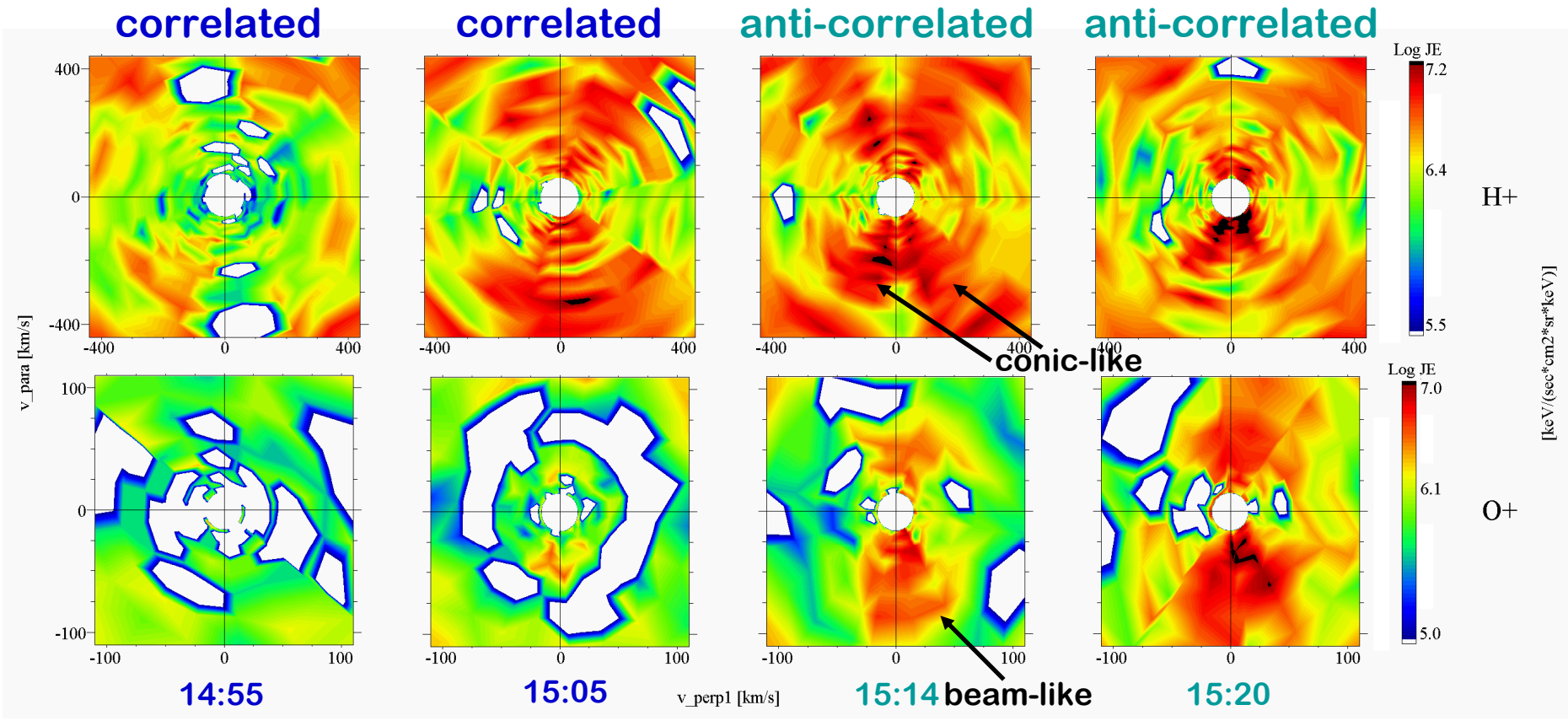

- Pitch-angle distribution functions reveals butterfly distributions (double conic-like distribution) peaking nearly field-aligned direction with the loss cone.
- Butterfly distributions are seen in H^+ for both the correlated and anti-correlated periods.
- O^+ do not have butterfly distribution.
- O^+ and H^+ originated from different sources.
- O^+ originated from a lower altitude.

Ion Outflow over the Polar Cap

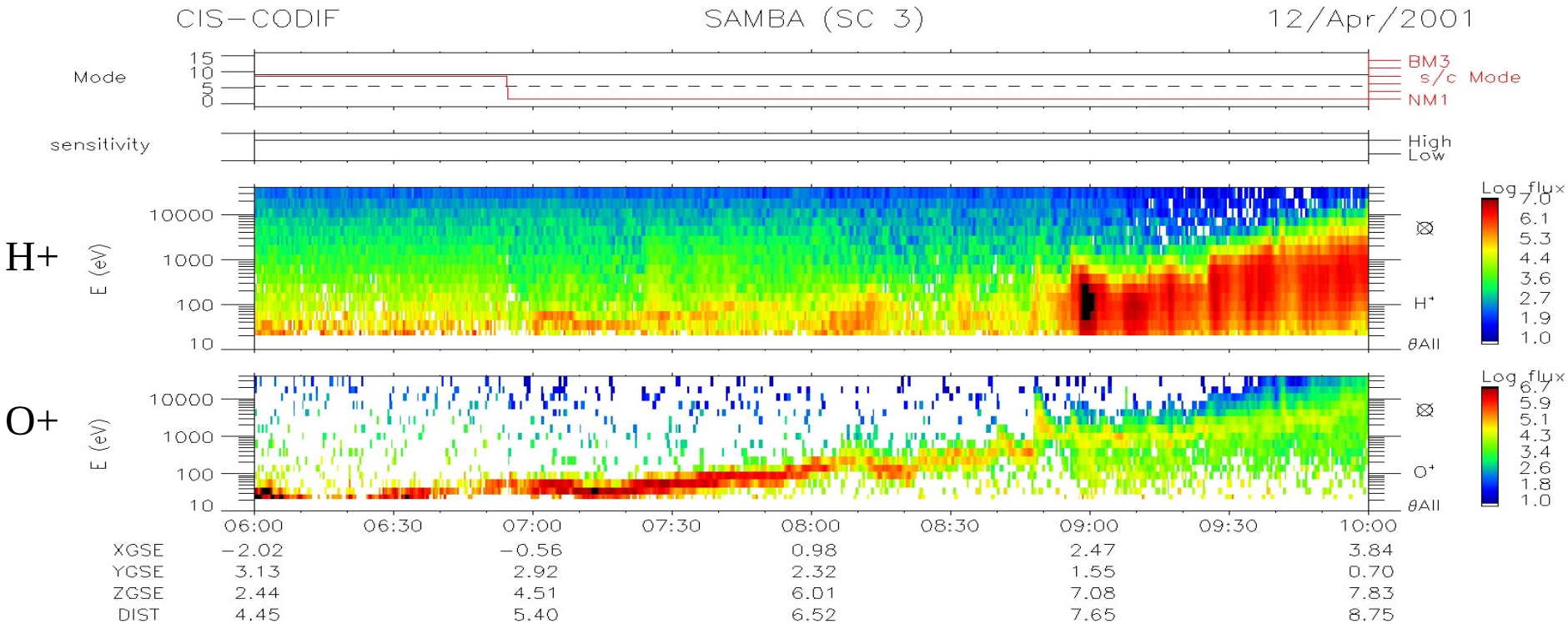

Martin Waara

martin.waara@irf.se

Swedish Institute of Space Physics, Kiruna

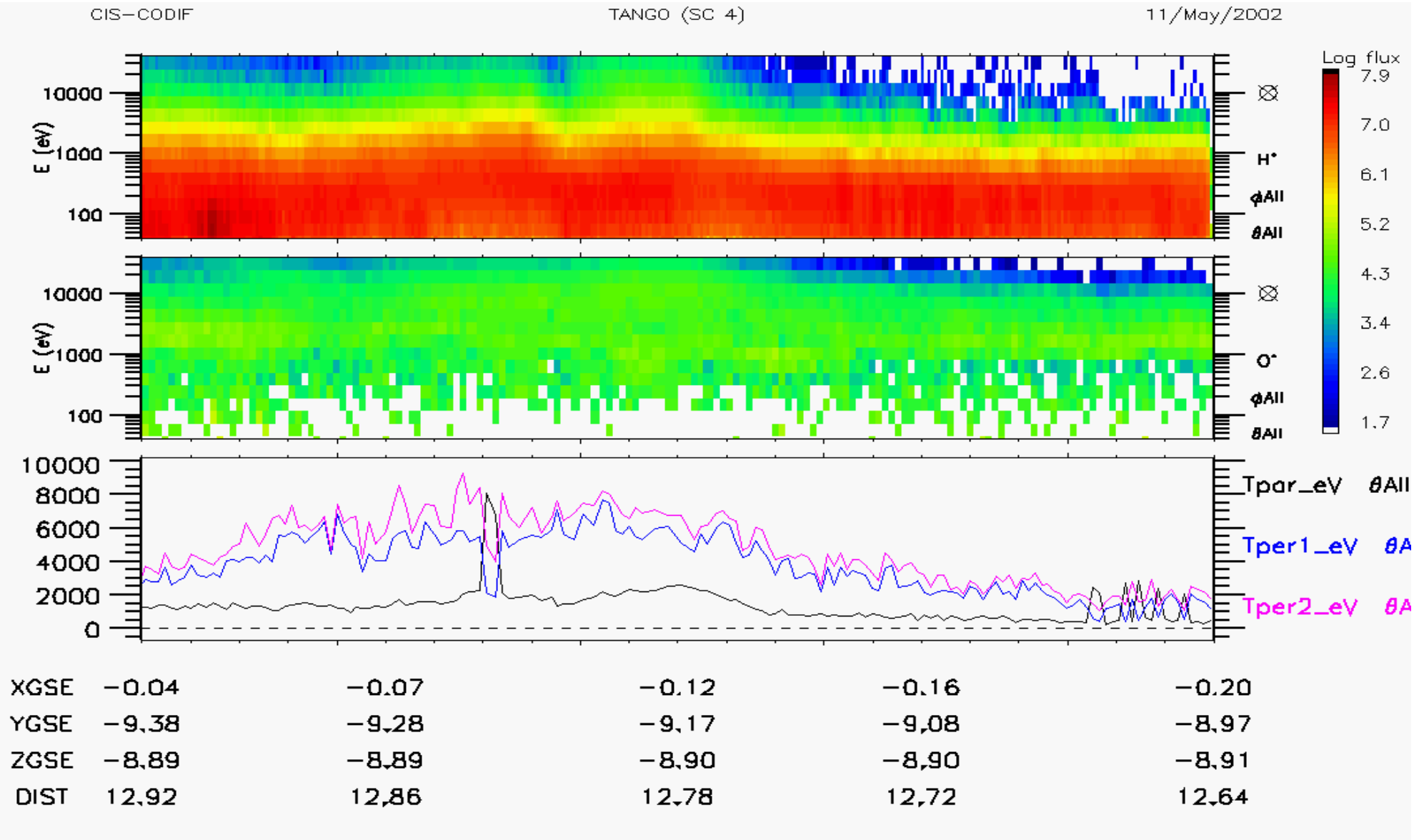
CIS–CODIF
TANGO (SC 4)
11/May/2002
E (eV)
10000
1000
100
H+
O+
φAll
θAll
Log flux
7.9
7.0
6.1
5.2
4.3
3.4
2.6
1.7
10000
8000
6000
4000
2000
0
Tpar_eV θAll
Tper1_eV θA
Tper2_eV θA
XGSE −0.04 −0.07 −0.12 −0.16 −0.20
YGSE −9.38 −9.28 −9.17 −9.08 −8.97
ZGSE −8.89 −8.89 −8.90 −8.90 −8.91
DIST 12.92 12.86 12.78 12.72 12.64
Time 17:51 18:00 18:13

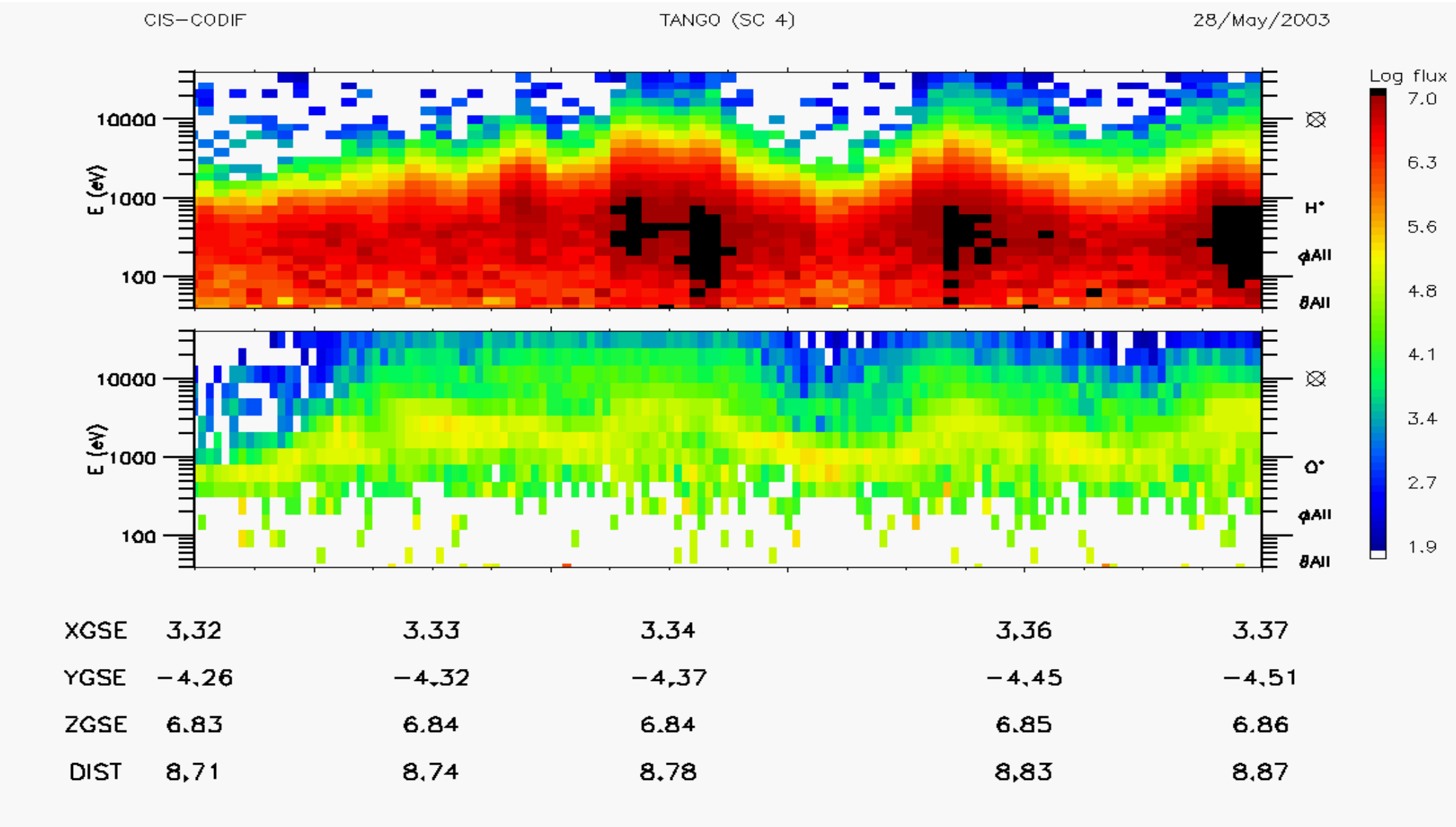
CIS–CODIF
TANGO (SC 4)
28/May/2003
Log flux
7.0
6.3
5.6
4.8
4.1
3.4
2.7
1.9
E (eV)
10000
1000
100
H+
φAll
θAll
O+
XGSE 3.32 3.33 3.34 3.36 3.37
YGSE −4.26 −4.32 −4.37 −4.45 −4.51
ZGSE 6.83 6.84 6.84 6.85 6.86
DIST 8.71 8.74 8.78 8.83 8.87
Time 02:30 2:35 02:40

Photo: Y. Ebihara

Scientific activities of ALIS & Optical auroral networks

- Optiska mätningar är verkligt viktiga om man vill förstå:
  - Norrsken
  - Tidsvariationer
  - Rumsvariationer

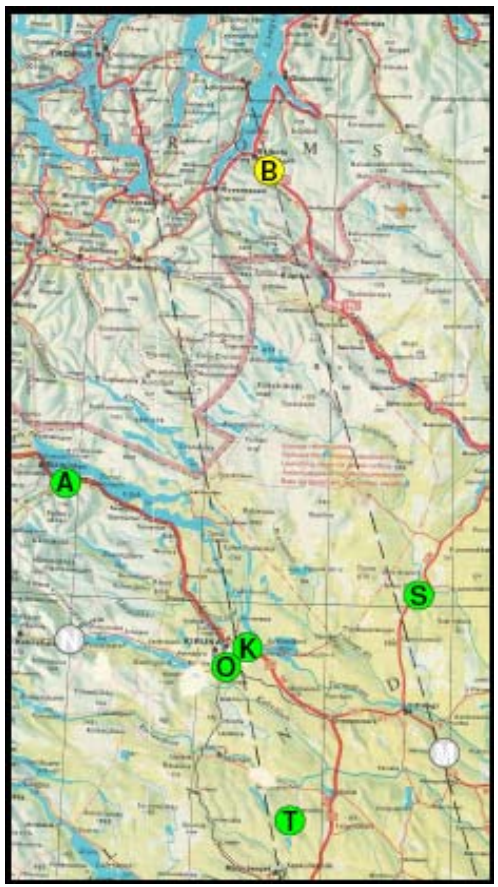

ALIS (Auroral Large Imaging System)

Finstruktur i norrsken

Heating

Meteorer

- CCD detektorer 1024x1024 pixels
- FOV 60 or 90 grader
- Maximal upplösning: 100 m at 100 km
- Filterhjul, 6 pos., interferensfilter
- Hög känslighet, klarar några Rayleigh
- Fjärrstyrning
- Kampanjmod
- Data på Internet

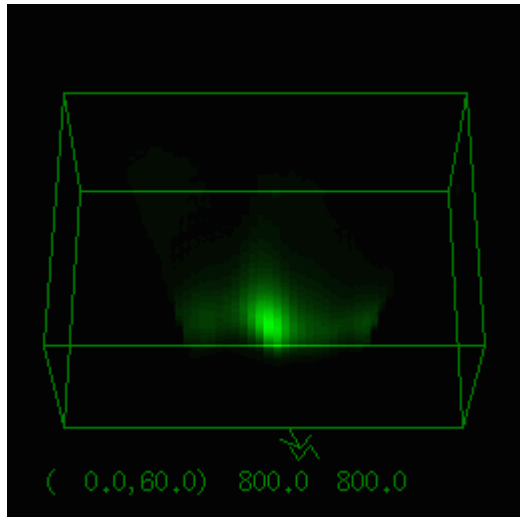

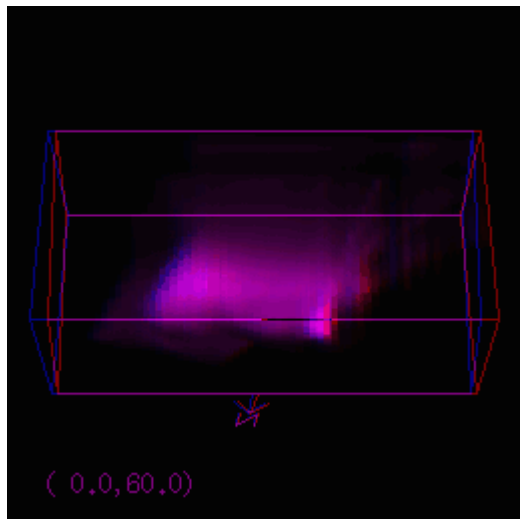

Auroral Optical Network

International Network for Auroral Optical Studies of the Polar Ionosphere

- IPY-projekt med fortsättning.
- Omfattar i stort sett alla grupper i världen som arbetar med optiska norrskensmätningar.
- ICESTAR/IHY cluster.
- Forum för att planera koordinerade mätkampanjer och sprida information.
- Interkalibrering.
- Hemsida: alis.irf.se/auropt.
- Mail-lista:auropt.irf.se.

Optical Auroral Research in the Arctic Region

- Projekt finansierat av Nordiska ministerrådet(IPY-relaterade projekt, 74 ansökningar/20 anslag)
- Deltagande: Apatity, Oulu, Sodankylä, Kiruna, Tromsö, Longyearbyen
- Workshops Sodankylä 19-23 februari
- Mobilitetetsprogram
- Framtidsplaner: Gemensamma doktorandkurser

Scientific topics, Rickard Lundin

- Polar cusp plasma dynamics
- Detached magnetosheath plasma / dynamo regions
- Departure from "frozen inness" in energy transfer regions
- Wave induced ponderomotive aceleration (Earth, Mars)
- Auroral acceleration process (Mars)
- Solar forcing of celestial bodies (Mars, Venus,comets…)

Energy, mass and momentum transfer - Violation of "ideal" MHD -

$$\frac{d\Phi}{dt} = \iint \left(\frac{\partial \vec{B}}{\partial t} - \nabla \times \vec{E}_{emf} \right) d\vec{S}$$

Boundary layer - extended regions of departure $d\Phi / dt \neq 0$

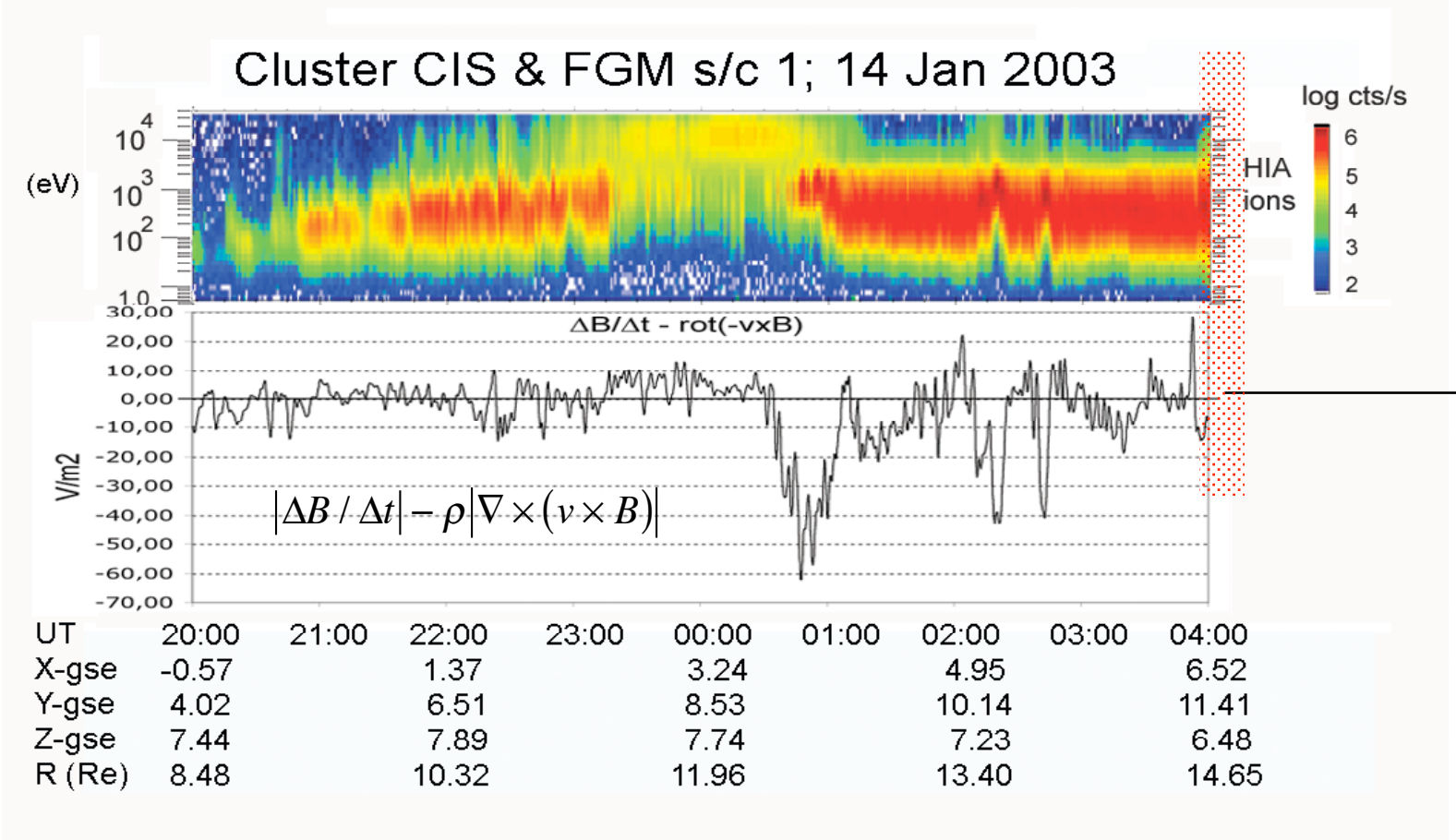

$d\Phi / dt > 0$
(e/m forcing)

$d\Phi / dt < 0$
(induction => particle forcing)

Auroral acceleration, $E_{||}$ and $j_{||}$ - also at Mars

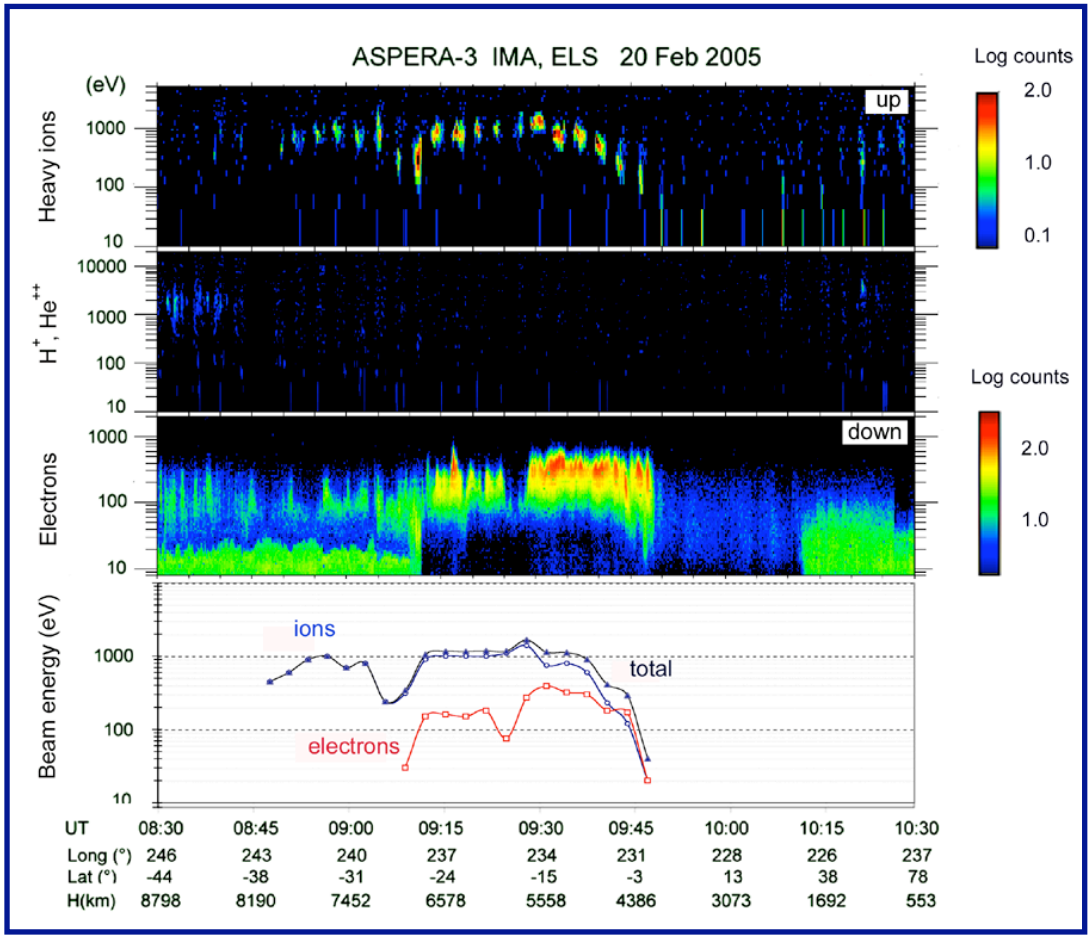

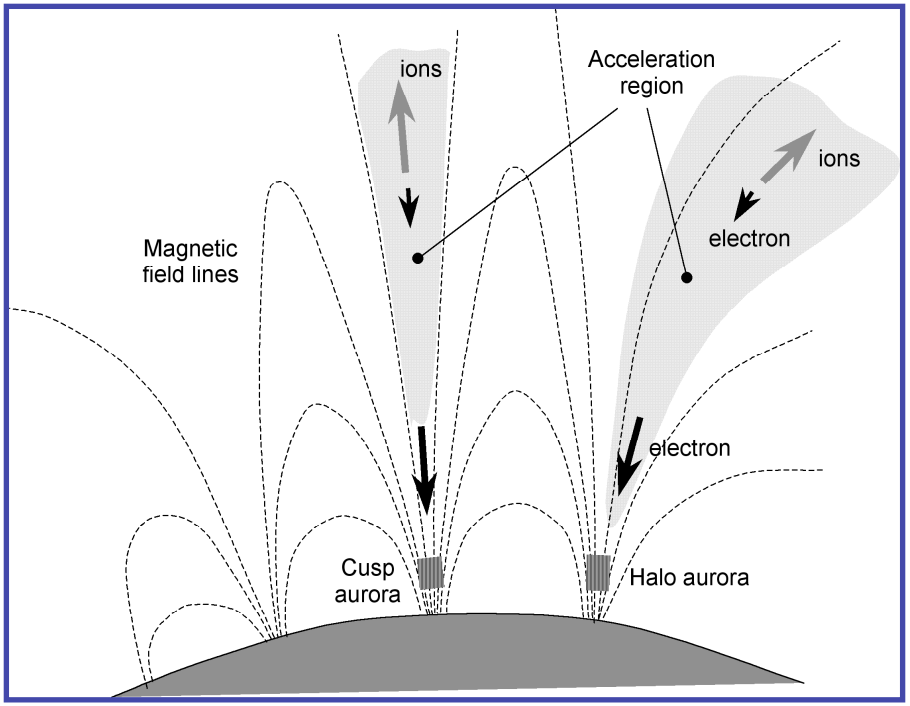

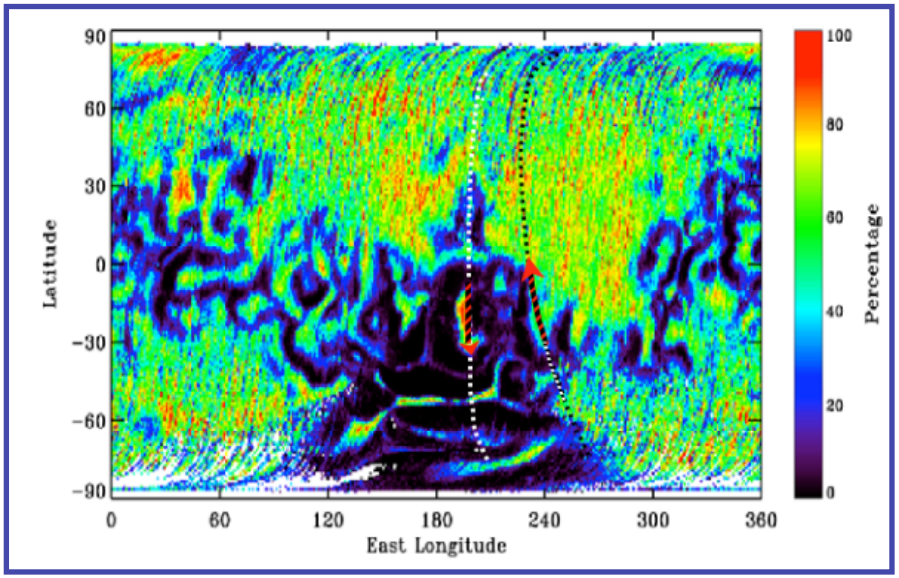

Combined energy ($E_{||}$) and velocity ($v_{||}$) field-aligned acceleration in the tail cavity of Mars

Height distribution of auroral accel.

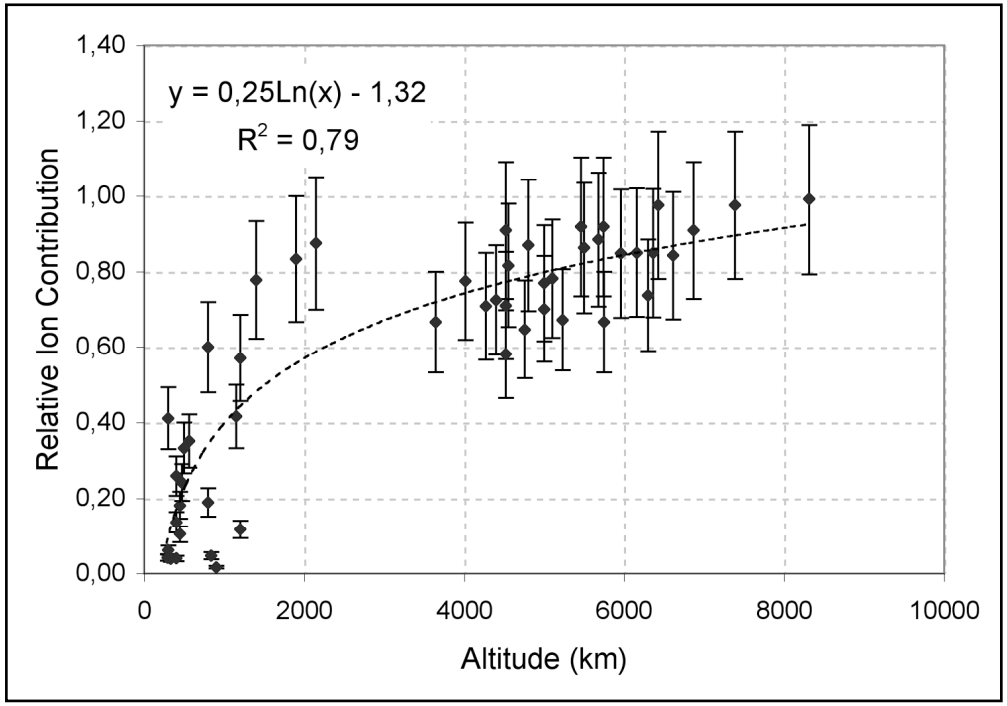

$$E = eV_0 + \frac{Nm_p v_{||}^2}{2}$$

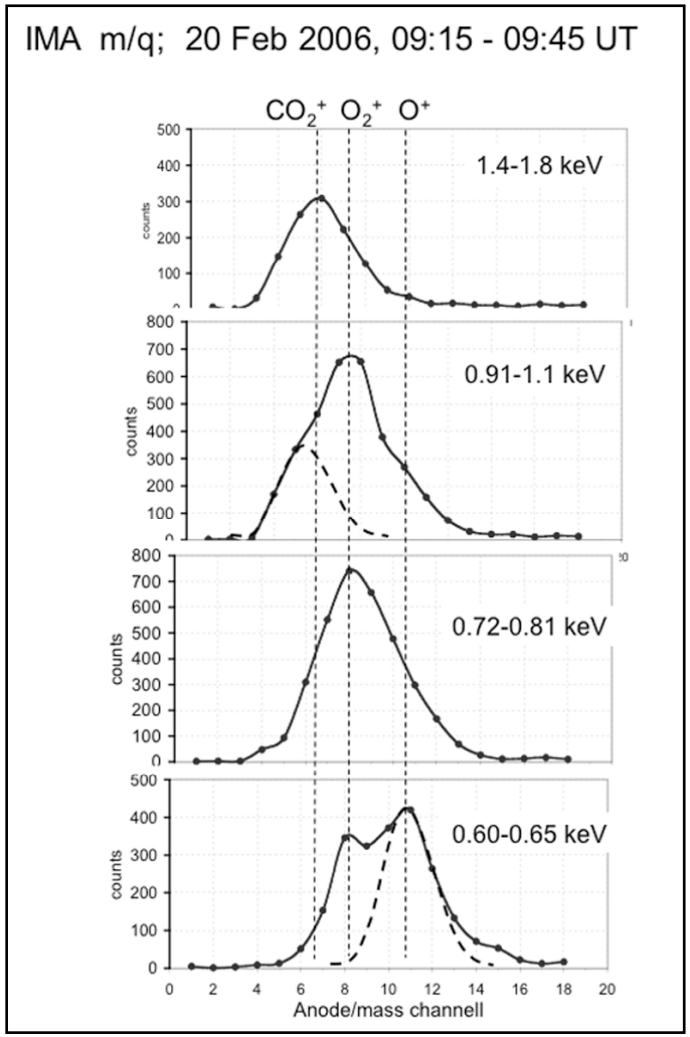

Peak energies

$CO_2^+ \approx 1.16$ keV

$O_2^+ \approx 0.93$ keV

$O^+ \approx 0.62$ keV

($v(O^+) \approx 85$ km/s, $v(O_2^+) \approx 71$ km/s and $v(CO_2^+) \approx 67$ km/s)

Plasma wave acceleration (Ponderomotive acceleration)

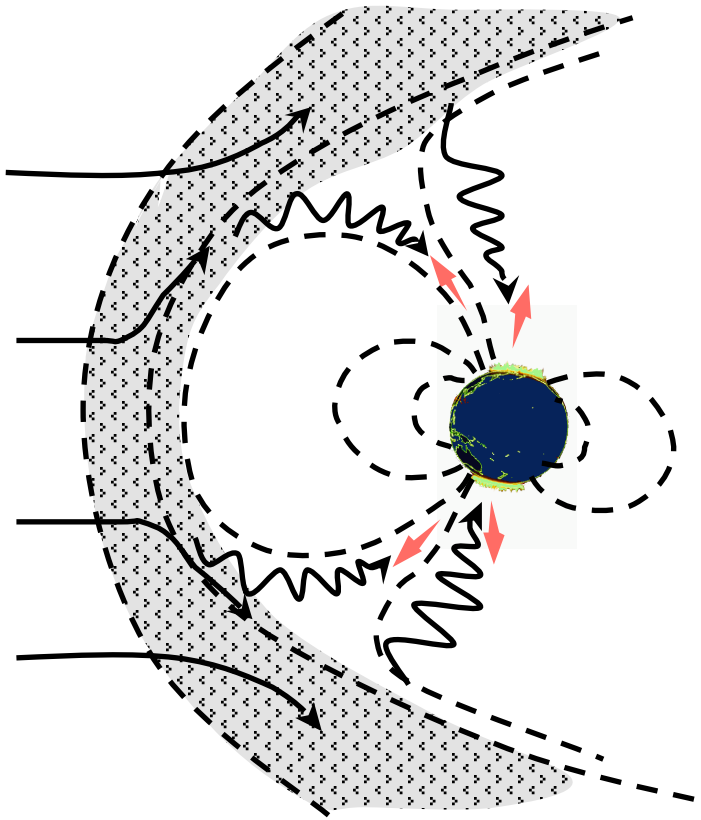

ULF waves generated in:
Earth's magnetosheath, cusp, boundary layer (Chaston et al, 2005)
Mars sheath (Espley et al, 2004)

Upward Acceleration by MMP in the Earth´s dipole field (E/B=0.5)

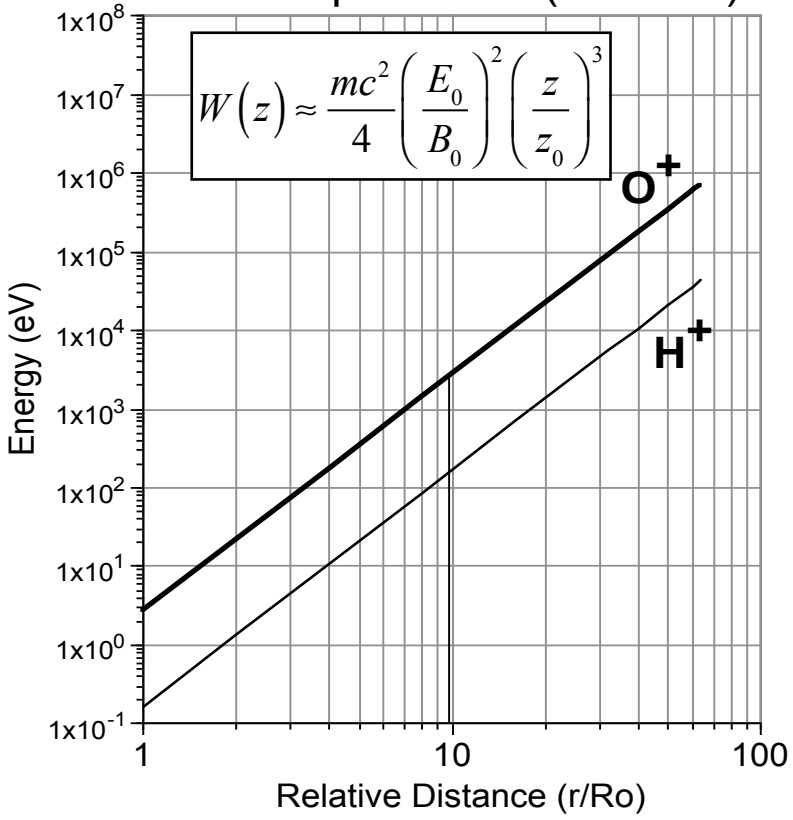

Exact formula for the energy gain by field-aligned ponderomotive acceleration :

$$\Delta W_{\parallel}(z) \approx \frac{e^2}{m}\int_0^z \frac{E_\Omega^2}{\nu B}\left|\frac{\partial B}{\partial z}\right| dz$$

Yama's works

Still using old satellites (Viking, Freja)

Moving from H+ (SW origin) to O+ (ionospheric origin)

Large-scale

Freja O+ injections

O+ = not well-studied

H+ = well-studied

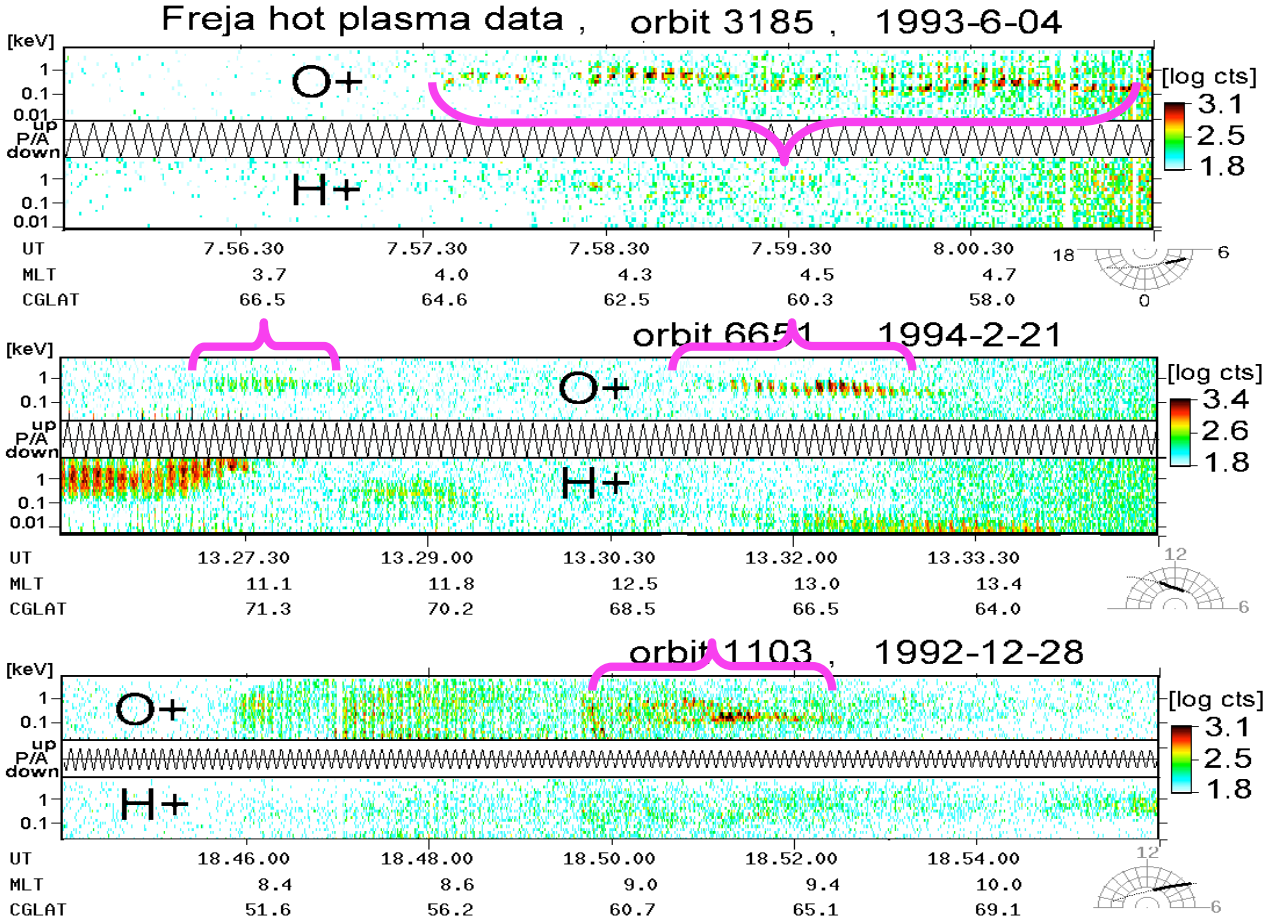

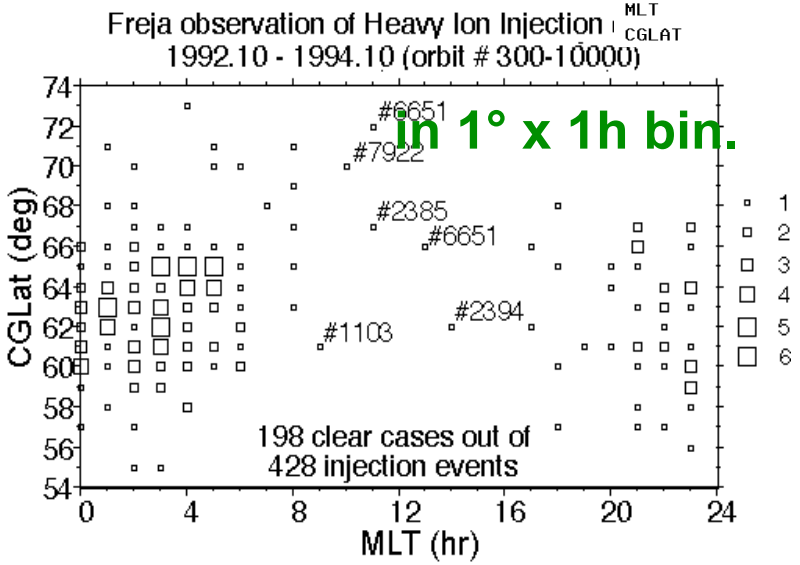

Freja O+ data is not well studied : need common database to analyze

Dayside sub-auroral heating

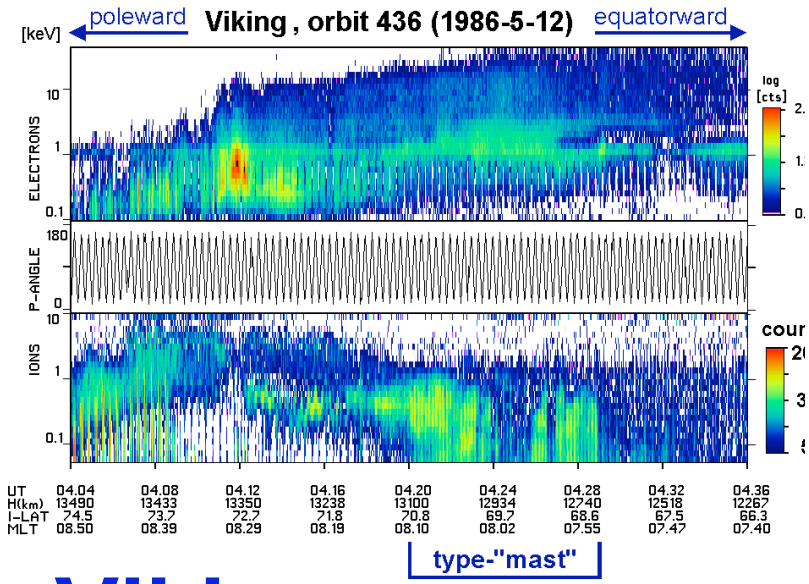

Viking

Wave?

Field?

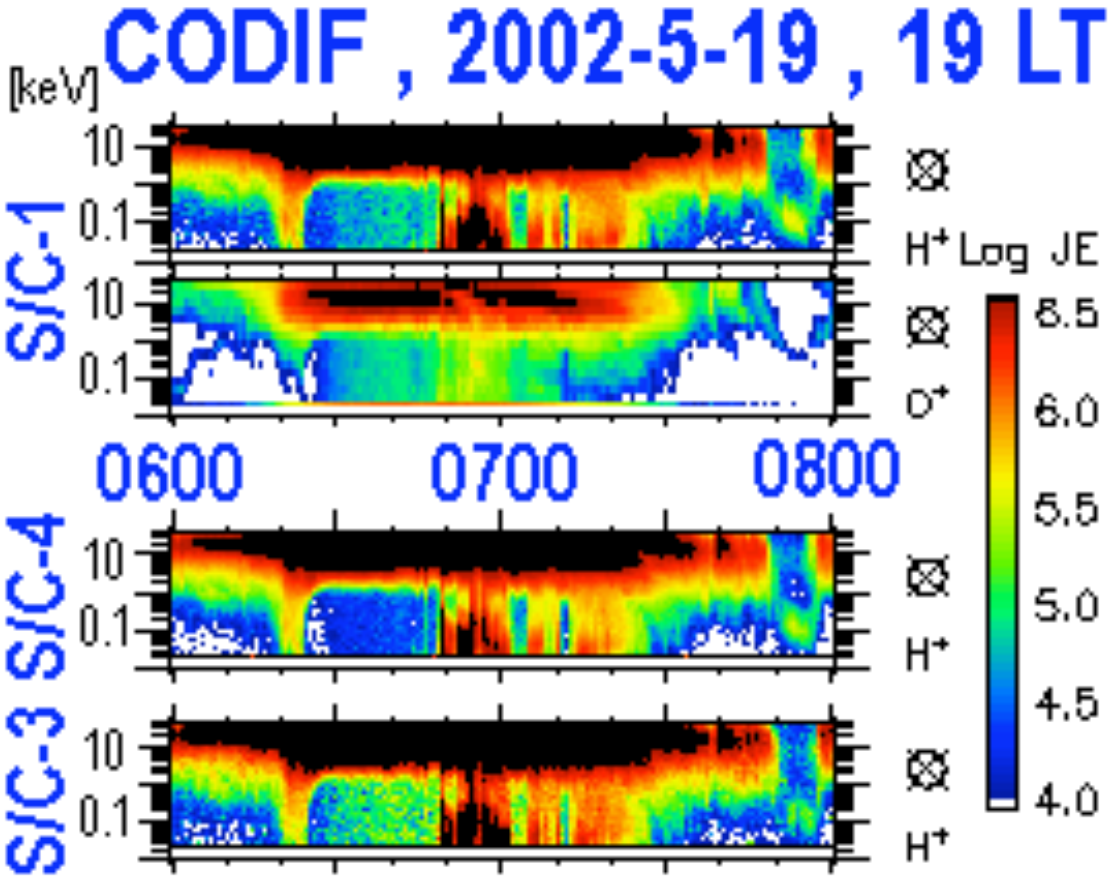

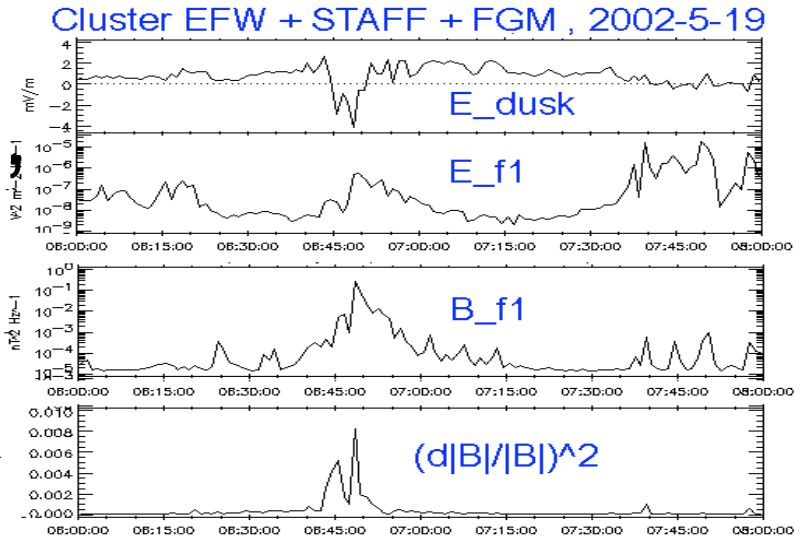

Knowing new results re-examine **Viking, Freja, Astrid : need common database**

Importance of ionosphere

Present Earth,
Ancient Earth?

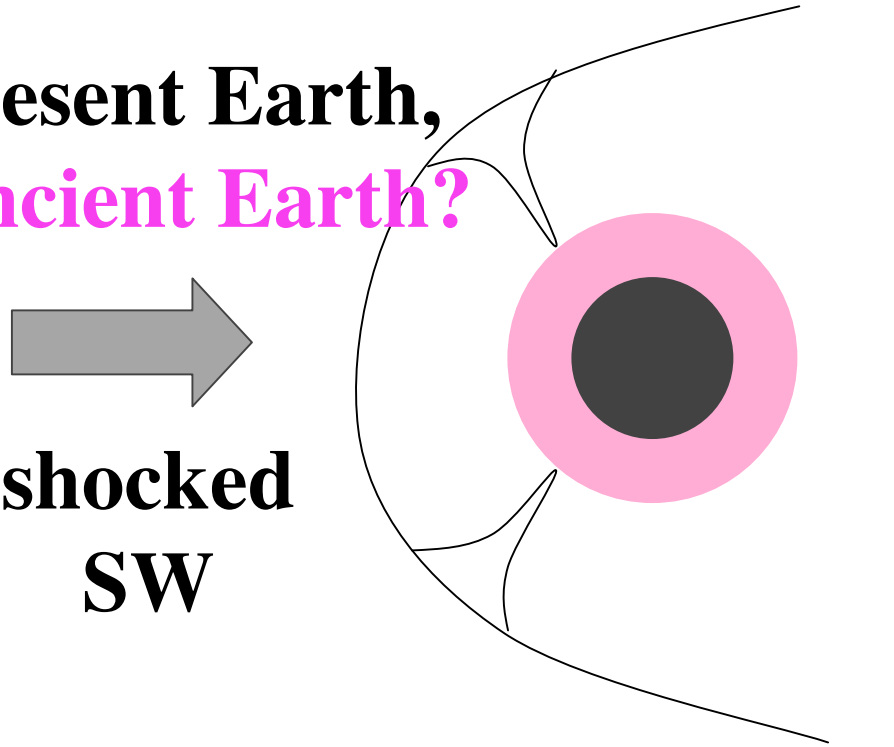

Mars, Venus,
Ancient Earth?

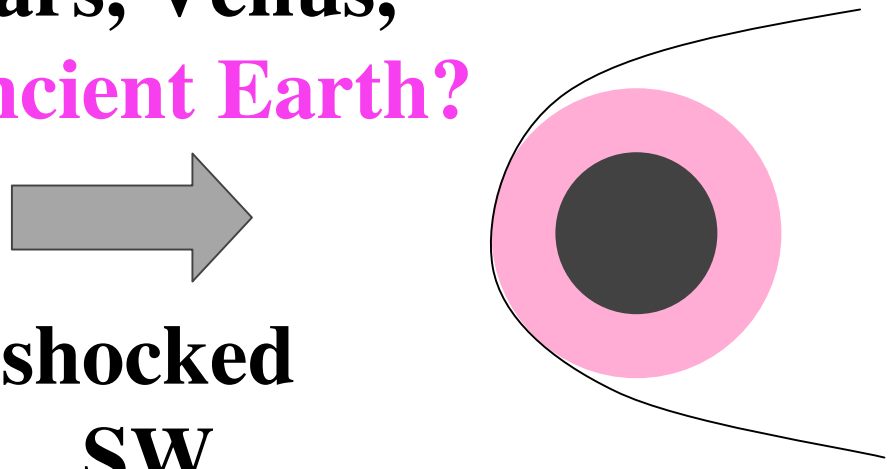

Because of IMF, ionosphere can stop SW through the piled-up magnetic field

Cycloid ions distribution in SW (Mars)

Bow-shock is quite different between Earth and Mars

Cycloid distribution

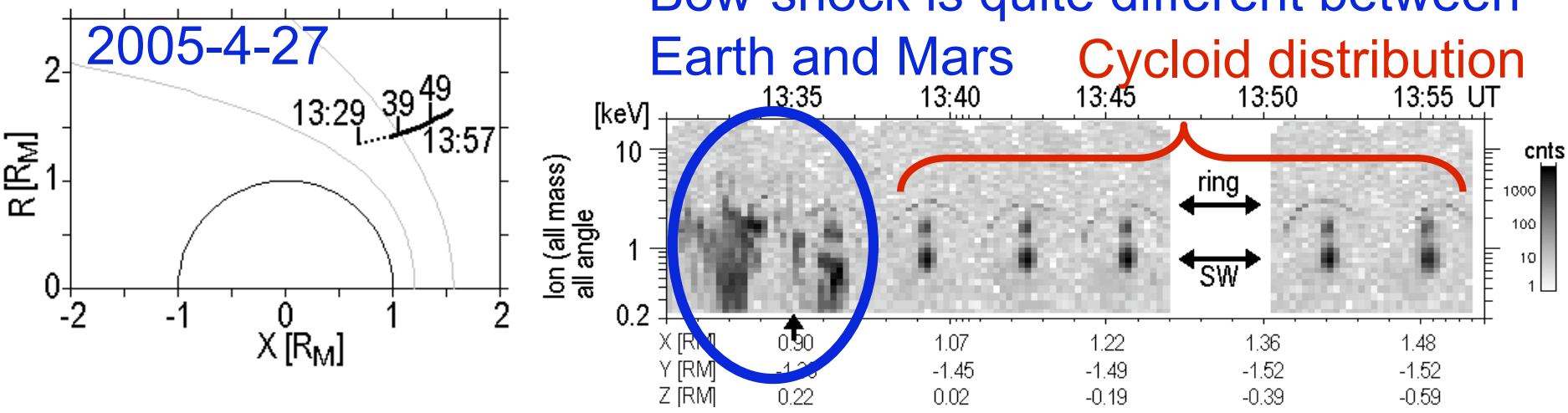

Minimum Variance Method to determine gyration plane

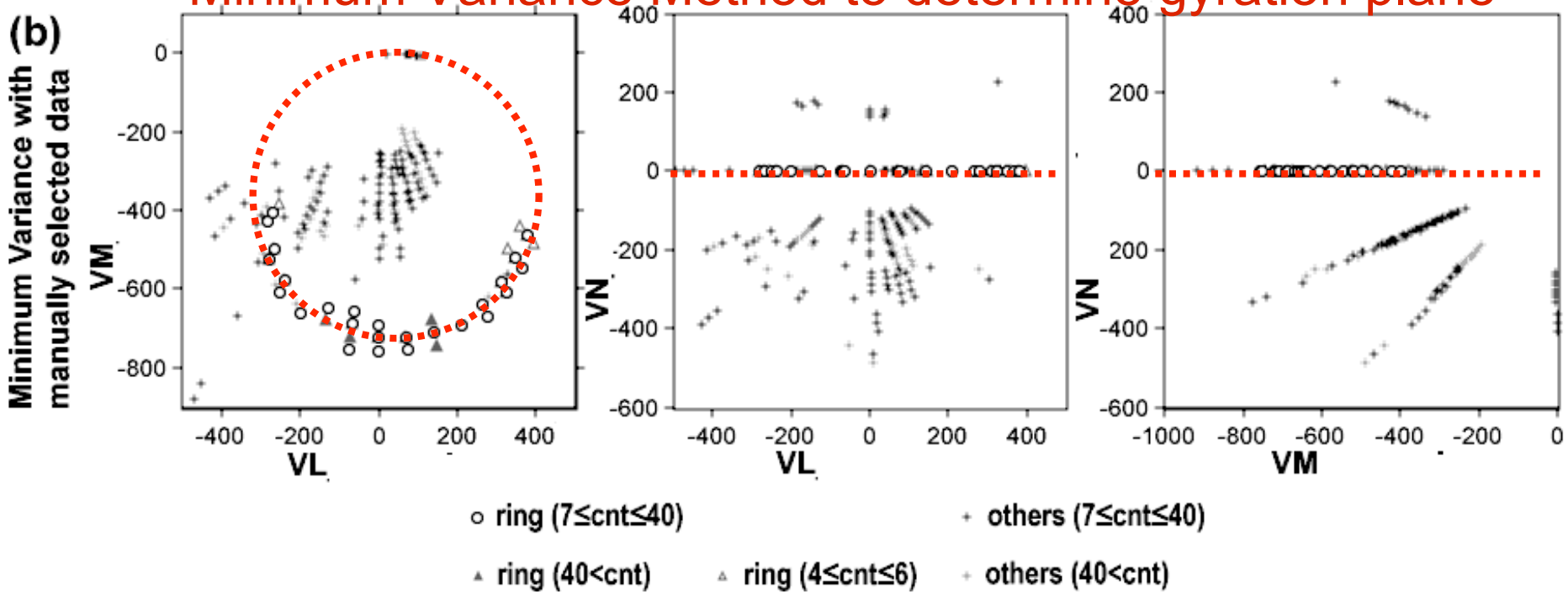

Substorm & sub-keV ring current

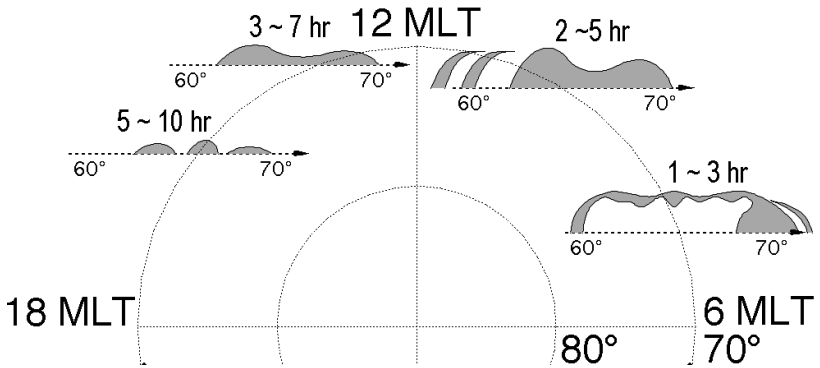

Viking
14 MLT

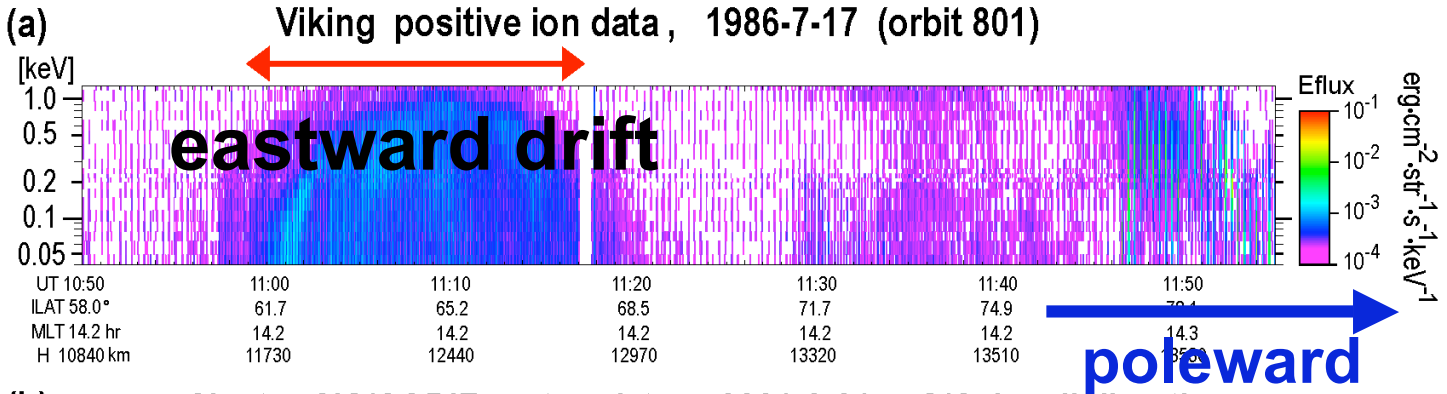

Cluster
Perigee, 11 MLT

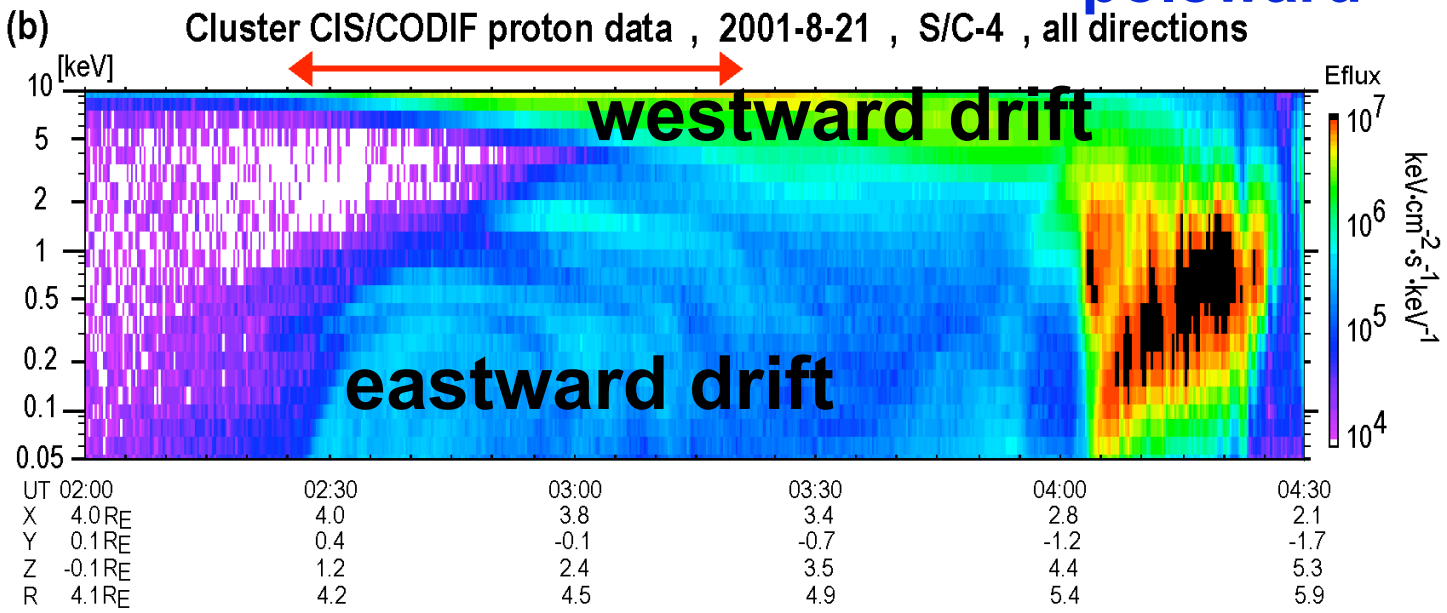

Statistics suggests morning source !

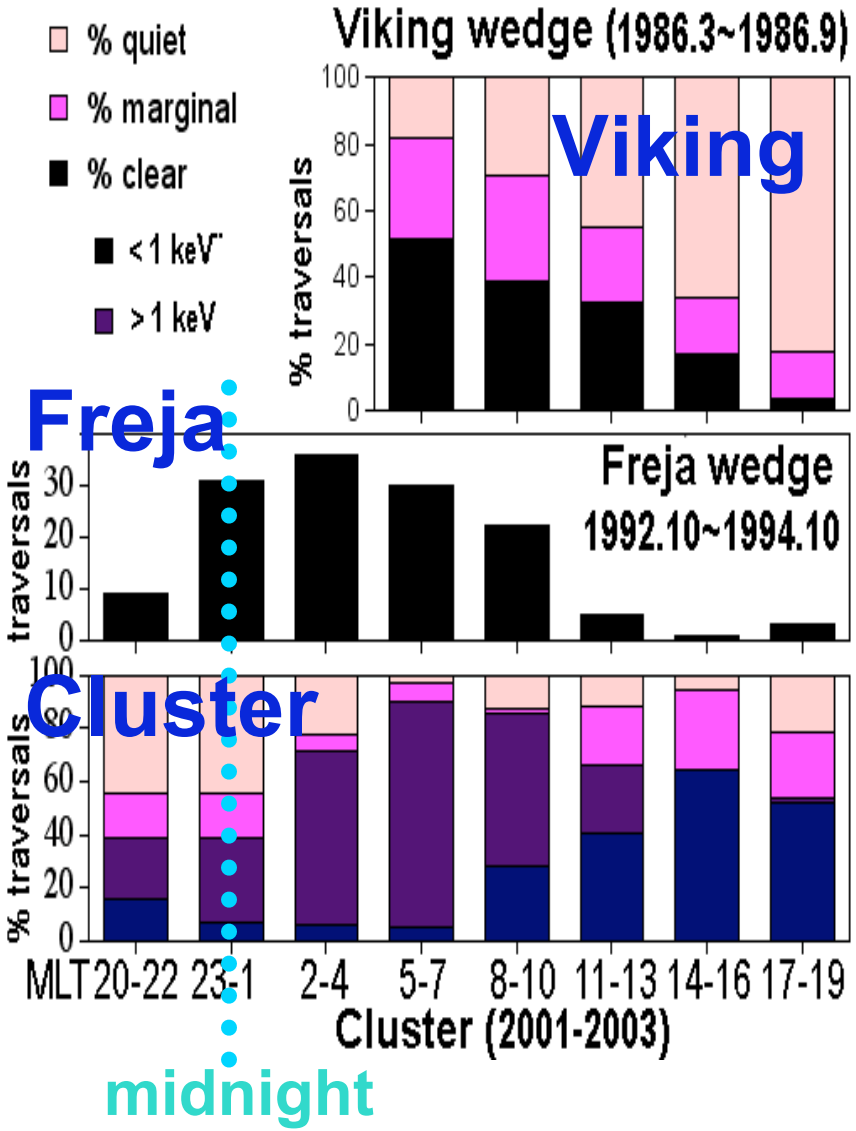

Viking probability of event

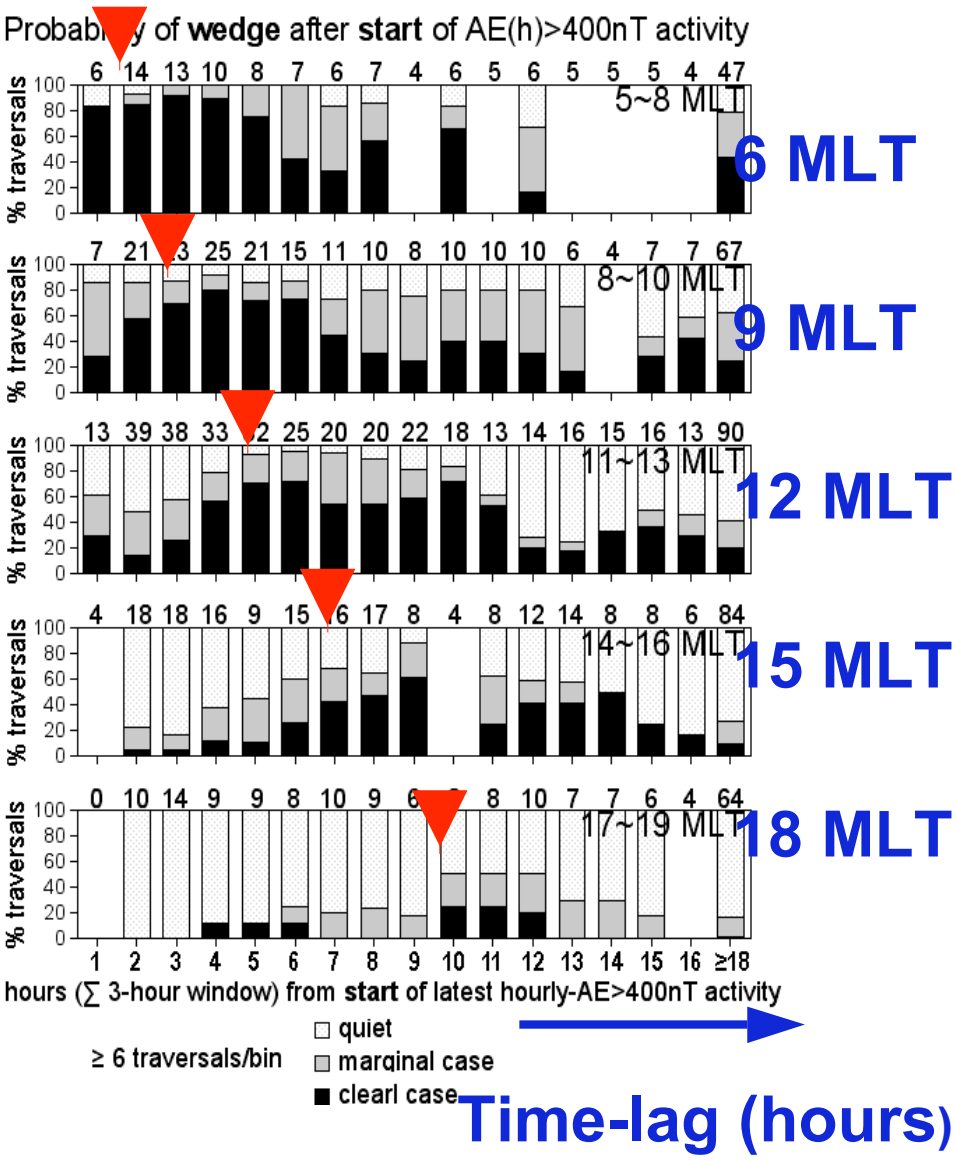

Backward Superposed Epoch Analyses using **700 traversals.**

Cluster case study

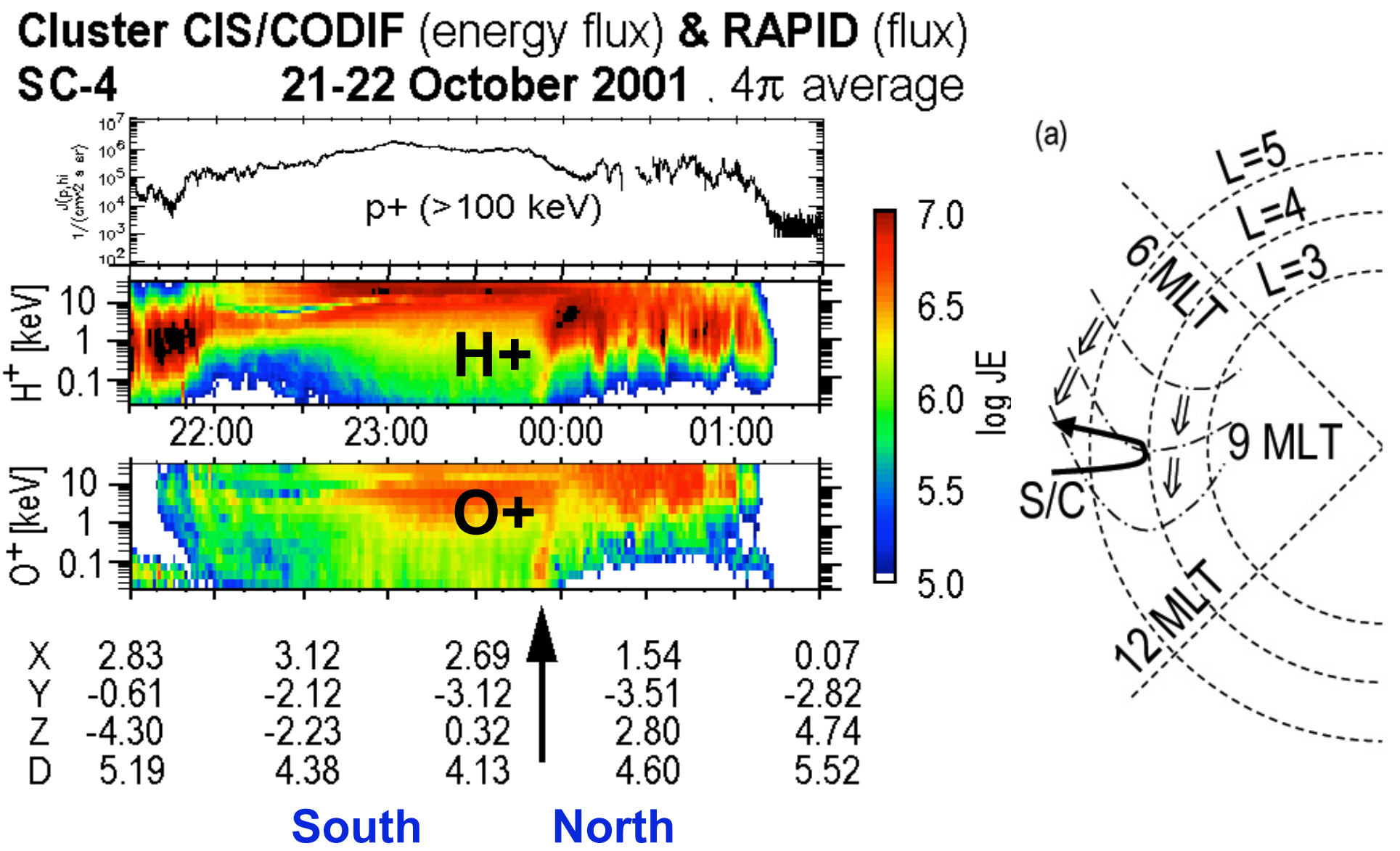

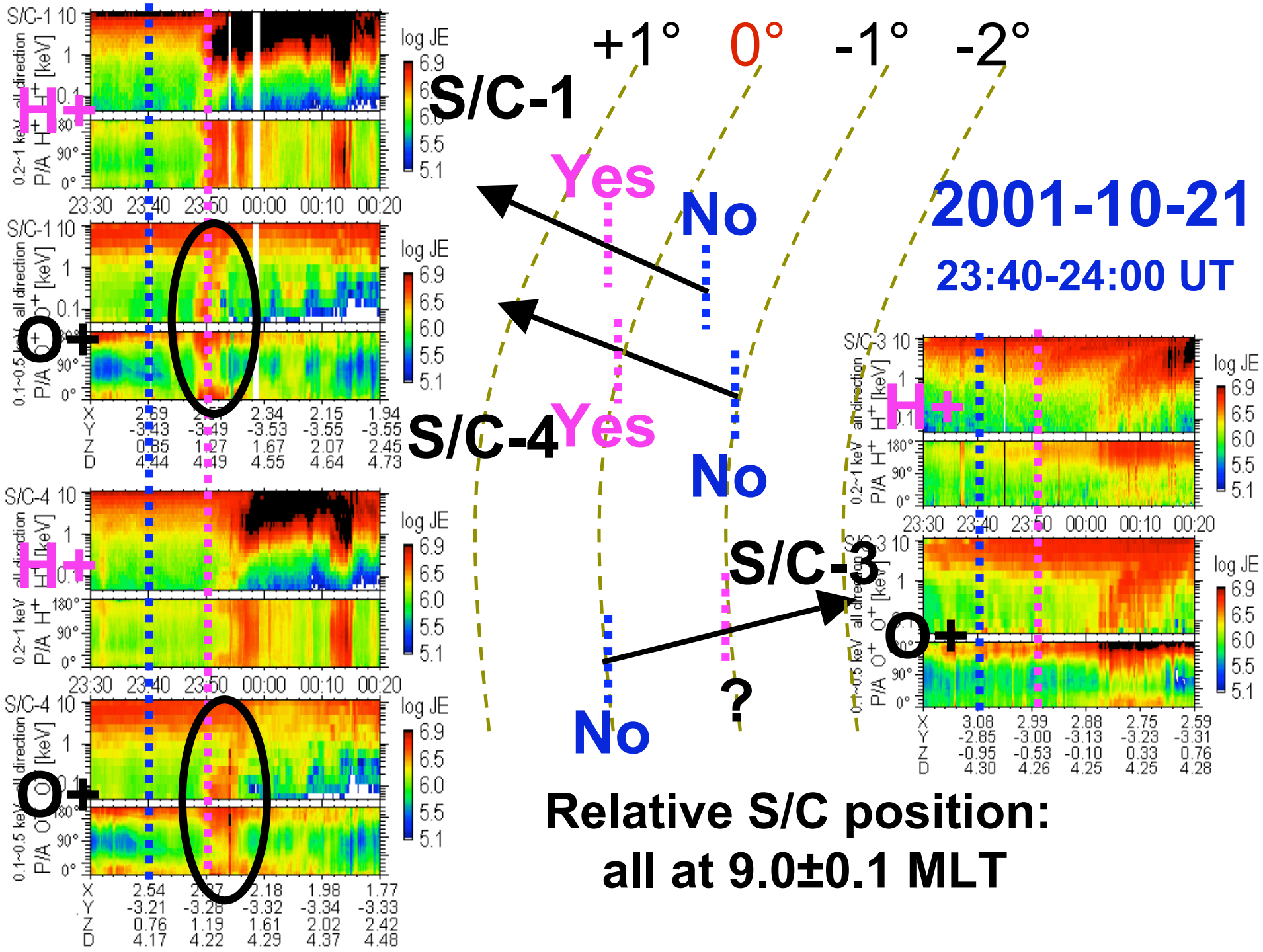
+1°
0°
-1°
-2°
S/C-1
S/C-4
S/C-3
Yes
No
Yes
No
No
?
2001-10-21
23:40-24:00 UT
H+
O+
H+
O+
H+
O+
log JE
Relative S/C position:
all at 9.0±0.1 MLT

Morning Source of Energized Ions during Substorm

Many statistics (Viking, Freja, Cluster)

Some of sub-keV ring current are formed in the morning sector (not midnight sector).

Case study from 2001-10-21 substorm

Dispersion started and O+ is ejected from 6~7 MLT.

(A) Strong **E-field** push ions quickly.
(B) **Scattering** of <10 keV ions to lower energy
(C) **Sputtering** of ionospheric ions by >10 keV ions
(D) Unknown **local energization** process.

Onset of 2003-10-29 substorm

Indepent substorm onset in the morning sector within 1 min, from evening-midnight onset.

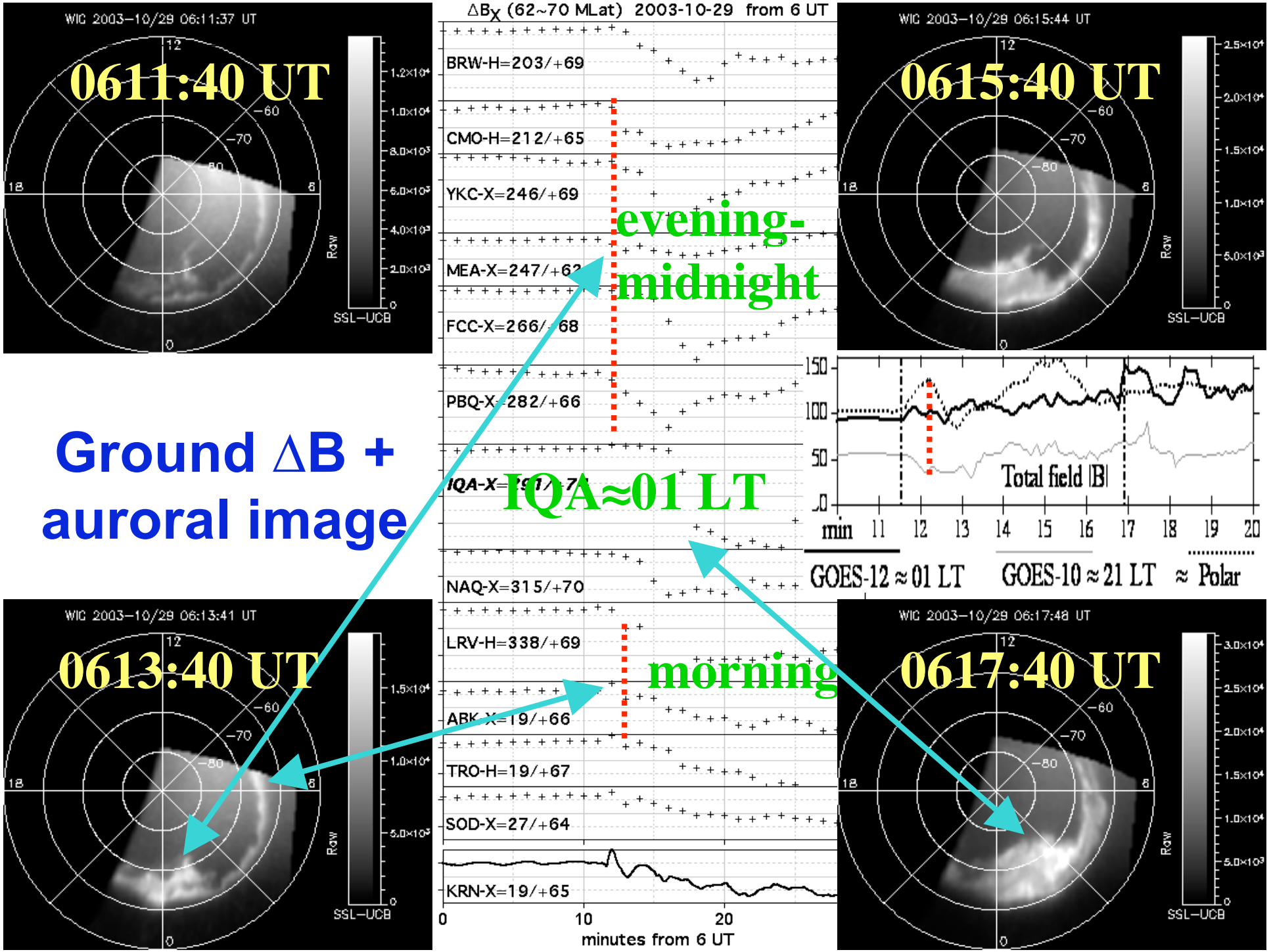
WIC 2003-10/29 06:11:37 UT
0611:40 UT
WIC 2003-10/29 06:15:44 UT
0615:40 UT
ΔBX (62~70 MLat) 2003-10-29 from 6 UT
BRW-H=203/+69
CMO-H=212/+65
YKC-X=246/+69
MEA-X=247/+62
FCC-X=266/+68
PBQ-X=282/+66
IQA-X=291/+71
NAQ-X=315/+70
LRV-H=338/+69
ABK-X=19/+66
TRO-H=19/+67
SOD-X=27/+64
KRN-X=19/+65
minutes from 6 UT
evening-
midnight
IQA≈01 LT
morning
Ground ΔB +
auroral image
Total field |B|
min
GOES-12 ≈ 01 LT
GOES-10 ≈ 21 LT
≈ Polar
WIC 2003-10/29 06:13:41 UT
0613:40 UT
WIC 2003-10/29 06:17:48 UT
0617:40 UT
SSL-UCB

Cheap Aurora camera (budget < 20 k kr)

Table 1. Example of day-to-day list of aurora visibility

date	aurora (UT)	activation (UT)	expansion (UT)	cloudy UT
050301	1940 ~ 0300	(2111 & 2154=north)	2132=north	
050302	2035 ~ 2105 / 2235 ~ 2335	(2035=far north), 2254=north		2010 ~ 2100
050303	unvisible			**~ 0000 / 0040 ~ 0220**
050304	2005 ~ 2100	far north		2300 ~
050305	1920 ~ 2300 / 0015 ~ 0025	1907=pseudo,	(1920=pseudo=)1952, (2139 through cloud)	~ 1830 / 2020 ~
050306	1800 ~ 2230 / 2300 ~ 0400	0007=omega	o 1804=1820, (2126 & 2254 & 0150 through cloud), (0127=omega through cloud)	2120 ~ 2300 / 0130 ~ 0230
050307	1735 ~ 1810 / 1940 ~ 2110 / 2225 ~ 2235	1939=pseudo north, 2018=pseudo	1749, 2038	~ 1740 / 2240 ~

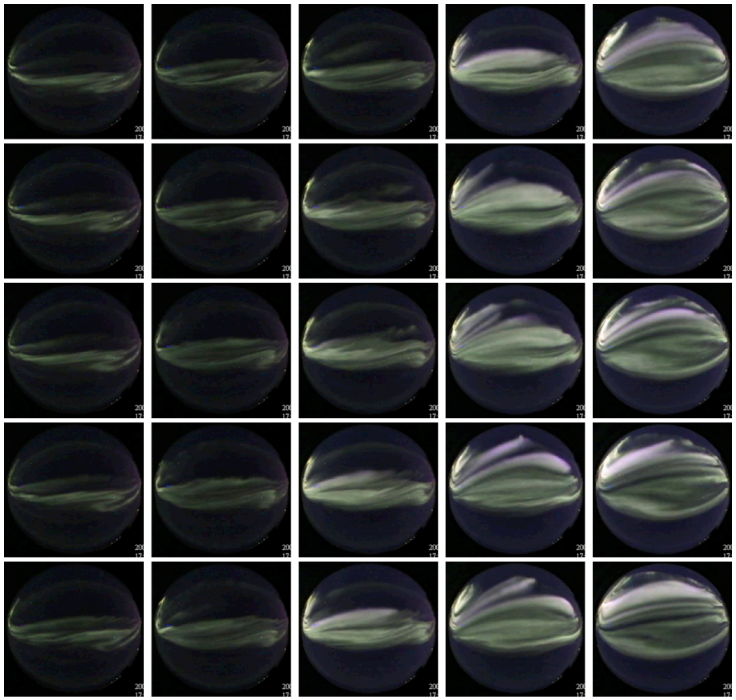

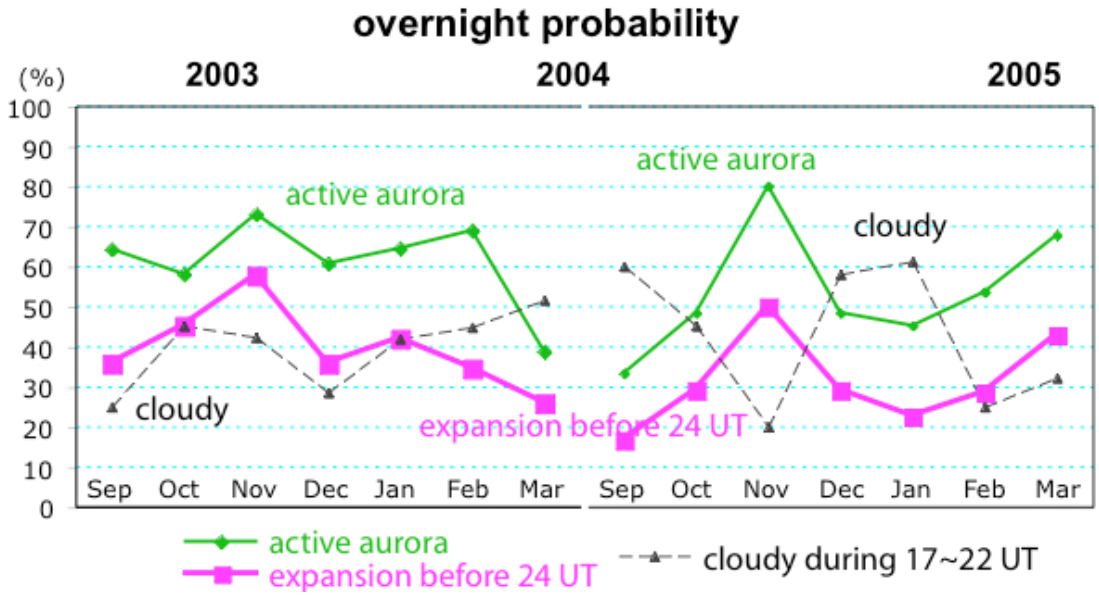

Generator and load regions in the plasma sheet as detected by Cluster

Then: M. Hamrin, O. Marghitu, … **Now: G. Stenberg, K. Rönnmark, …**

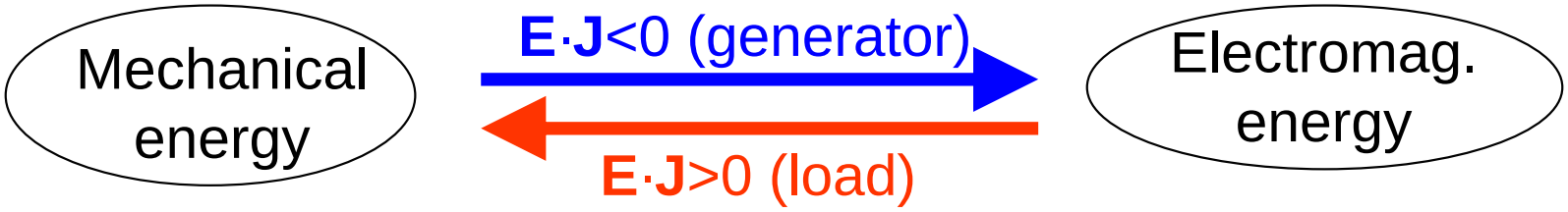

- Study of concentrated generator regions (CGR) near PSBL.
- 19 – 20 Sep 2001, h=18 RE.
- First *in-situ* experimental evidence for generators.
- CGRs correlate with auroral electrons observed by FAST.

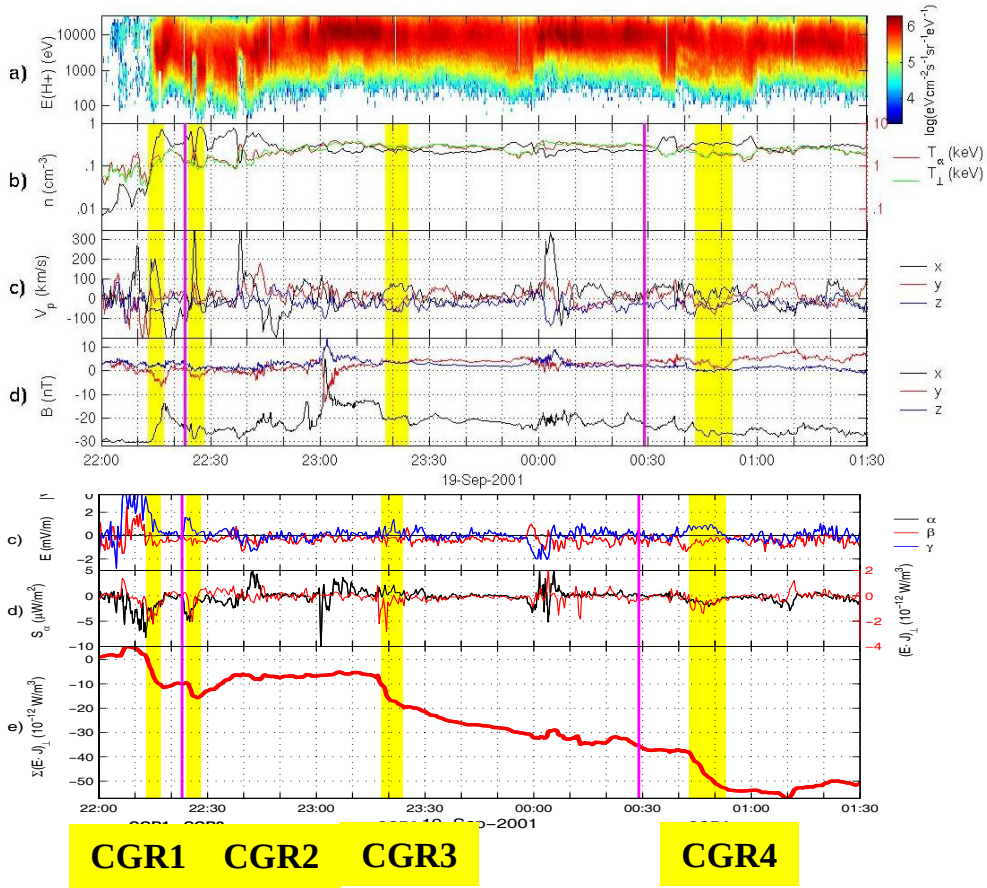

- Statistical study (Aug–Nov 01) of PS crossings.
- Energy Conversion Regions (ECR) observed.
- The PS behaves, on average, as a load.
- Typically load close to the neutral sheet.

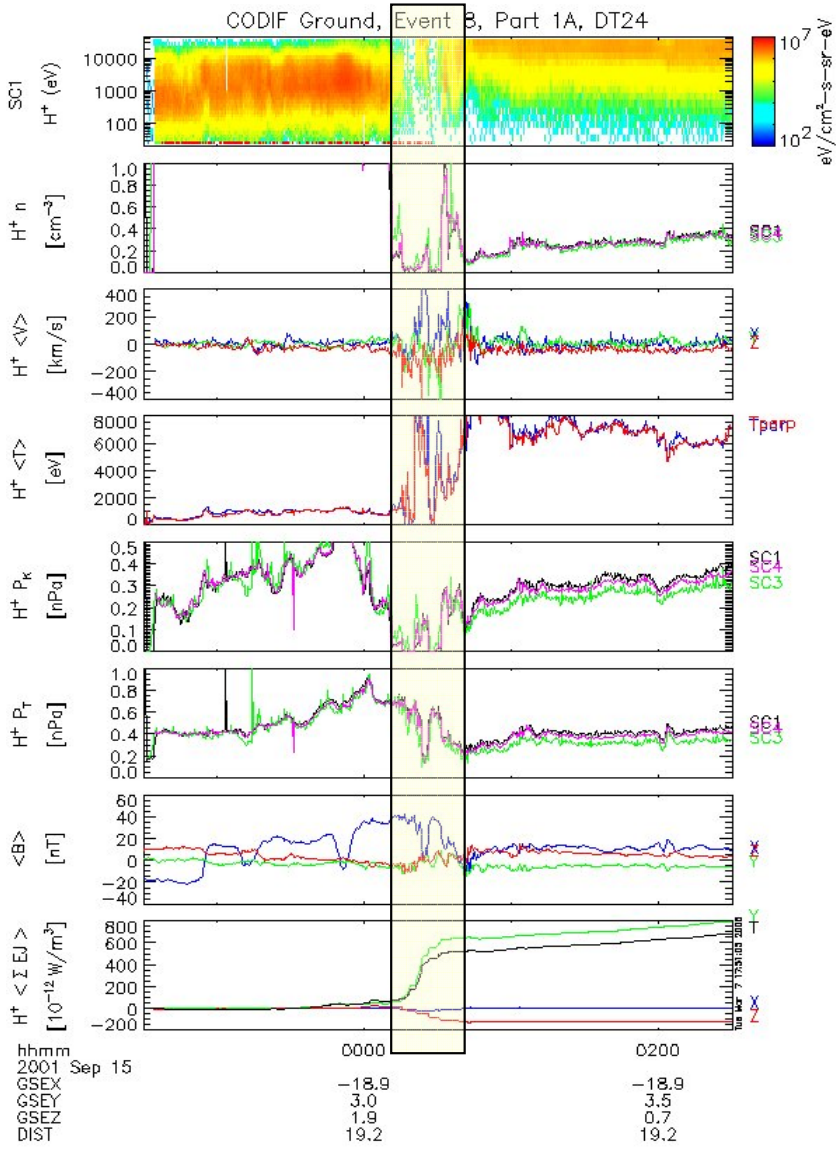

Ex:
a load

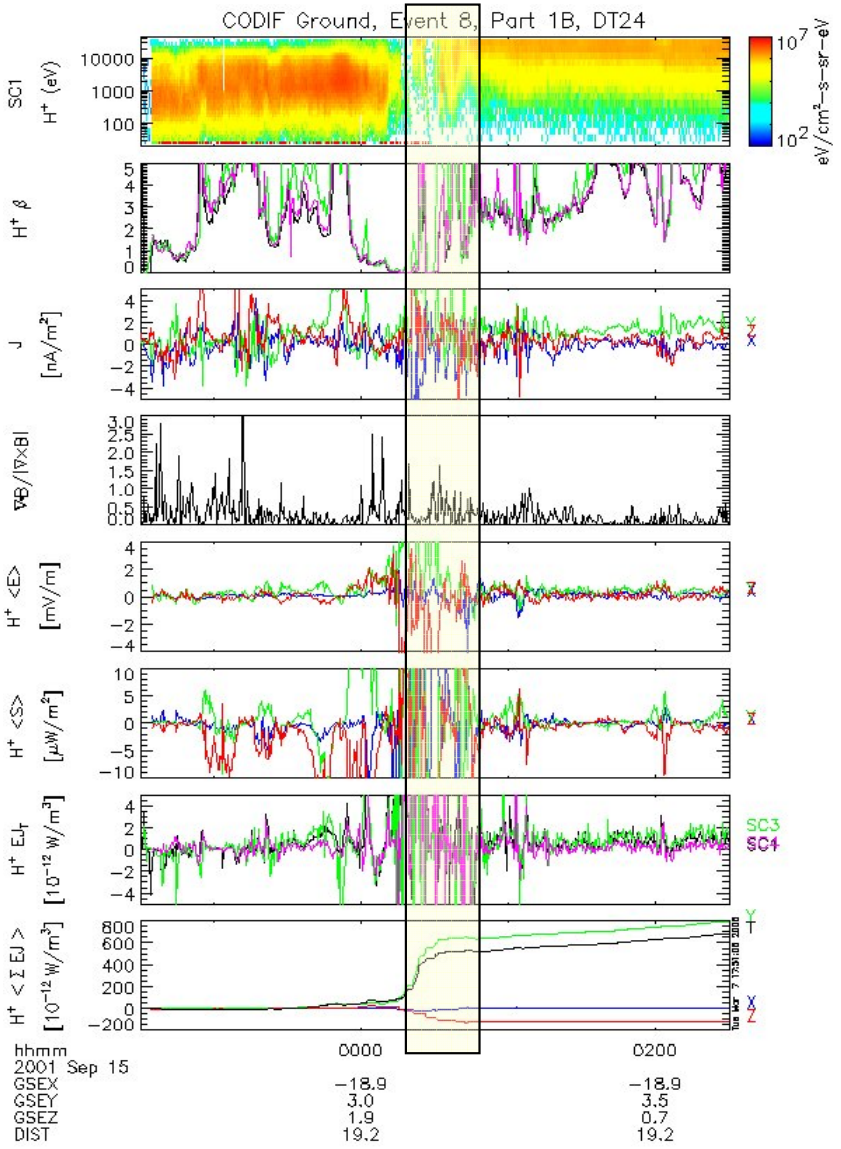

Good agreement with simulations, Birn & Hesse, AG 2005

- ECRs: Mostly load character; Related to bulk flow (along B); Few minutes time scale.
- (Integrated) loads close to midnight, generators on the sides.
- CGRs close to PSBL.
- Net Poynting flux from generators.

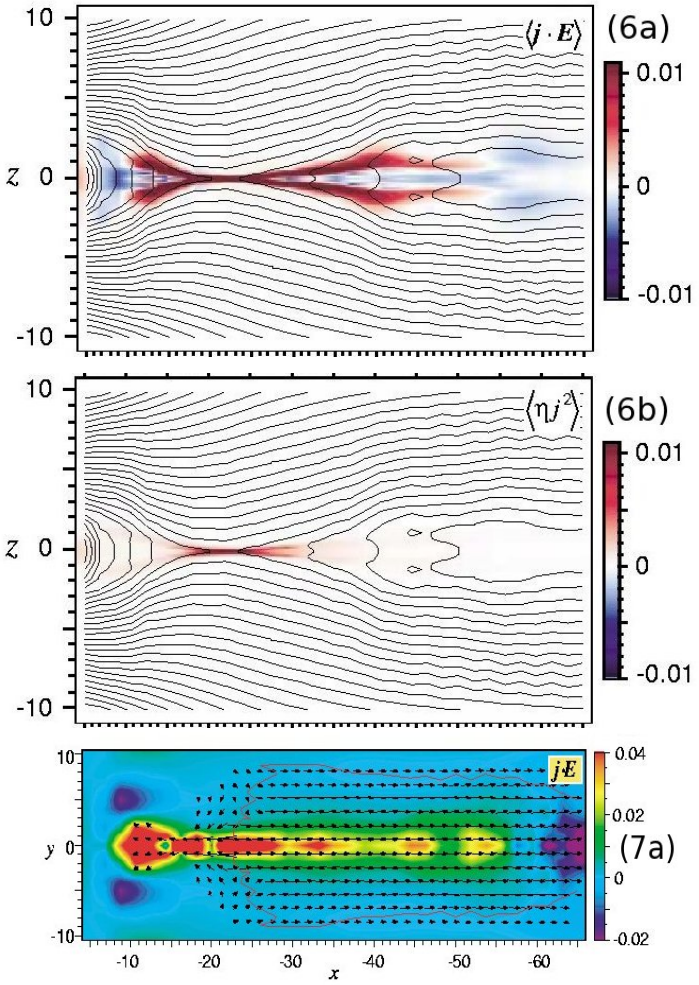

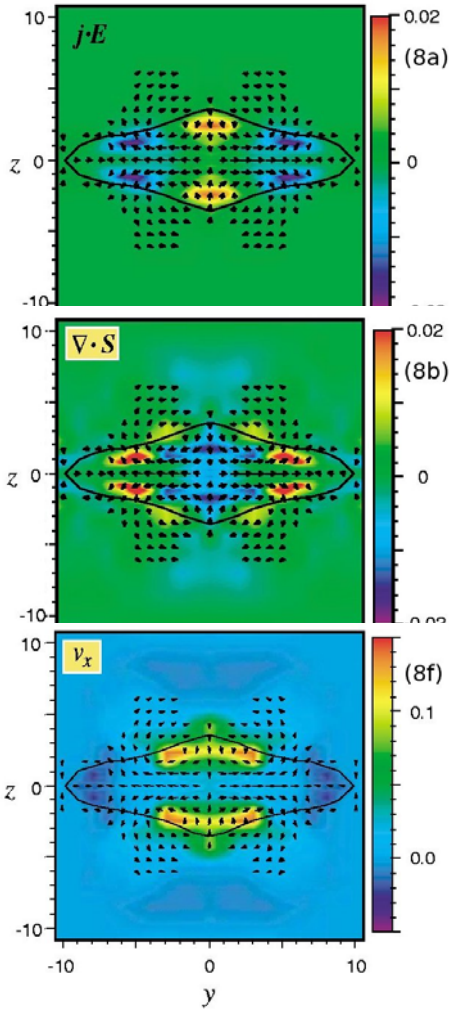

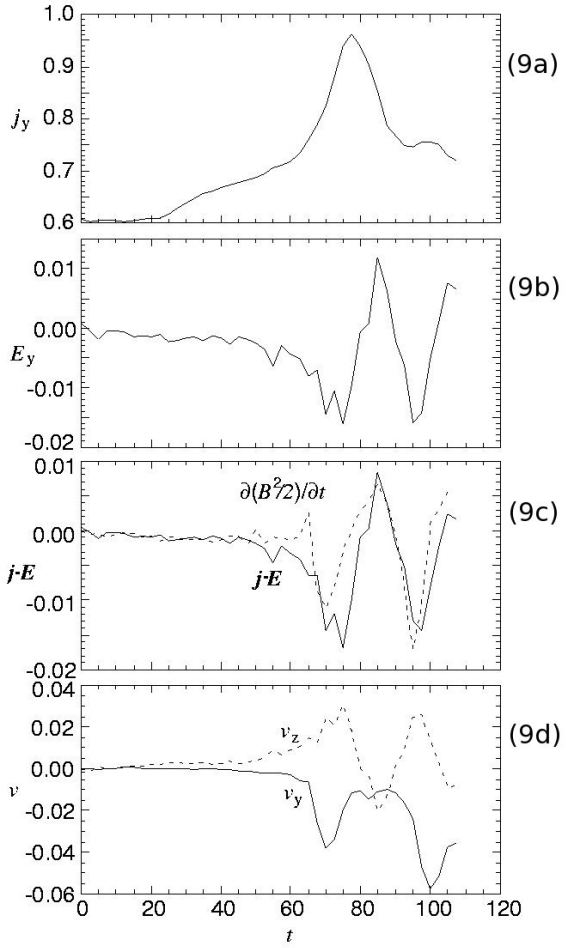

Magnetic reconnection sites - strong / narrow currents and potential jumps

- Understand how strong currents and potential jumps can form within narrow layers close to reconnection sites

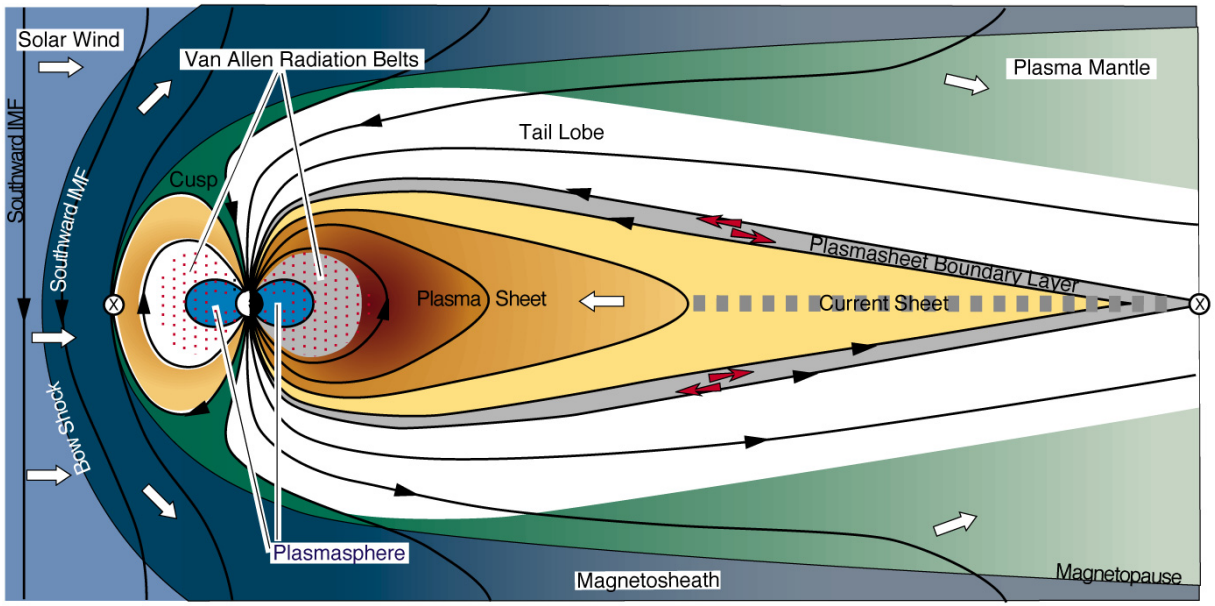

What has been done?

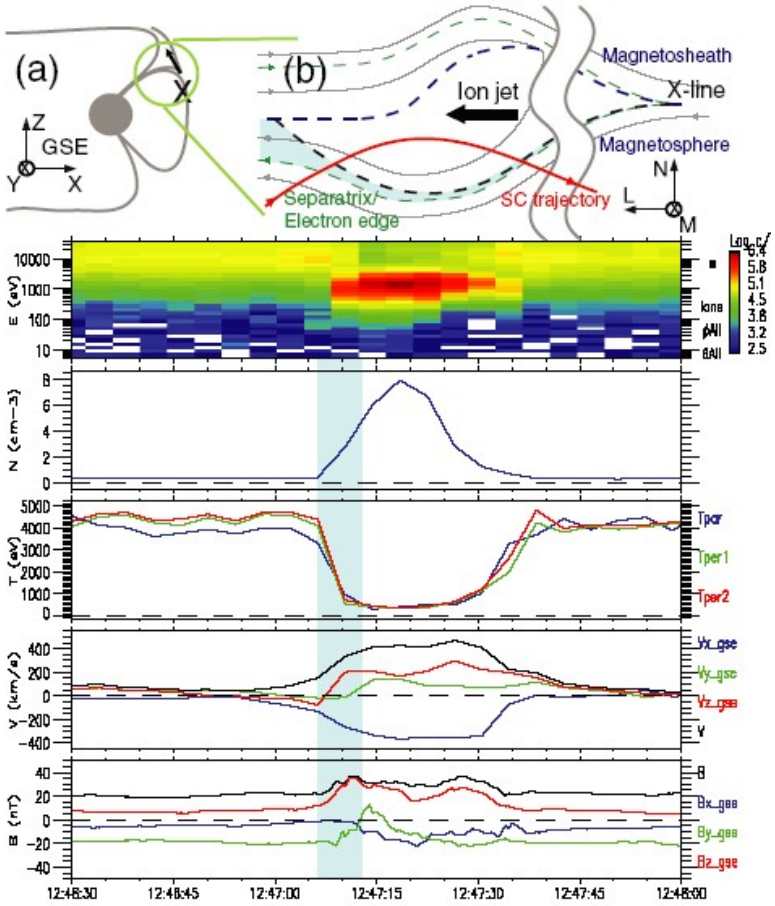

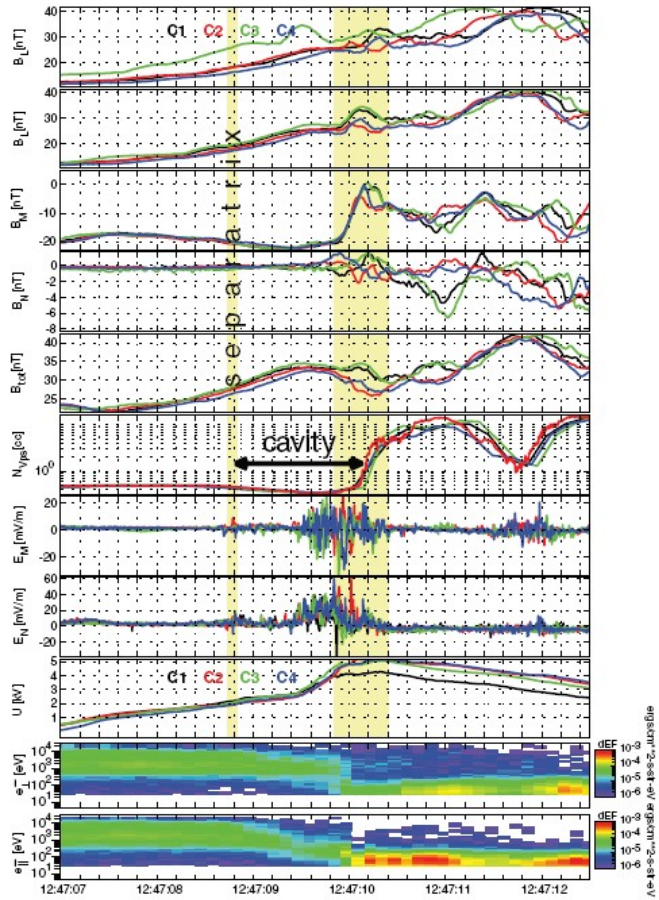

Khotyaintsev et al, PRL 97, 205003 (2006)

What will I do?

- Identify magnetopause crossings
- Identify current sheets and potential jumps
- Determine if these are due to reconnection or other processes
- Study under other reconnection conditions
- Study at different distances from reconnection region
- Study coupling to the ionosphere

Ionospheric heating

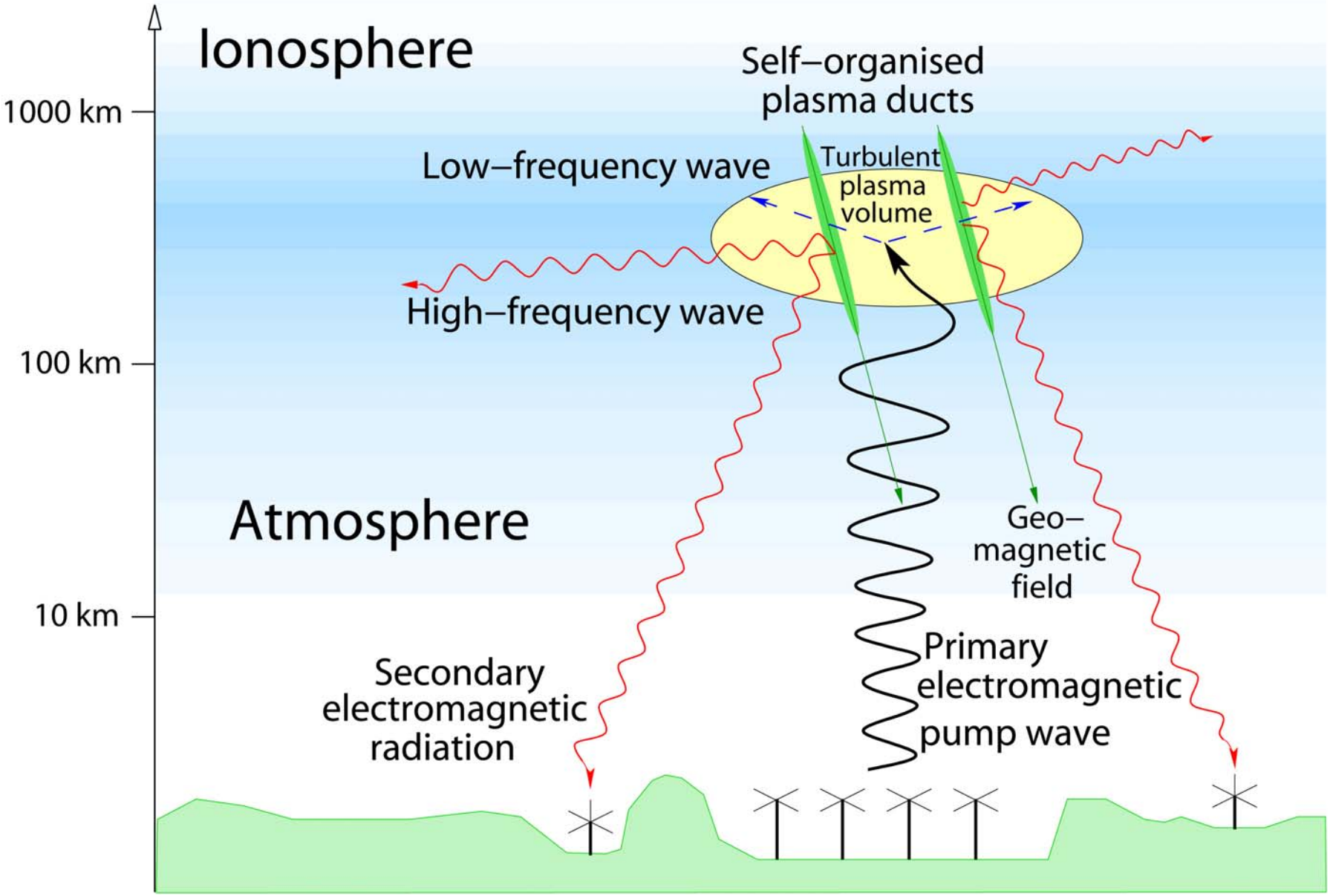

Blueshifted frequency components (+14-200 kHz)

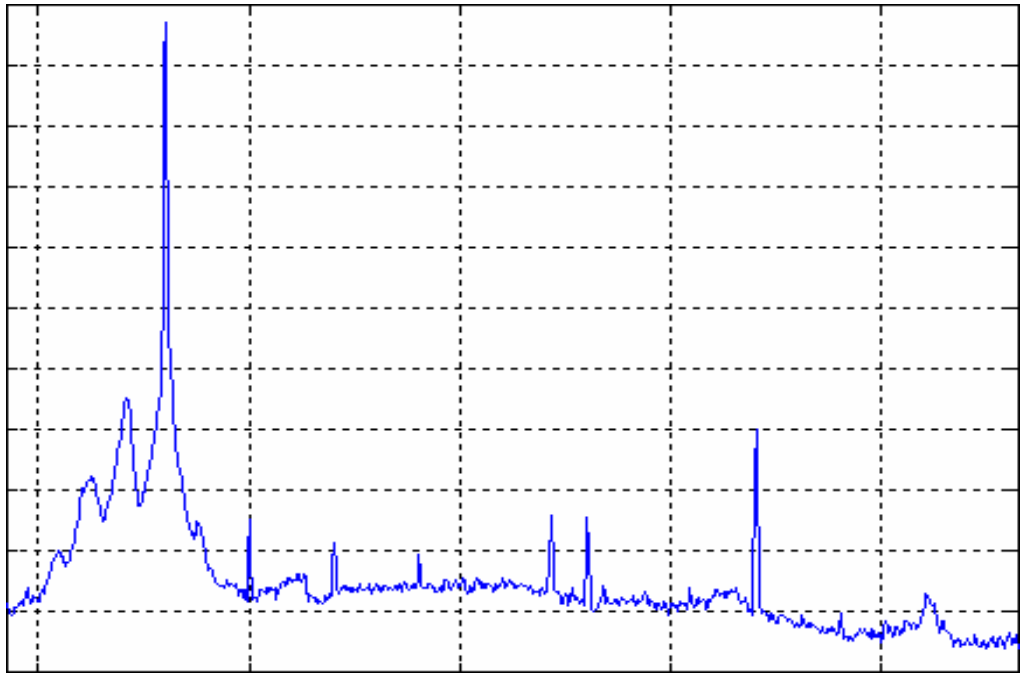

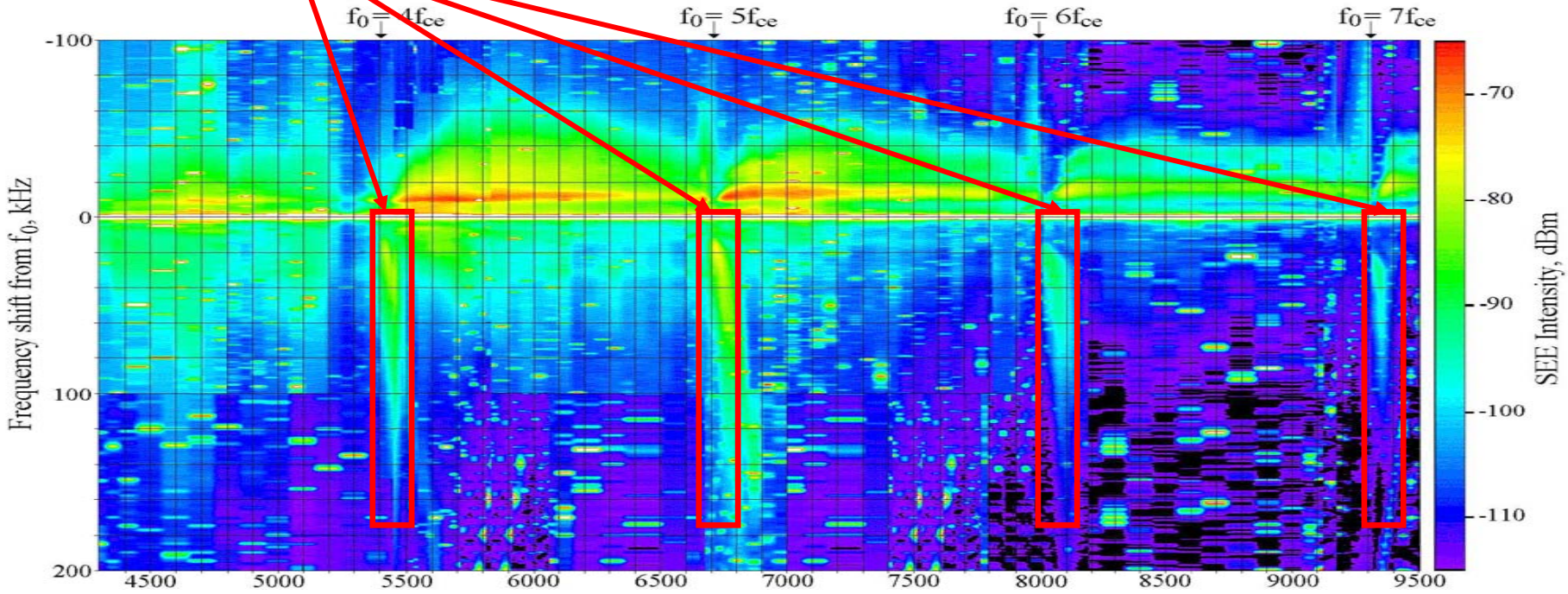

Theoretical model

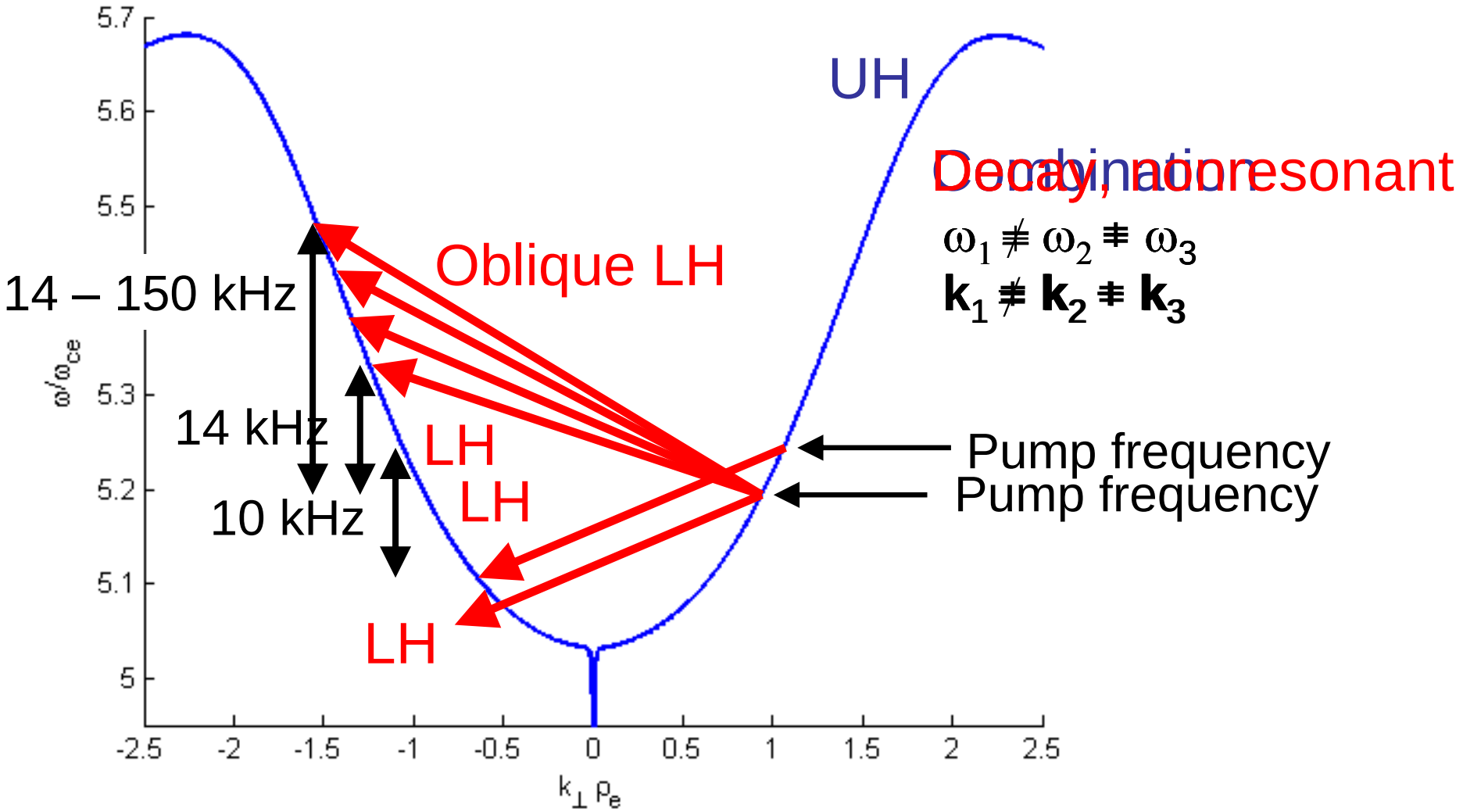

Vlasov simulation of wave interaction

Radio Pumping of plasma

Lars K. S. Daldorff[1]

[1]Department of Astronomy and Space Physics
Uppsala, Sweden

1 Feb. 2007

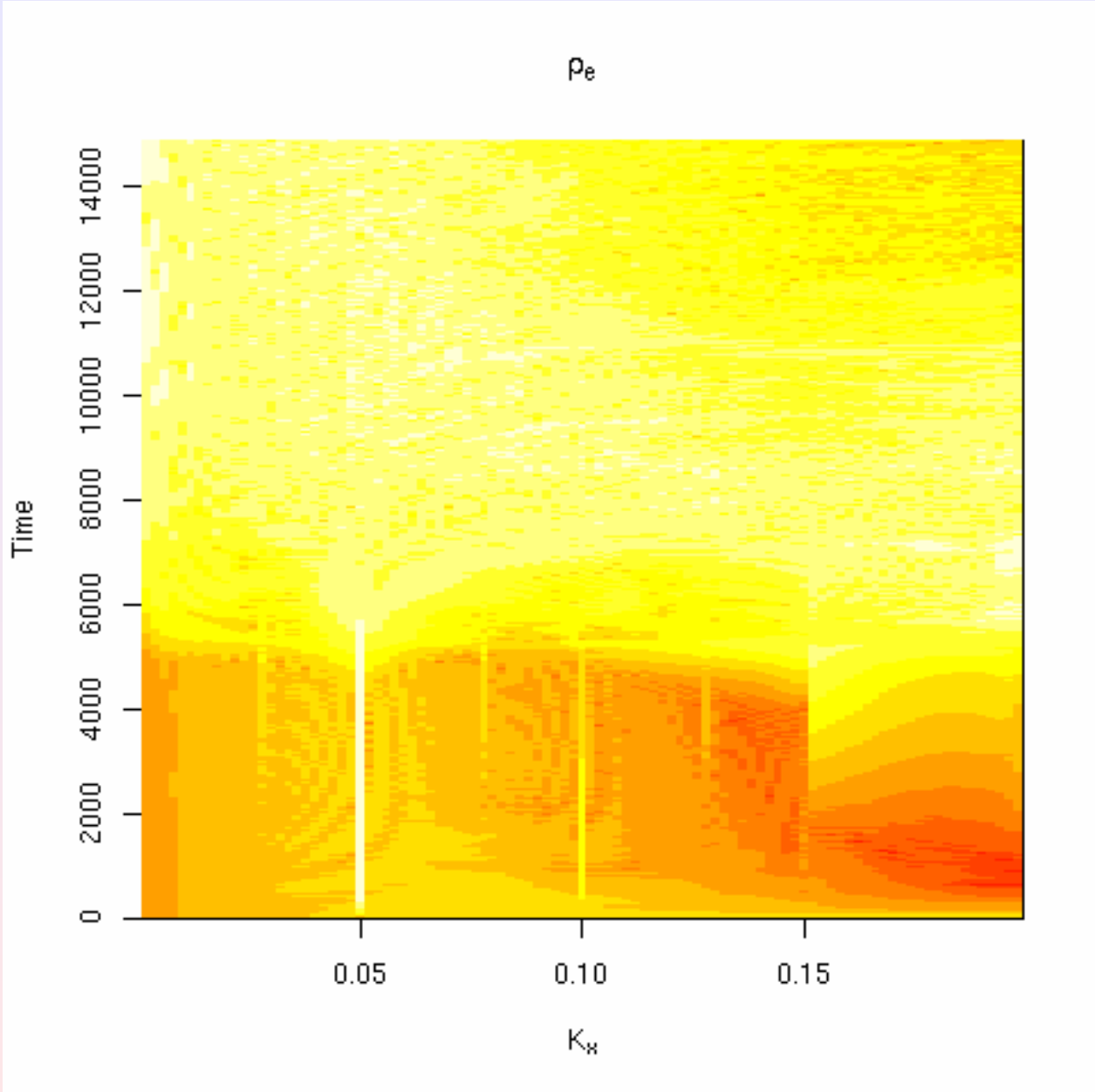
ρ_e
Time
0
2000
4000
6000
8000
10000
12000
14000
0.05
0.10
0.15
K_x

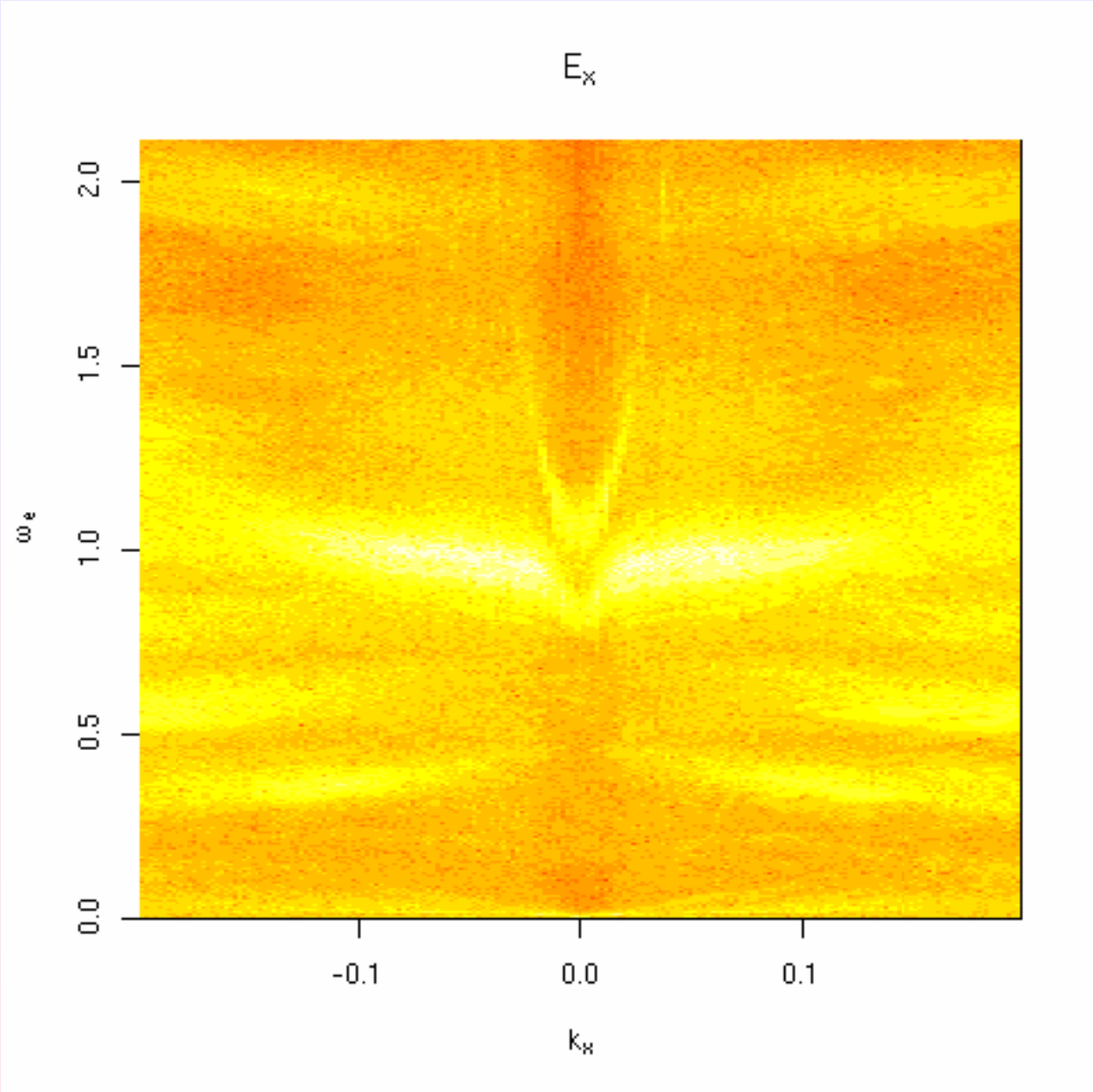
E_x
2.0
1.5
1.0
0.5
0.0
ω_e
-0.1
0.0
0.1
k_x

Nonlinear MHD Structures in Space Plasmas

Erik Nordblad, IRF-U

Linear and nonlinear stationary waves

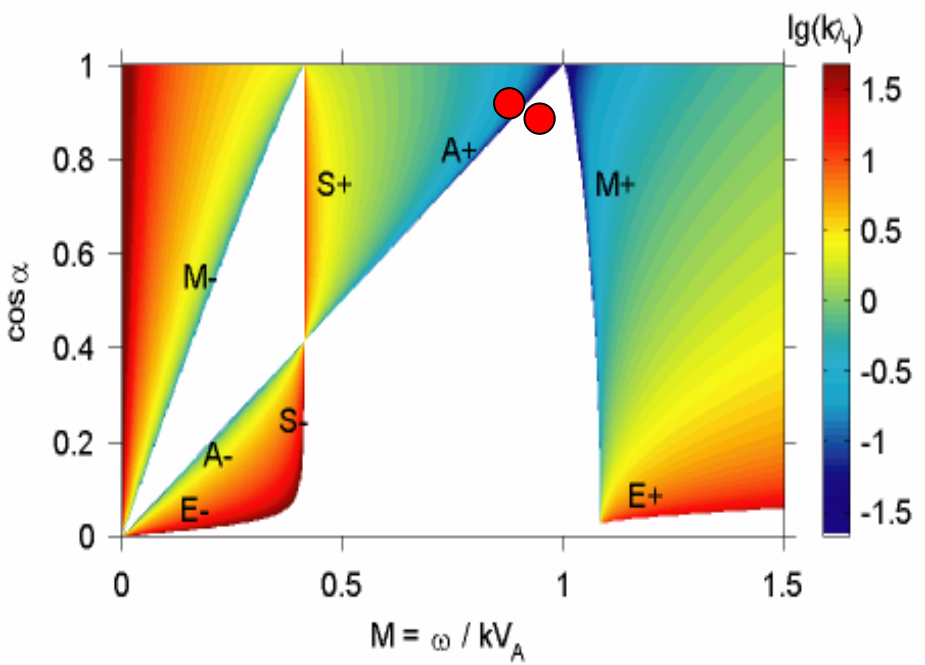

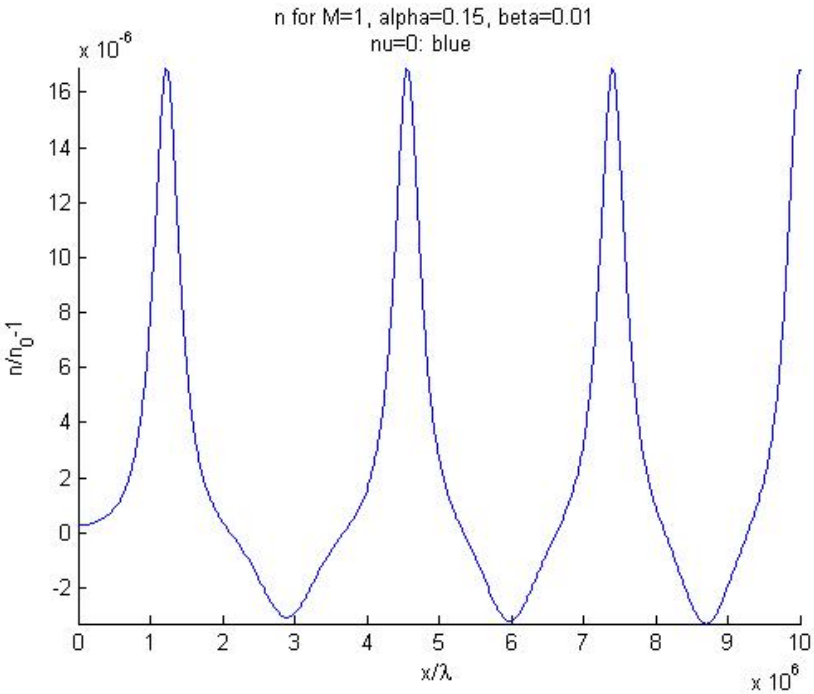

$\alpha =$ propagation angle relative to $\vec{B}$

M = phase velocity in units of v_A

Generalization to nonstationary case

For instance:

- collisions, resistivity $\Longrightarrow$ damping
- non-uniform background $\Longrightarrow$ ”surf waves”

Needed to understand the emergence and evolution of nonlinear structures, e. g. in the solar corona.

Approach:

- numerical solutions of time-dependent fluid equations
- analytical methods: how useful are KdV-like formulations?

Electric fields at electron scales

Mats André

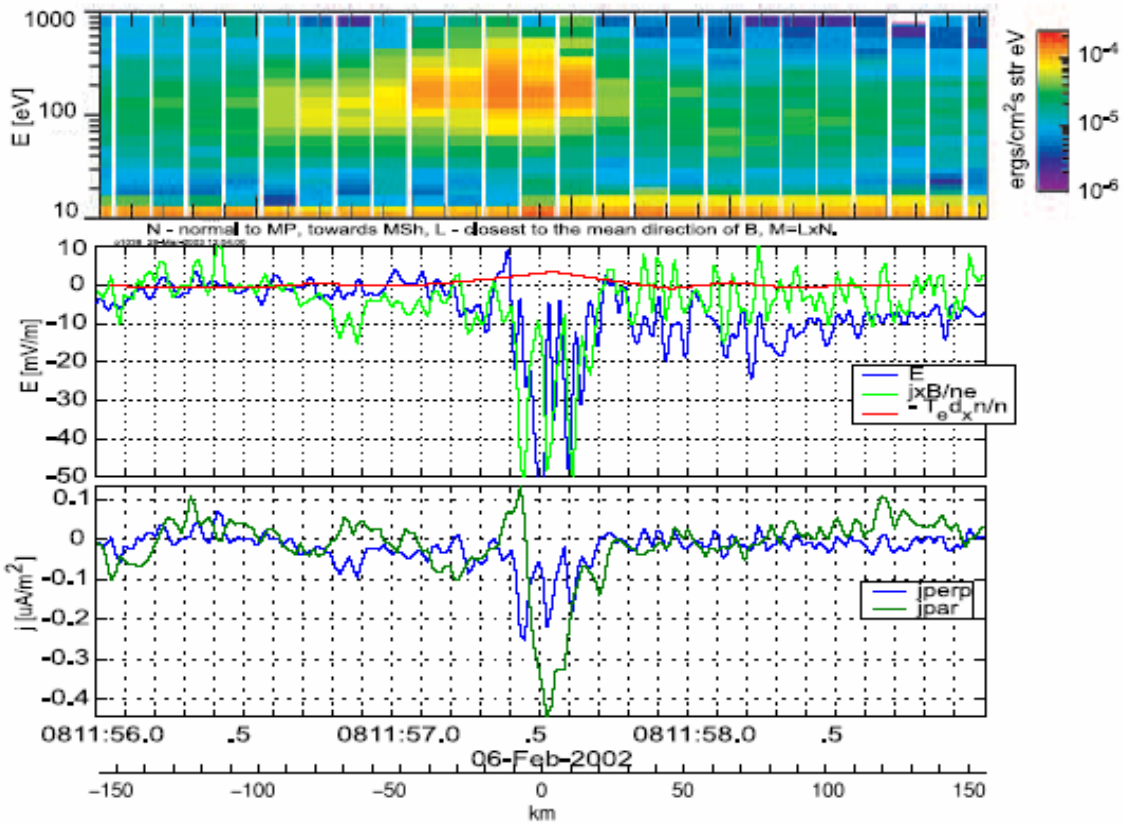

André et al. GRL, 2004

10 c/ω_{pe}

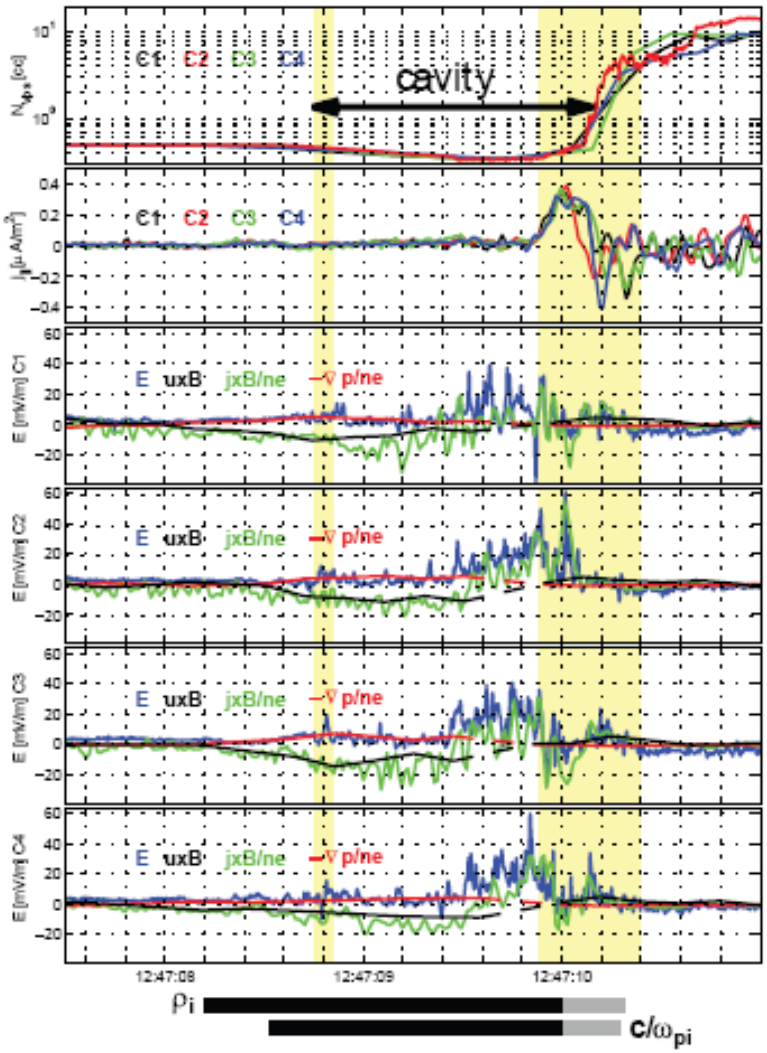

Khotyaintsev et al., PRL, 2006

Electric fields at electron scales in magnetic reconnection regions

- Strong fields down to electron scales
- Importance for start and
  dynamics of reconnection
- Identification: thin sheets, LH; e^- pres. grad. etc.
- Dream event: EFW internal burst, including:
  interferometry (single SC), δn from SC pot. (<100 Hz)

Cluster Chorus Emission in terms of Canonical Electromagnetic Observables

- Canonical EM Observables (CEO)
  - Unique decomposition of EM (**E**,**B**) sixtor matrix in covariant space-time tensors

$$\begin{pmatrix} E_xE_x^* & E_xE_y^* & E_xE_z^* & E_xB_x^* & E_xB_y^* & E_xB_z^* \\ E_yE_x^* & E_yE_y^* & E_yE_z^* & E_yB_x^* & E_yB_y^* & E_yB_z^* \\ E_zE_x^* & E_xE_y^* & E_zE_z^* & E_zB_x^* & E_zB_y^* & E_zB_z^* \\ B_xE_x^* & B_xE_y^* & B_xE_z^* & B_xB_x^* & B_xB_y^* & B_xB_z^* \\ B_yE_x^* & B_yE_y^* & B_yE_z^* & B_yB_x^* & B_yB_y^* & B_yB_z^* \\ B_zE_x^* & B_zE_y^* & B_zE_z^* & B_zB_x^* & B_zB_y^* & B_zB_z^* \end{pmatrix} \Leftrightarrow F^{\alpha\beta}\overline{F}^{\gamma\delta}$$

- CEO in space-time classifications
  - 1+1+9+9+6+10=36 observables

CEO 4-tensor	Rank (Symmetry)	Proper + Pseudo –	Number of Observables
C_+	0	+	1
C_-	0	–	1
T	2(S)	+	9
U	2(S)	–	9
Q	2(A)	–	6
W	4(M)	+	10

- Three CEO are well known,

Lagrangian $C_+ = (\bar{F}_{\alpha\beta} F^{\alpha\beta} - {}^*\bar{F}_{\alpha\beta}\, {}^*F^{\alpha\beta})/2 \rightarrow (|\mathbf{E}|^2 - |\mathbf{B}|^2)/2$

Pseudo Lagrangian $C_- = (\bar{F}_{\alpha\beta} F^{\alpha\beta} + {}^*\bar{F}_{\alpha\beta}\, {}^*F^{\alpha\beta})/2 \rightarrow -\mathrm{Re}\left[\bar{\mathbf{E}} \cdot \mathbf{B}\right]$

Energy Stress Tensor

$$T^{\alpha\beta} = (\bar{F}^{\alpha}_{\mu} F^{\alpha\beta} + {}^*\bar{F}^{\alpha}_{\mu}\, {}^*F^{\alpha\beta})/2 \rightarrow \begin{pmatrix} (|\mathbf{E}|^2 + |\mathbf{B}|^2)/2 & \mathrm{Re}\left[\bar{\mathbf{E}} \times \mathbf{B}\right] \\ \mathrm{Re}\left[\bar{\mathbf{E}} \times \mathbf{B}\right] & T^{00}\mathbf{1}_3 - \mathrm{Re}\left[\bar{\mathbf{E}} \otimes \mathbf{E} + \bar{\mathbf{B}} \otimes \mathbf{B}\right] \end{pmatrix}$$

- Two CEO are less well known,
  - $U^{\alpha\beta}$ is similar to $T^{\alpha\beta}$
    - Contains energy densities that depend on "handedness" (spin, helicity, polarization, chirality)
  - $Q^{\alpha\beta}$ is very different
    - Contains reactive energy densities, such as the imaginary part of the complex Poynting vector
- One CEO is completely new!
  - $W^{\alpha\beta\gamma\delta}$ is a rank 4 tensor
  - Same structure as the Weyl tensor
  - Contains a four-dimensional generalization of Stokes parameters

- CEO as 3-tensors
  - 4×(1+3+5)=36 observables

	Scalars	Vectors	Tensors
(active) total	*u*	**N**	**M**
(active) handed	*h*	**S**	**C**
reactive total	*l*	**R**	**X**
ractive handed	*a*	**O**	**Y**

- 2D version of CEO
  - 4×(1+1+2)=16 observables

Symbol	Detailed Name
u_{2D}	Total energy
N_z	Total energy flux
M_{σ_z}	Total energy stress σ_z component
M_{σ_x}	Total energy stress σ_x component
h_{2D}	Handed energy
S_z	Handed energy flux
C_{σ_z}	Handed energy stress σ_z -component
C_{σ_x}	Handed energy stress σ_x -component
l_{2D}	Vacuum proper-Lagrangian
R_z	Reactive energy flux
X_{σ_z}	EM Stokes parameter Q auto-type
X_{σ_x}	EM Stokes parameter U auto-type
a_{2D}	Vacuum pseudo-Lagrangian
O_z	Reactive handed energy flux
Y_{σ_z}	EM Stokes parameter Q cross-type
Y_{σ_x}	EM Stokes parameter U cross-type

- Cluster Chorus Emission
  - STAFF-SA data
    - Auto/cross correlations of **E** and **B** fields
  - Cluster lacks third **E** component
    - 2D 16 parameter version of the CEO
    - Reprocessing of high-band part of an event discussed by Parrot *et al* (2003)

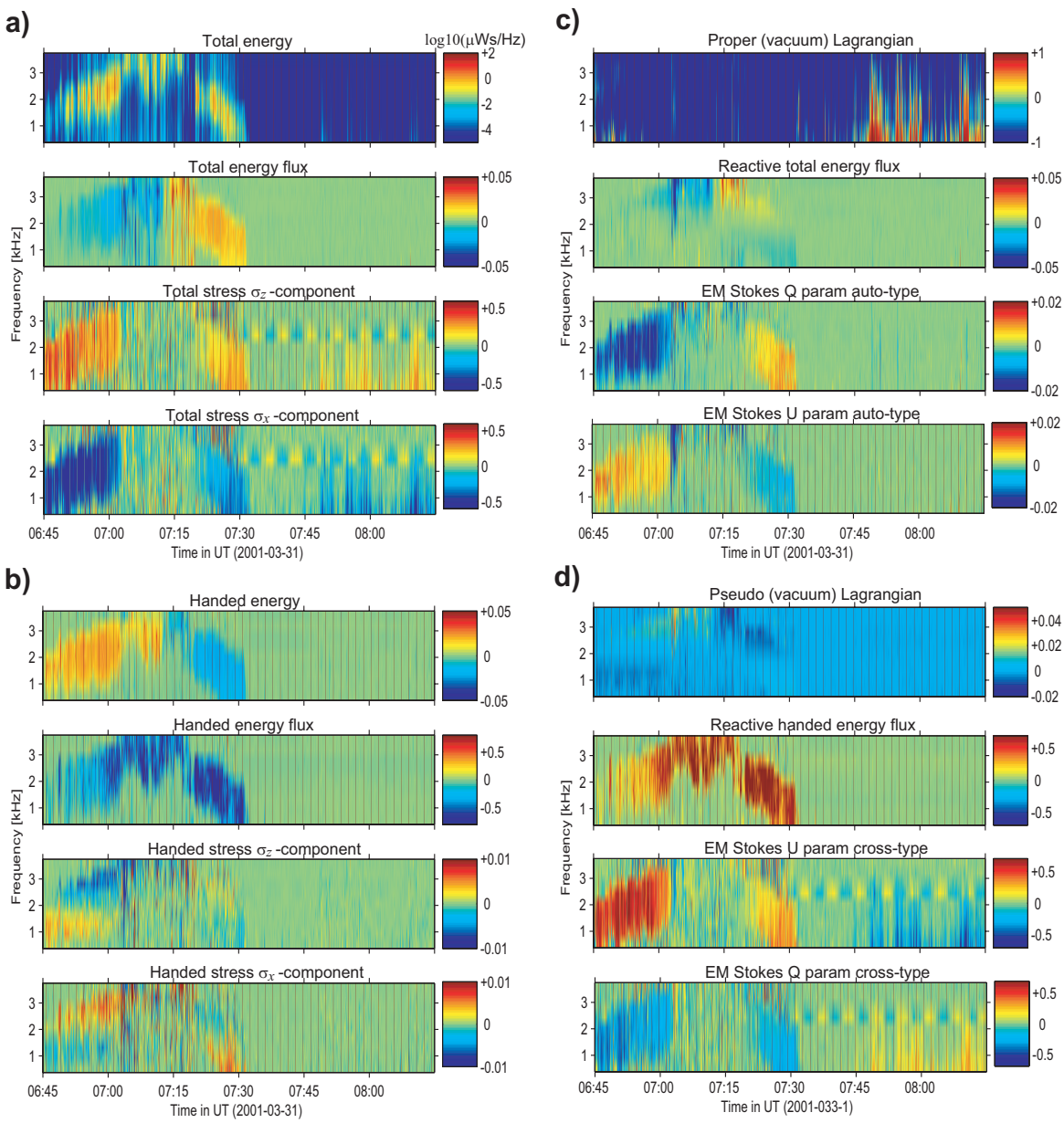

The characteristics of thin current sheets

G. Stenberg & E. Yordanova

The spacecraft orbit

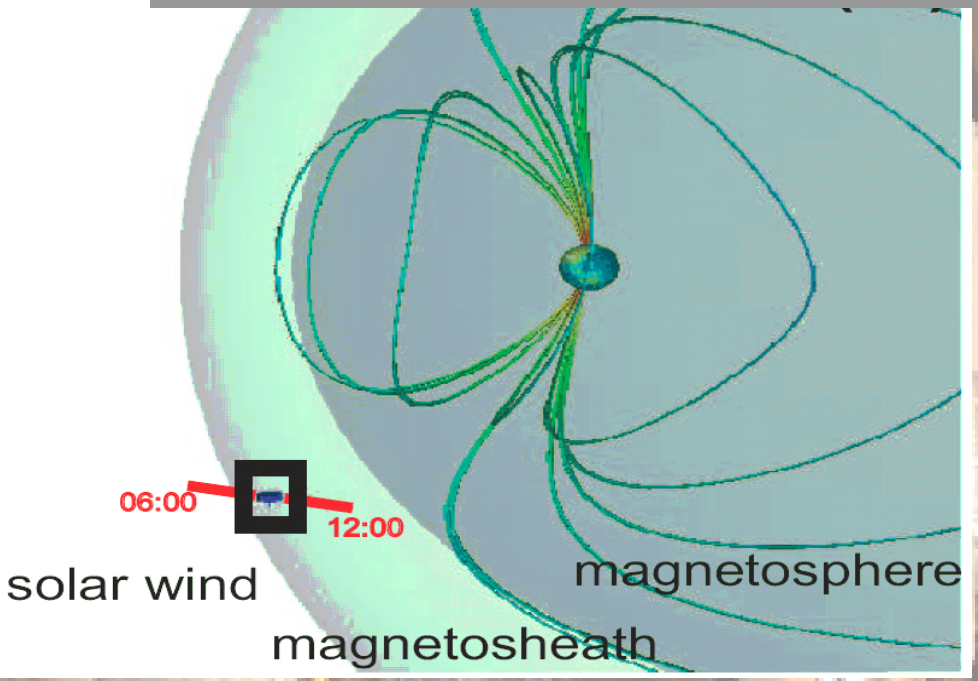

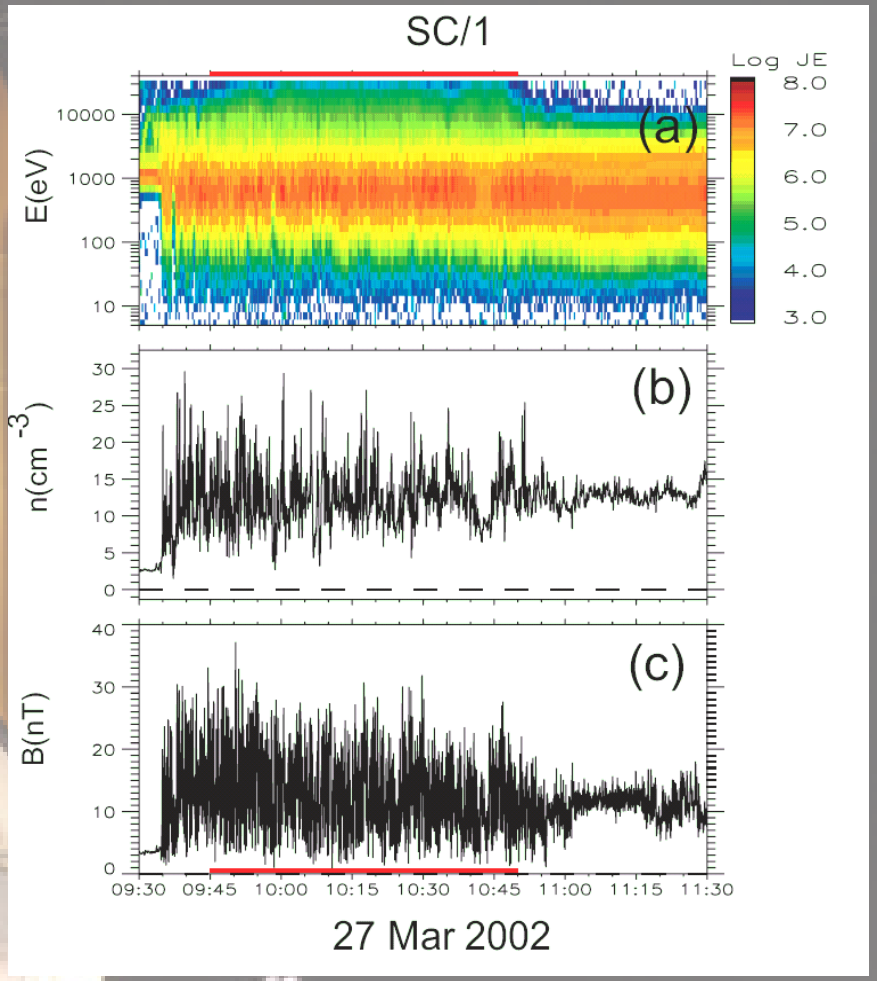

Pictures are from Retinò et al., submitted to Nature Physics, 2006.
Retinò and his colleagues show that reconnection takes place in turbulent plasmas.

(a) Ion energy flux
(b) Ion density
(c) Total magnetic field

The red bars indicate the time interval where current sheets as well as heated and accelerated ions are observed.

The time series approach

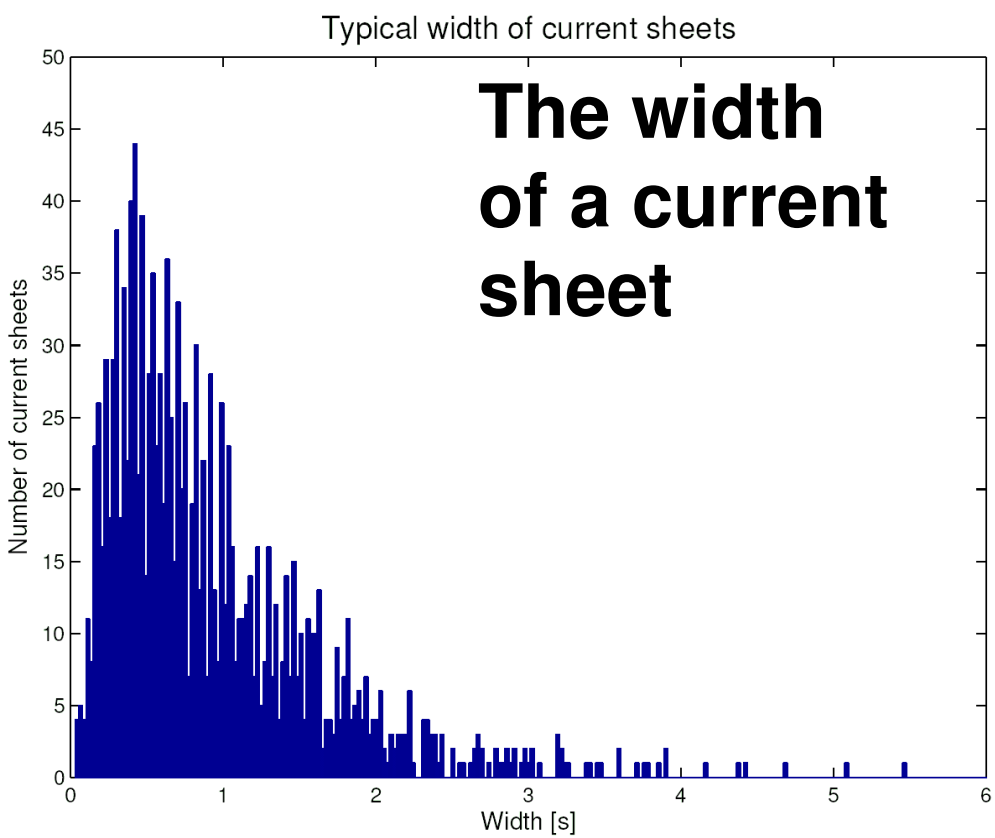

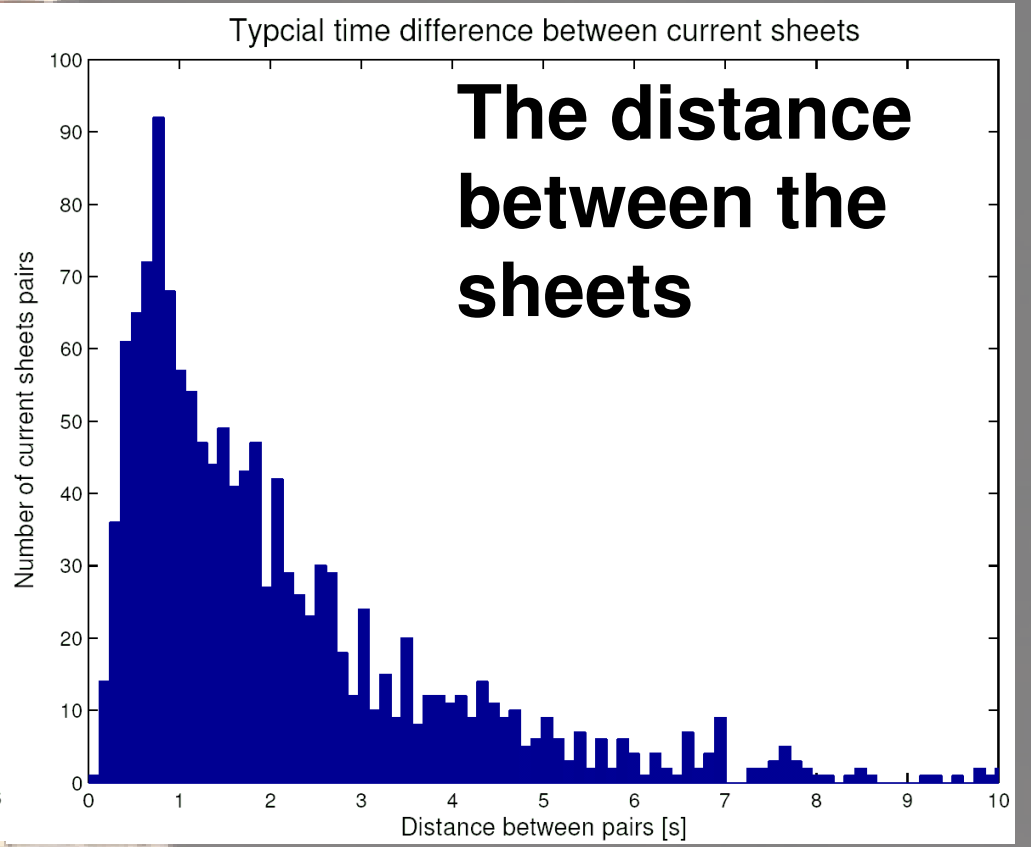

Conclusions

Flow velocity of 200 km/s gives...

The typcial width of a current sheet: 100 km (an ion gyro radius)

The typcial distance between current sheets: 100-200 km.

The turbulence approach

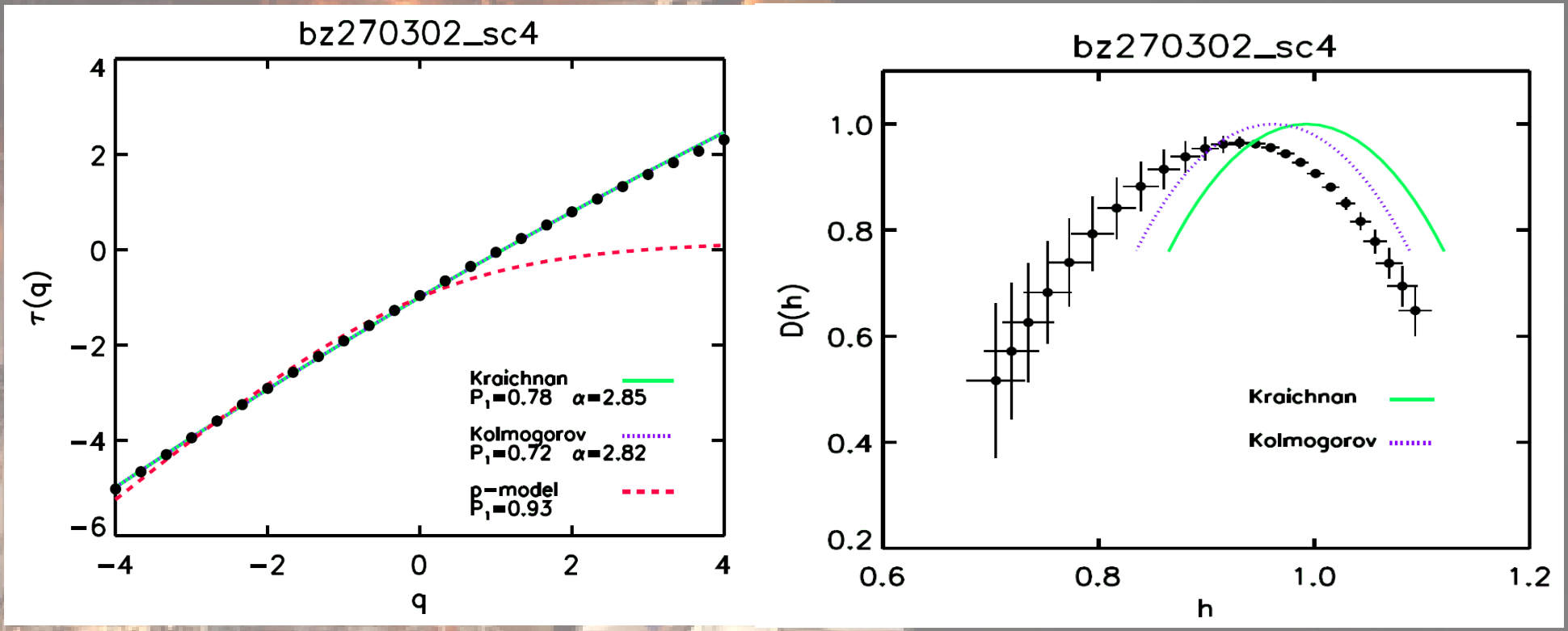

Conclusions

τ(q) has a non-linear behavior. Hence, the observed tubulence is intermittent.

The extended Kolmogorov model resemble the observed turbulence better than the Kraichnan model. This suggests that the turbulence is dominated by flow eddies.

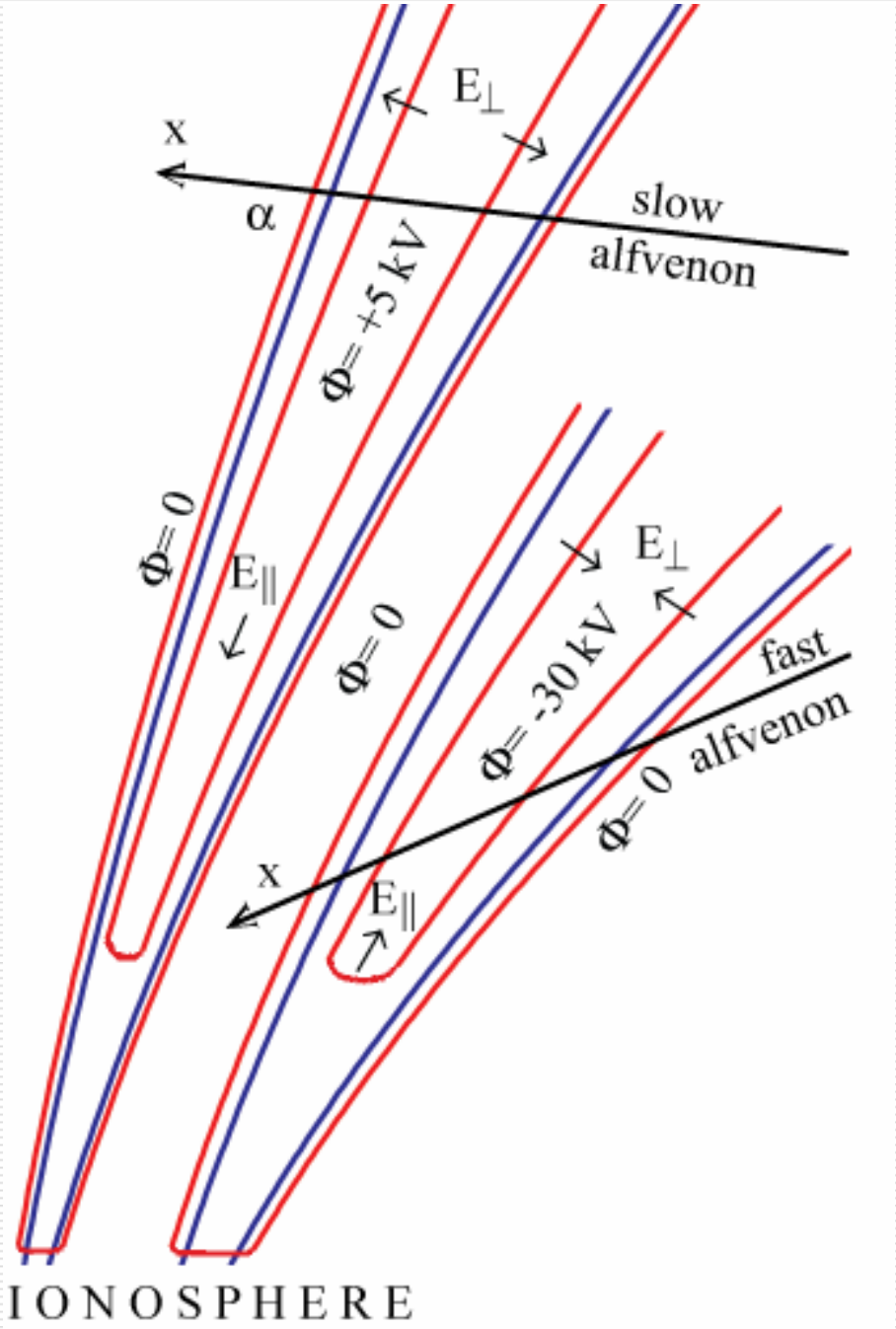

Auroral acceleration structures

Divergent electric fields

Convergent electric fields

Popular knowledge on MHD waves

Dispersion relations for:
1. Alfven, 2. slow 3. fast magnetosonic

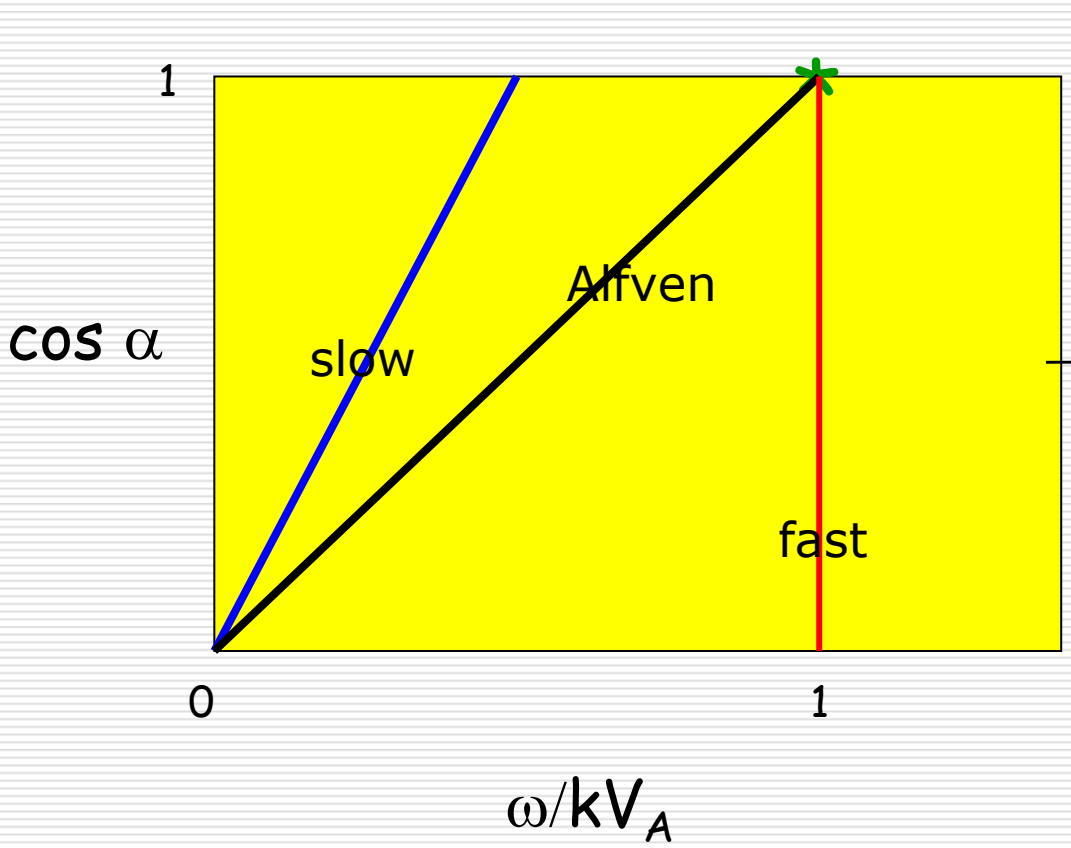

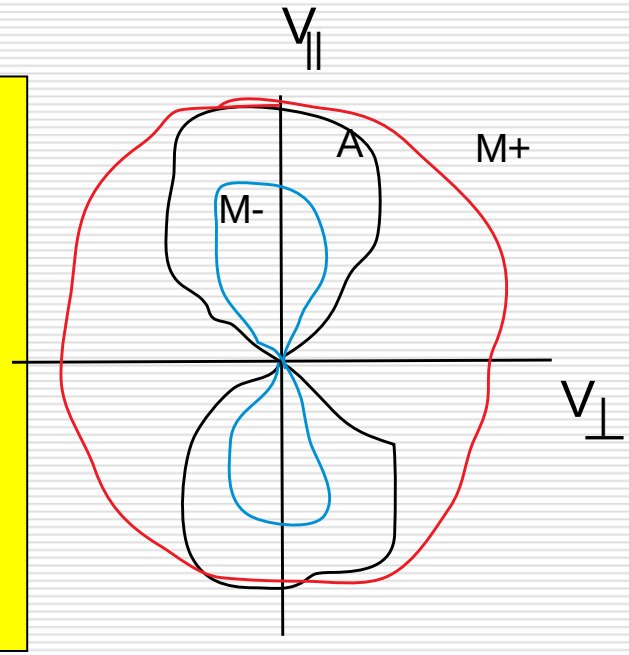

Correct dispersion for linear modes ~ sin(kx): β=0.2 including ion & electron inertia, finite β

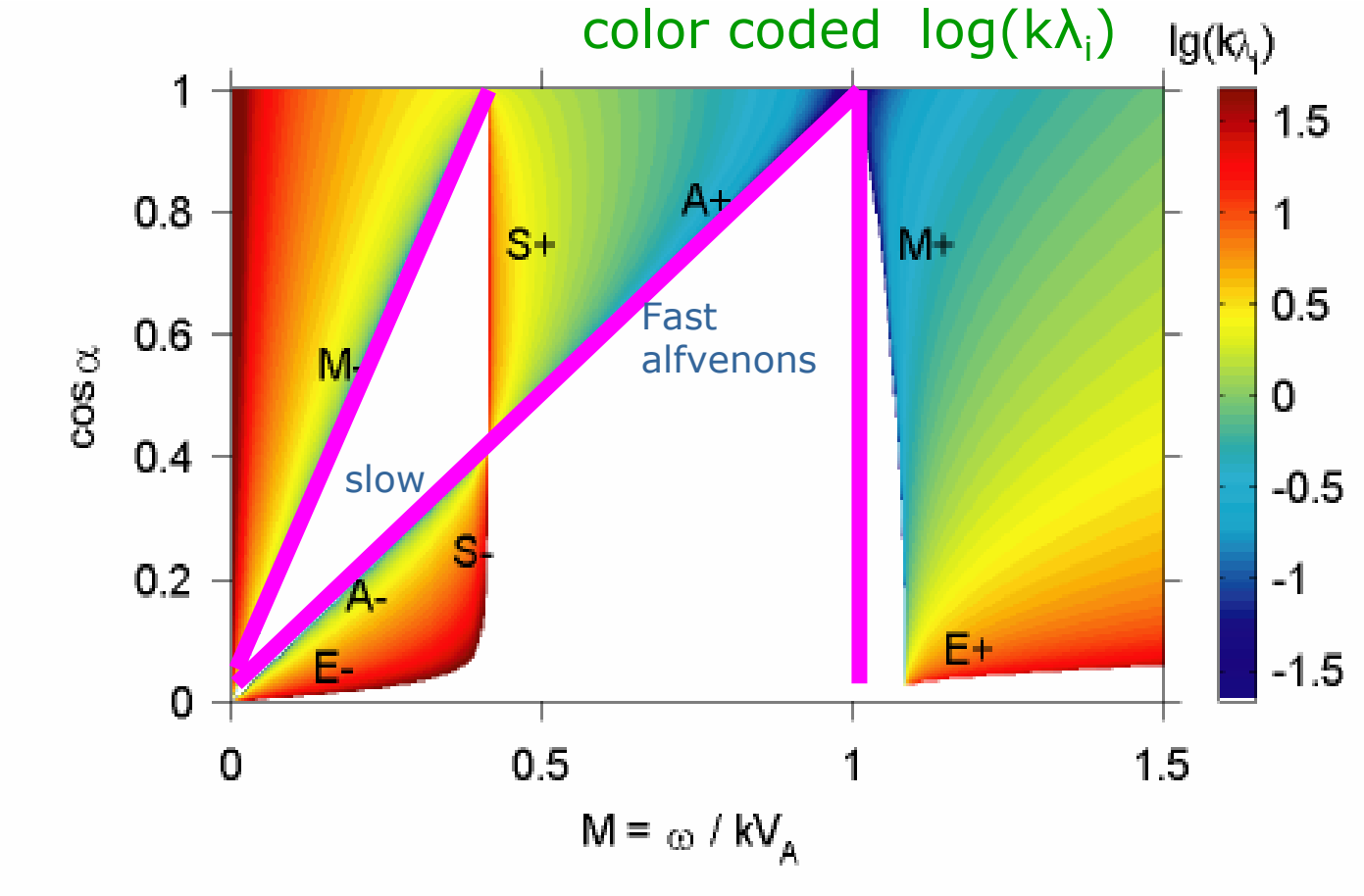

Alfvén speed profile in the magnetosphere

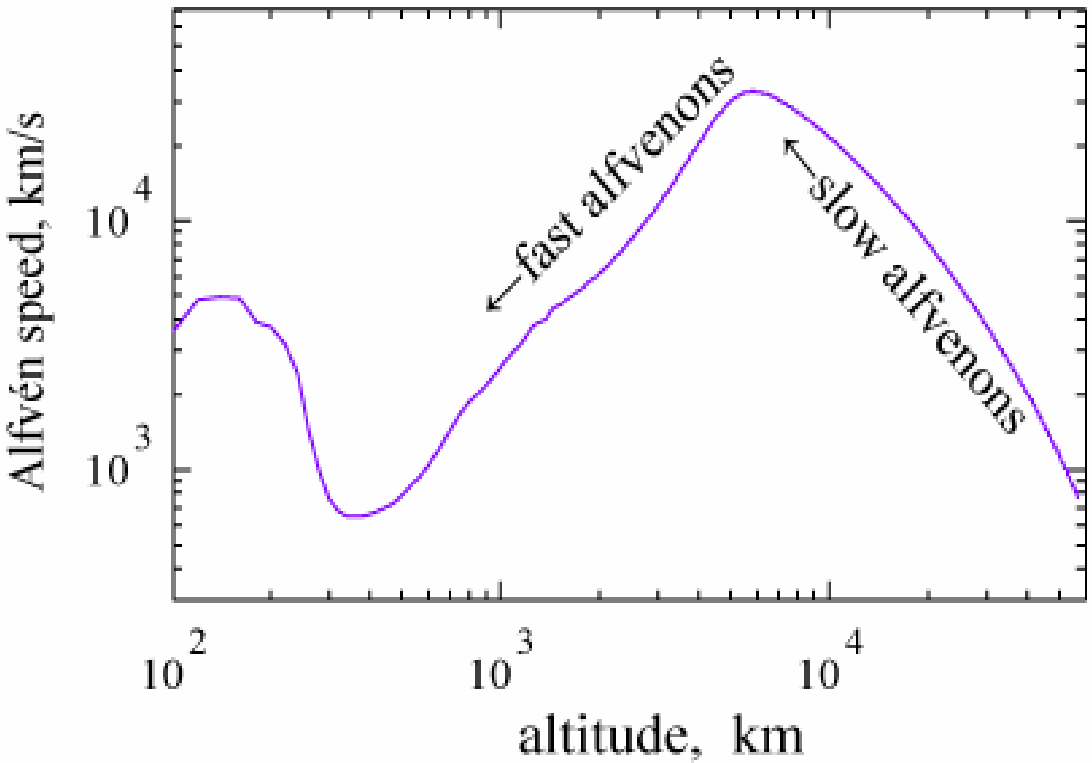

Perturbation from the magnetotail

Nonlinear surf in shallow water

Vaivads et al.,

The source of whistlers at the dayside magnetopause

submitted to GRL

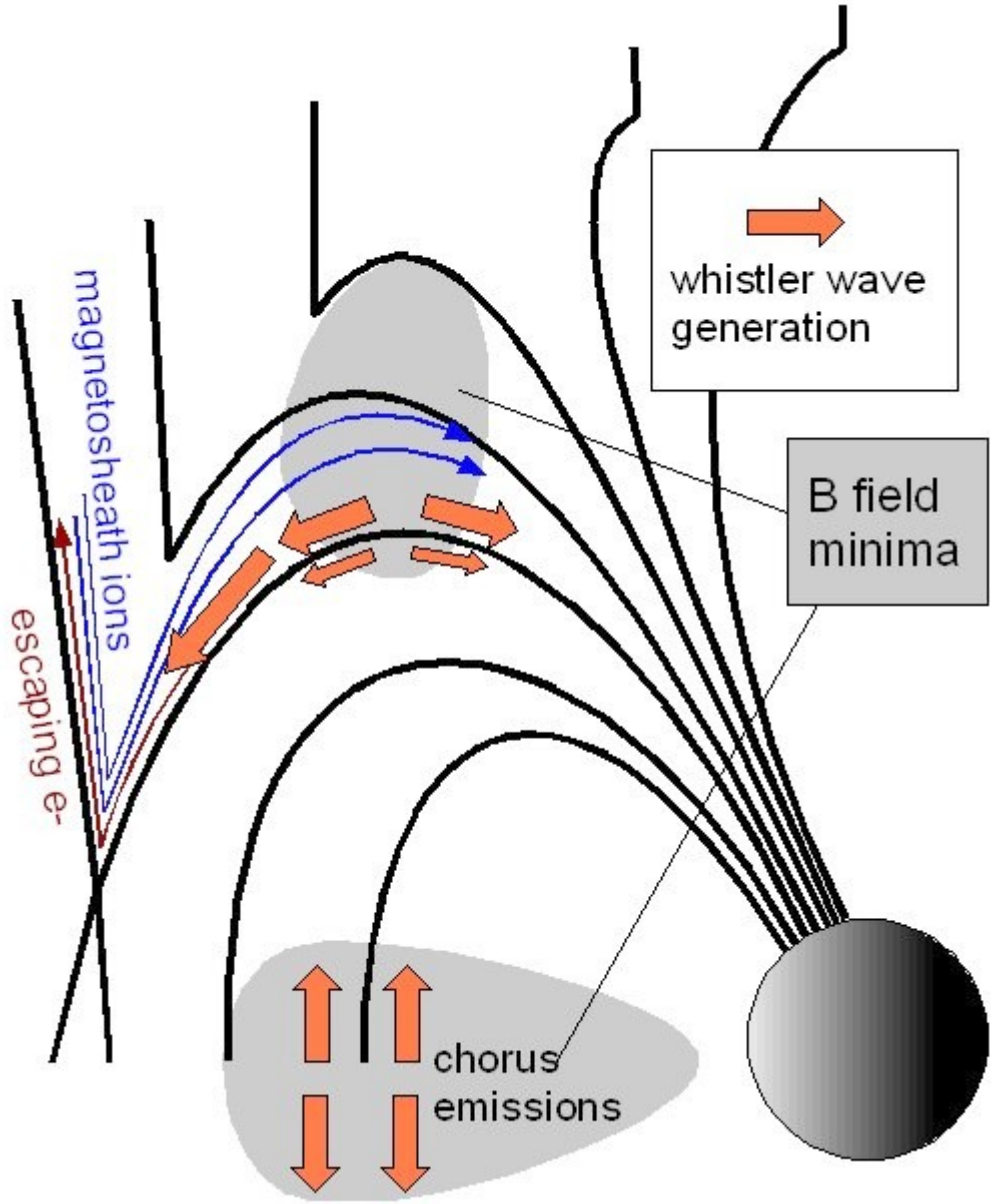

- ✔ |B| minima at high latitudes
- ✔ Whistlers on MP side
- ✔ Poynting flux away from minima
- ✔ Maximum wave amplitude at first open field lines
- ✔ Results consistent with earlier statistical studies of chorus emissions
- ✔ Whistlers can be used to remotely analyze dynamics of reconnection site

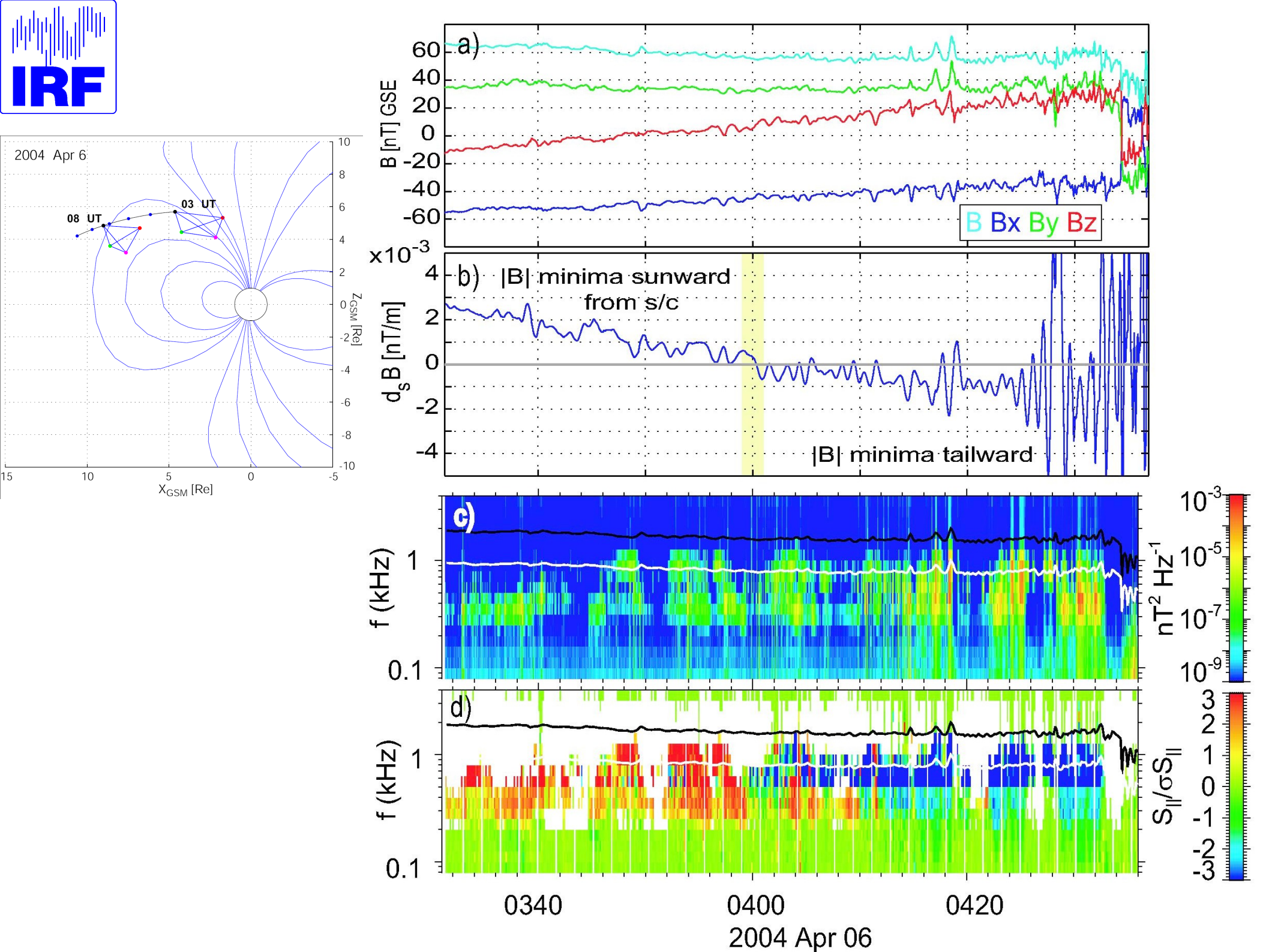
IRF
2004 Apr 6
08 UT
03 UT
X_{GSM} [Re]
Z_{GSM} [Re]
a)
B [nT] GSE
B Bx By Bz
b) |B| minima sunward from s/c
|B| minima tailward
$d_s B$ [nT/m]
x10^{-3}
c)
d)
f (kHz)
nT^2 Hz^{-1}
$S_{||}/\sigma S_{||}$
0340
0400
0420
2004 Apr 06

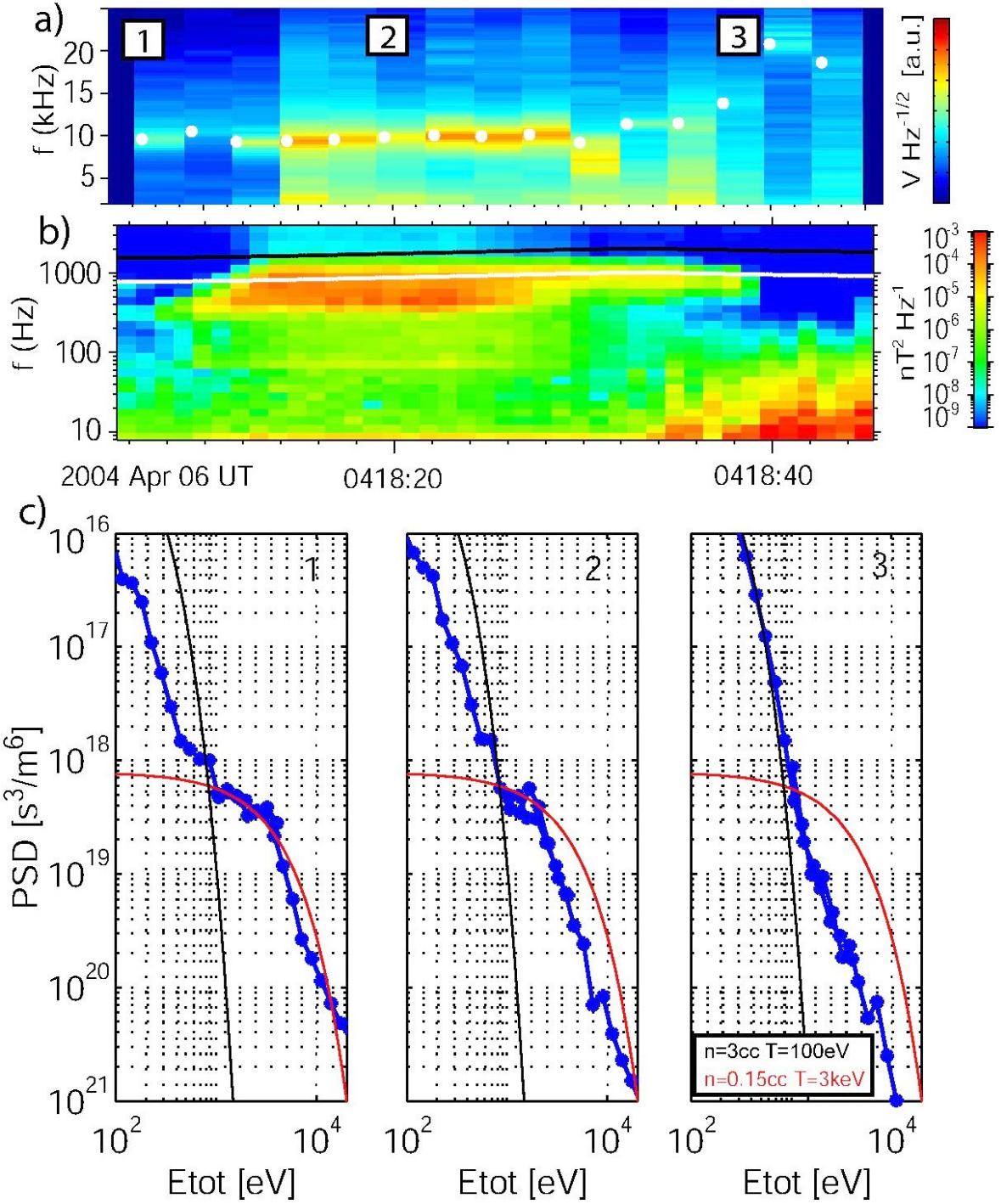
a)
1
2
3
f (kHz)
20
15
10
5
V Hz$^{-1/2}$ [a.u.]
b)
f (Hz)
1000
100
10
nT^2 Hz^{-1}
10^{-3}
10^{-4}
10^{-5}
10^{-6}
10^{-7}
10^{-8}
10^{-9}
2004 Apr 06 UT
0418:20
0418:40
c)
PSD [s^3/m^6]
10^{16}
10^{17}
10^{18}
10^{19}
10^{20}
10^{21}
1
2
3
10^2
10^4
Etot [eV]
n=3cc T=100eV
n=0.15cc T=3keV

Dust-plasma interaction near the E-ring

J-E. Wahlund et al.

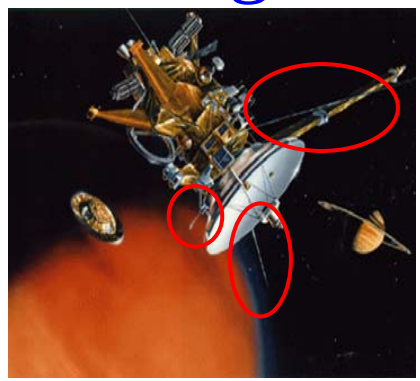

Saturnus radie
60 000 km

nordpol

rotationsriktning

Saturnus

Plasmat närmast Saturnus växelverkar elektriskt med det negativt laddade stoftet i E-ringen. I detta område närmar sig plasmats hastighet den hos Saturnus månar och ringens stoft.

De flesta forskare trodde att plasmats hastighet i stället skulle minska linjärt hela vägen in.

Ytterst har plasmat samma omloppstid som Saturnus och dess magnetfält.

km/s

Magnetfältstyrd hastighet

Gravitationsstyrd hastighet

Plasmats hastighet

100

50

0

A-ringen

B-ringen

D-ringen

F-ringen

C-ringen

(Ringarna är namngivna i den ordning de upptäcktes)

Magnetfält

Janus

Mimas

Enceladus

Tethys

Dione

Rhea

Plasma

Vattengruppjoner

(H_3O^+, H^+ och e^-)

E-ringen

Består av negativt laddat stoft och ispartiklar på en tusendels millimeter.

KARL ÅSTRAND UNT GRAFIK

E- vs E+ phase

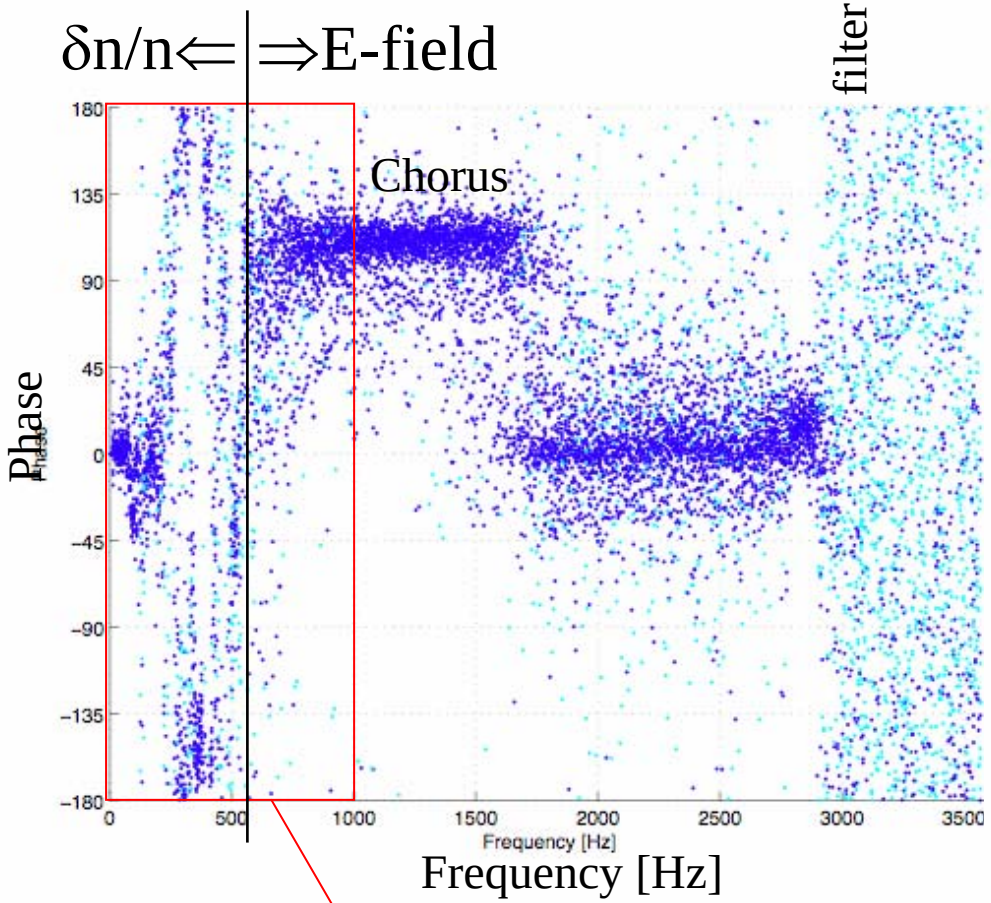

- 512 fft, 32 averages
- All 13 such averages

- 2 δn/n-signature slopes!
  - 42-55 km/s (θ_{sd}= 0 assumed)
    - Co-rot: 46-48 km/s
    - CAPS happy!
  - 12-14 km/s (θ_{sd}= 0 assumed)
    - Keplerian: 11.5 km/s
    - LP happy!

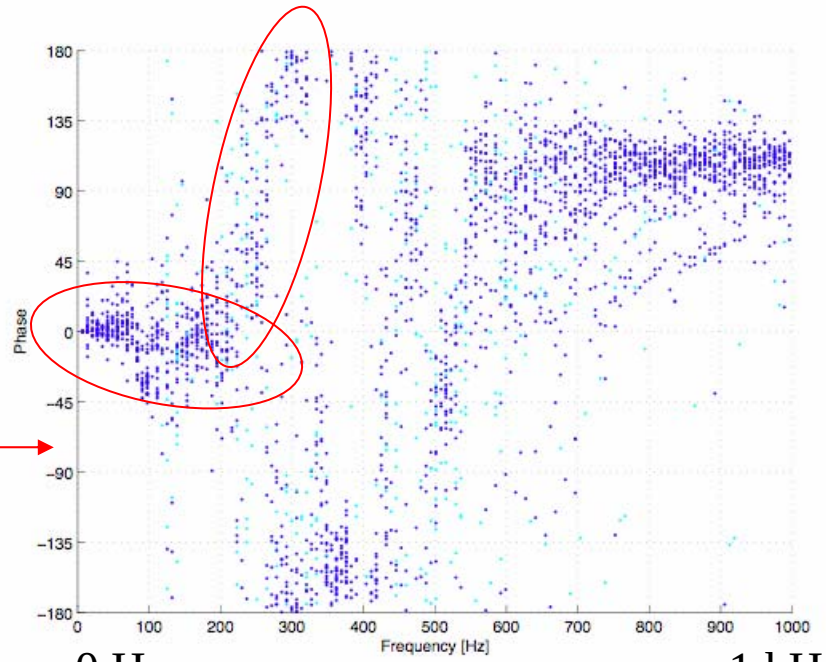

- Long antenna measurements
  - depend on 1/RC coupling to plasma
    ⇒ δn/n below 500 Hz

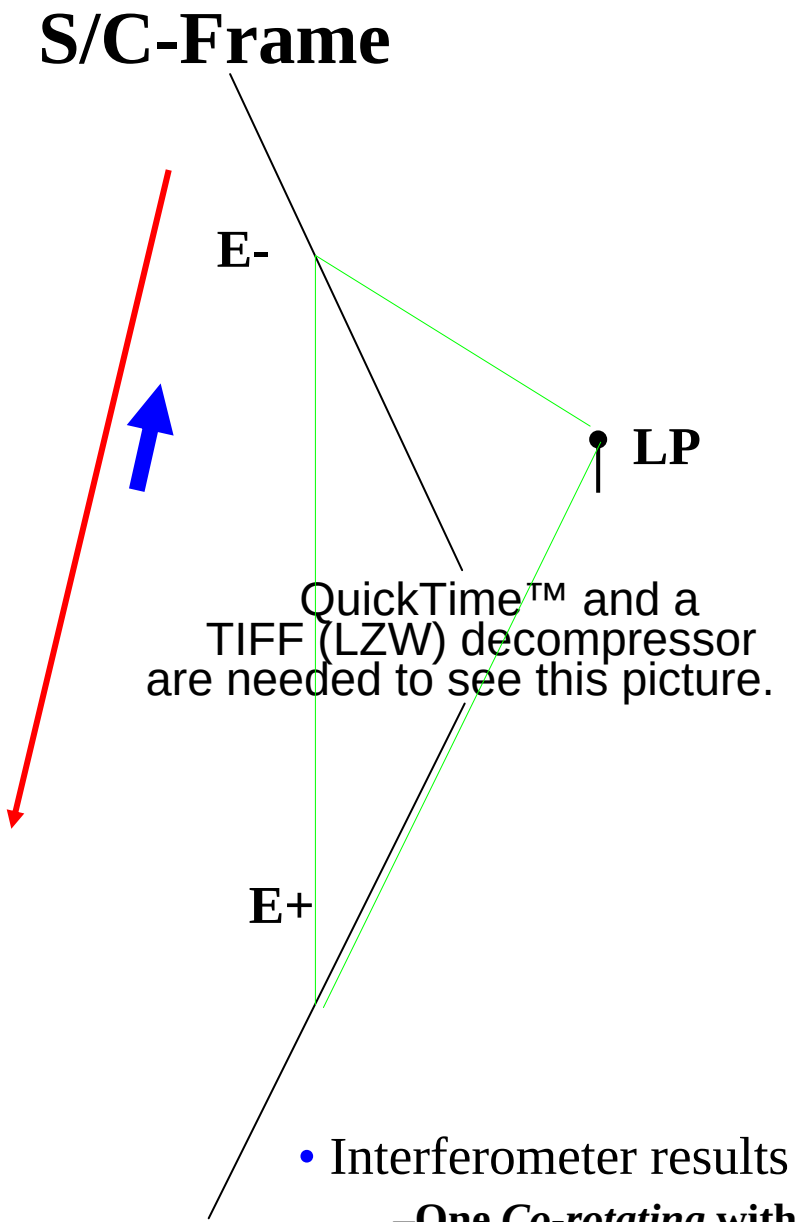

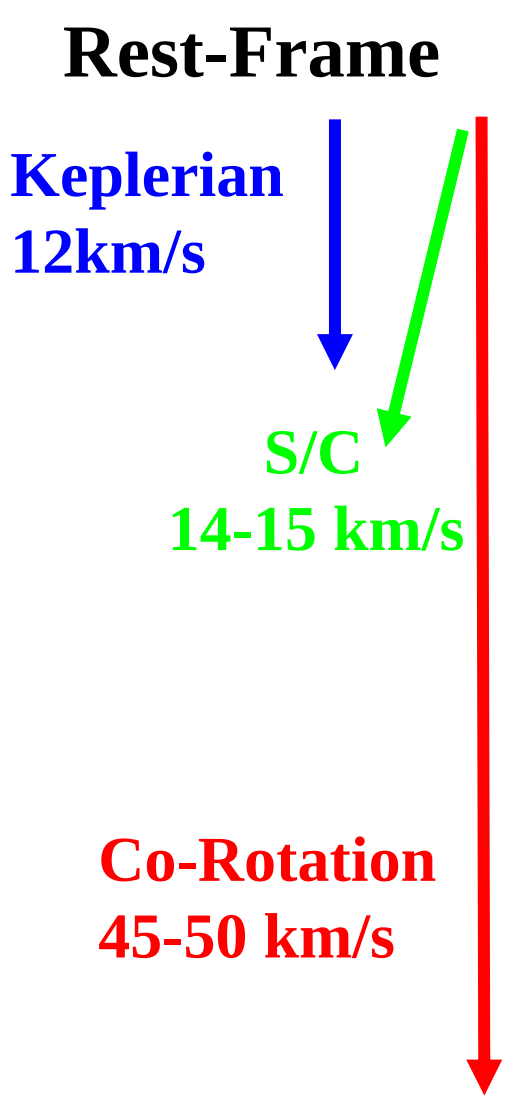

- Interferometer results suggests that two ion populations exist
  - **One *Co-rotating* with magnetic field (45-50 km/s)**
  - **One rotating with close to *Keplerian* speed (11-14 km/s)**

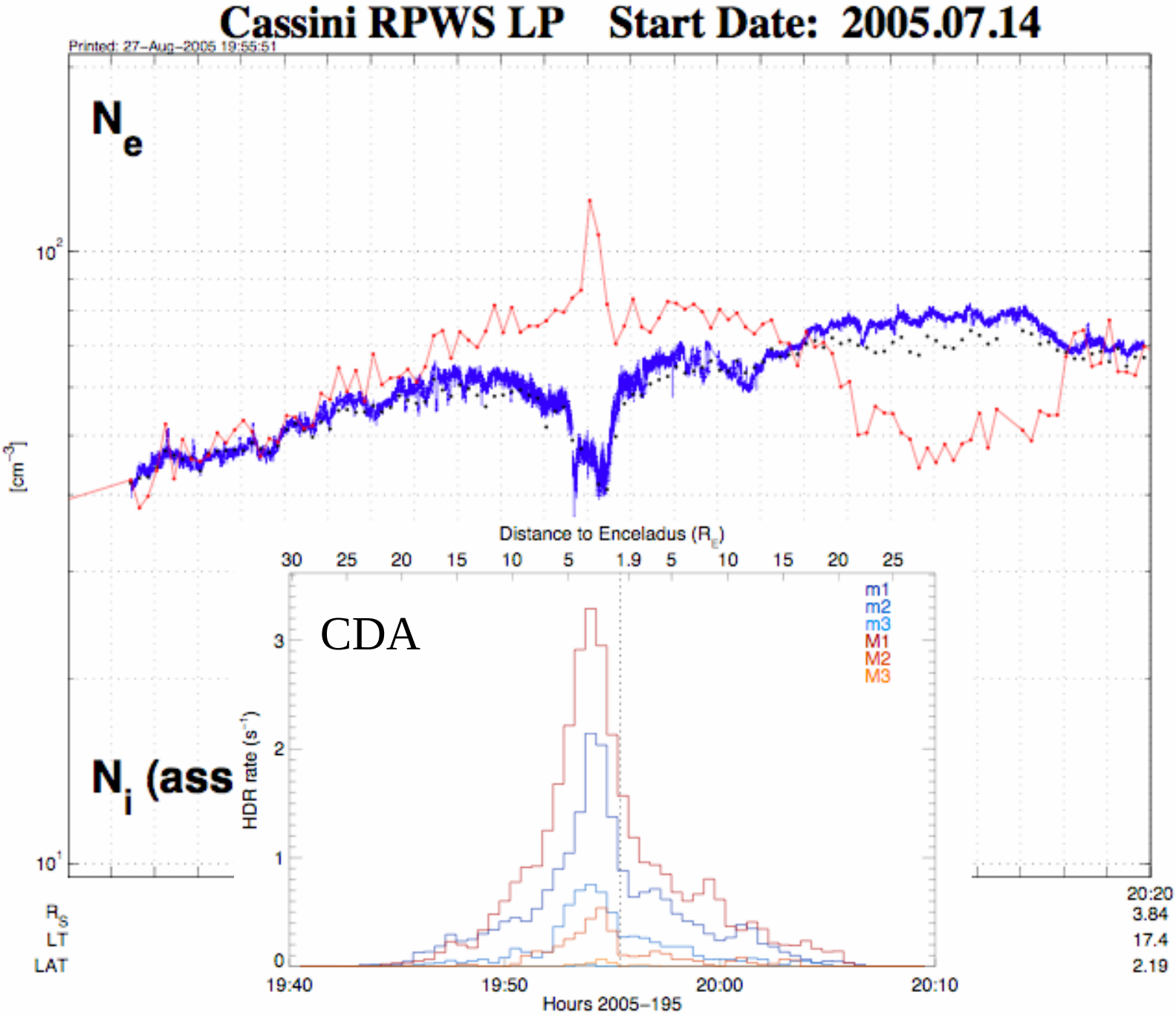
Cassini RPWS LP Start Date: 2005.07.14
Printed: 27-Aug-2005 19:55:51
N e
10 2
[cm -3]
Distance to Enceladus (R E)
30 25 20 15 10 5 1.9 5 10 15 20 25
CDA
m1
m2
m3
M1
M2
M3
N i (ass
HDR rate (s -1)
3
2
1
0
10 1
19:40
19:50
20:00
20:10
Hours 2005-195
20:20
R S
3.84
LT
17.4
LAT
2.19

Dust-Plasma Coupling?

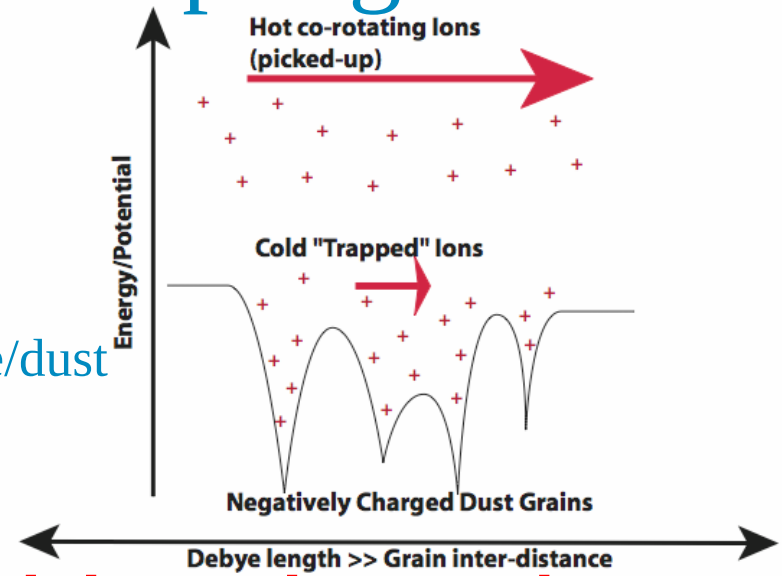

- Dust Charge from U_{sc} : -2 to -5 V
  - q_d ~ 700 e/Volt ⇒ 2000-4000 e/dust
  - CDA, q_d ~ 0.5 - 5 fC = 3000 - 30000 e/dust
    - [*Kempf et al.*, PSS, 2006]
- Cold ions (T_i < 5 eV) will be trapped close to dust particles
  - CDA & RPWS detects 0.1 m^{-3} for r_d > 2 μm ($r_d^{-2.8}$ distribution)
  - n_d ~ 20 m^{-3}, 0.7 μm dust etc, expect several hundred dust-particles within λ_D
  - $r_d << d << \lambda_D$ within most of E-ring
    - Charged dust participate in screening & collective dynamics of ensemble
    - In dust-plasma physics: "A true dusty plasma"
  - Havnes parameter [Havnes et al., 1987; Horanyi et al., 2004]

$$P = \frac{4\pi\varepsilon_0 a}{e^2}\left(\frac{Q_d n_d}{n_e}\right) T_p[eV] \approx 10-100$$

Relative importance of low & high latitude transpolar potential dynamos

---

Aim: To determine how much of the cross polar potential drop is driven by low latitude (closed field-line) dynamos such as viscous interaction and impulsive penetration, relative to magnetic reconnection at high latitudes.

DMSP F13
Altitude: 850 km
Orbit: 05.45 – 17.45 LT

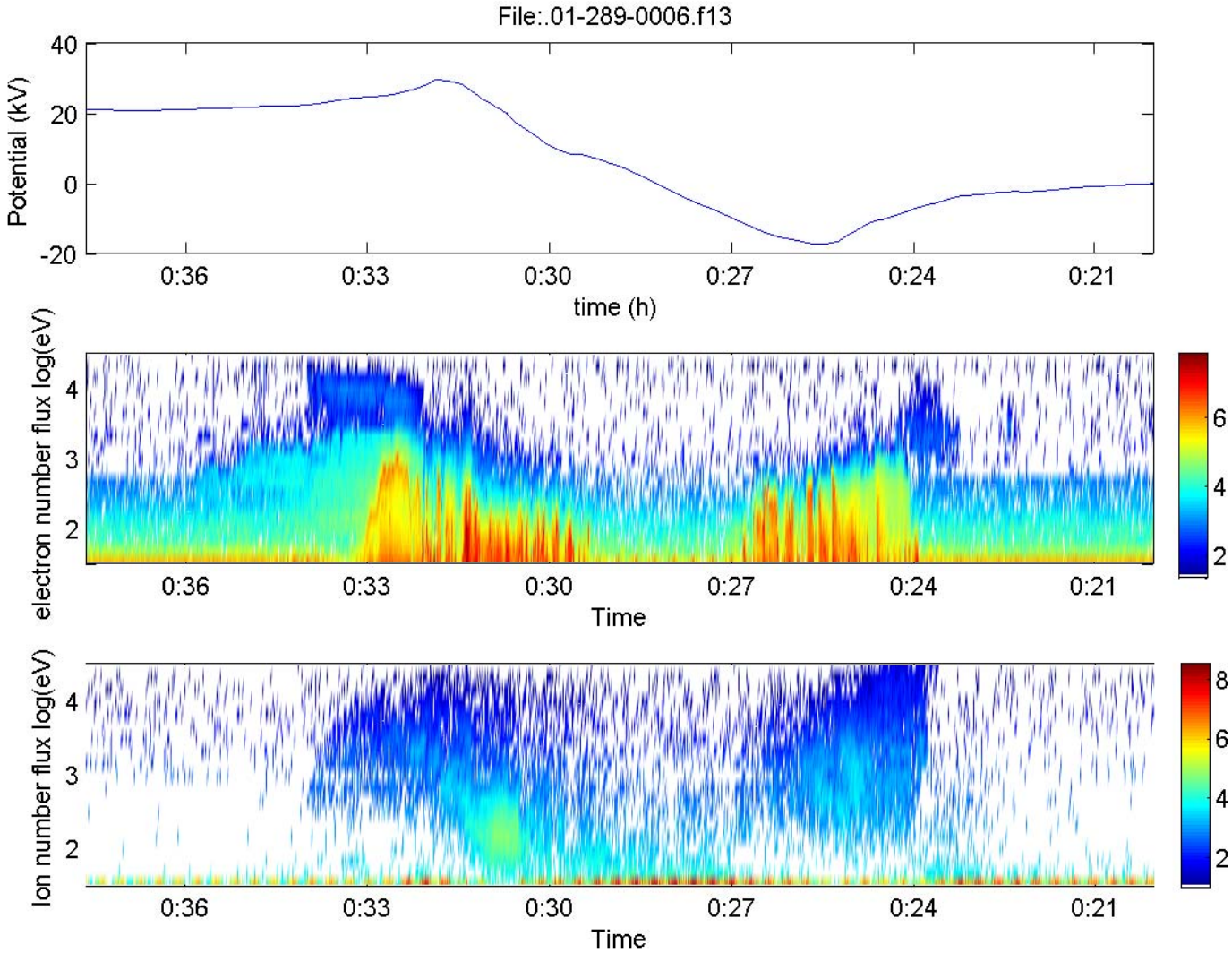
File:.01-289-0006.f13
Potential (kV)
40
20
0
-20
0:36
0:33
0:30
0:27
0:24
0:21
time (h)
electron number flux log(eV)
4
3
2
Time
6
4
2
ion number flux log(eV)
4
3
2
Time
8
6
4
2

Recent Cluster auroral research

Göran Marklund

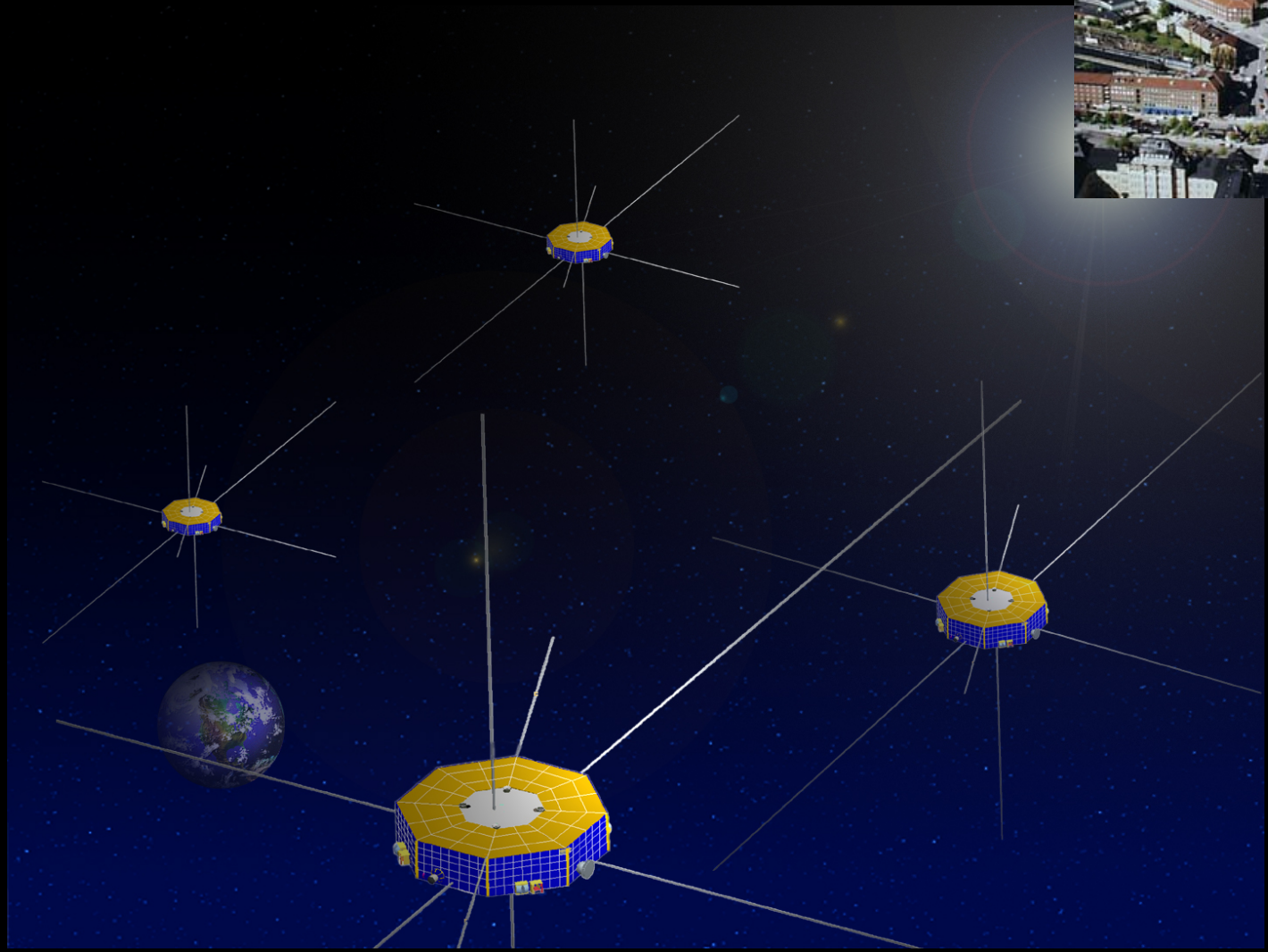

1. U-potential evolution in adjacent up- & downward FAC regions

Marklund et al, 2006

14 FEB 2001 EVENT SUMMARY

- Bipolar, diverging E-field of 1.7 V/m
- Located at PSBL / CPS boundary
- Scale size of 8 km
- $\Delta\Phi_{\perp}$, grows from 0.4 to 2.7 kV in 100 s
- $\Delta\Phi_{//}$ in $j_{||}^{up} \approx -\Delta\Phi_{\perp}$ in $j_{||}^{down}$
- Local density min, E-region density hole
- Downward FAC ≈ 10 μA/m^2

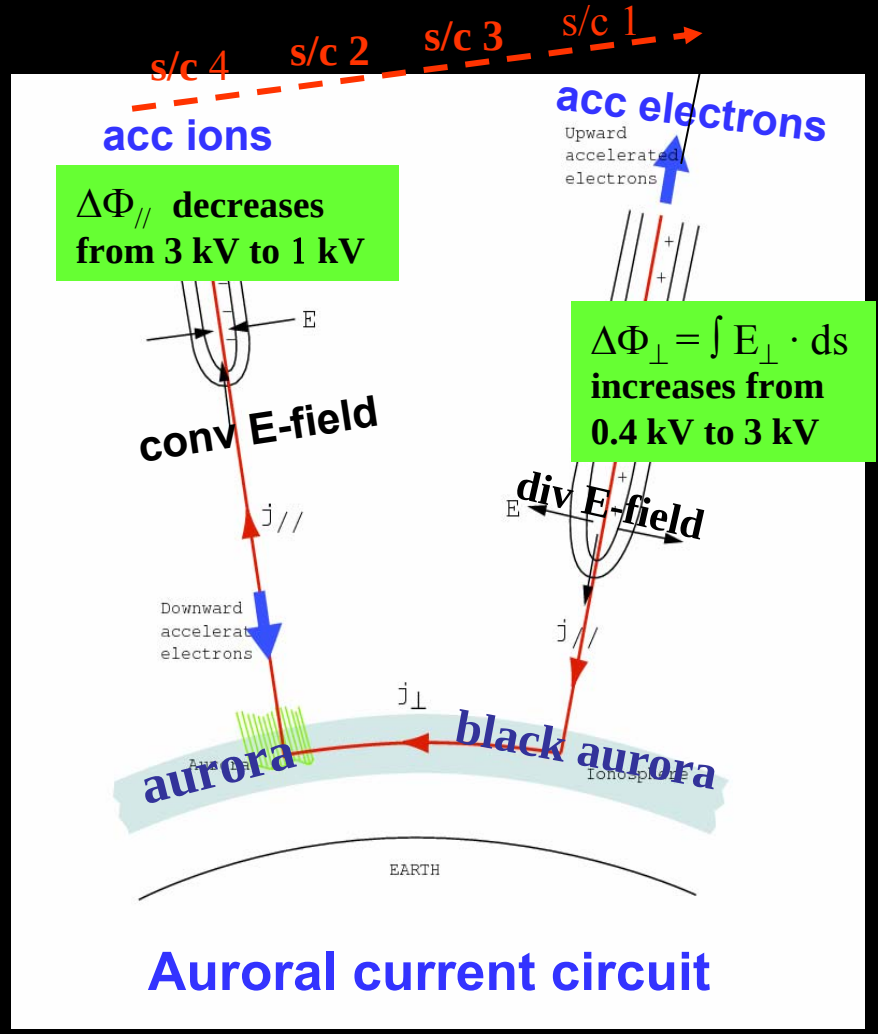

2. Auroral potential & FAC reconfiguration

Marklund et al, JGR 2007

Cluster s/c 1 t= t_0

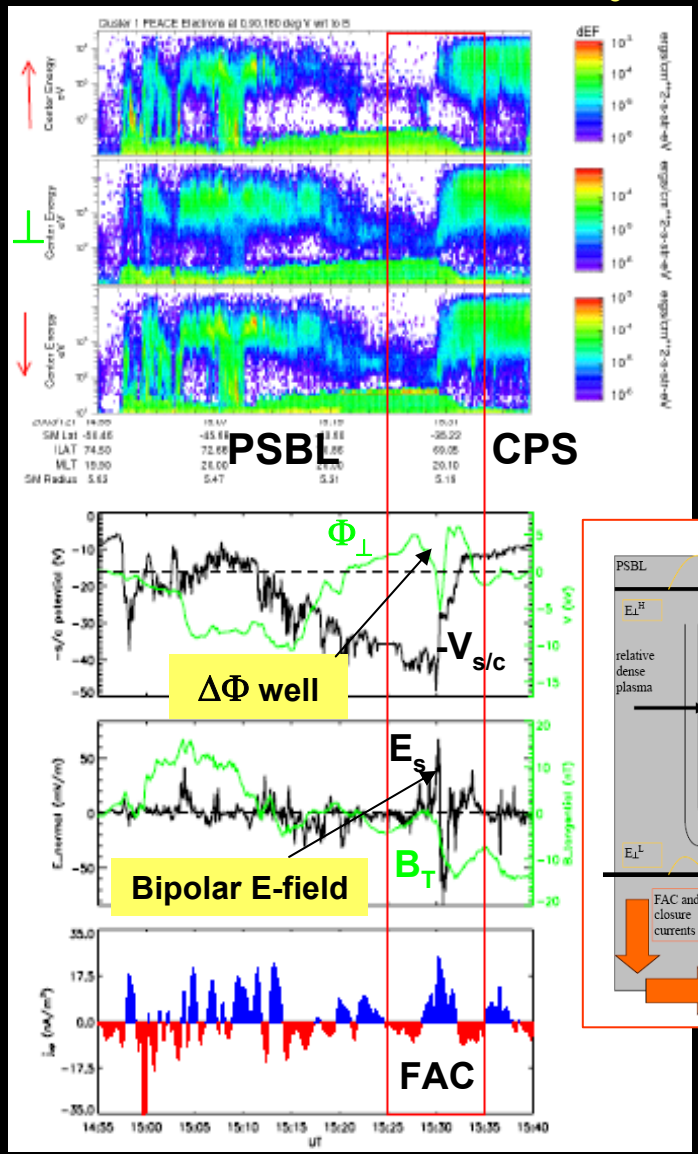

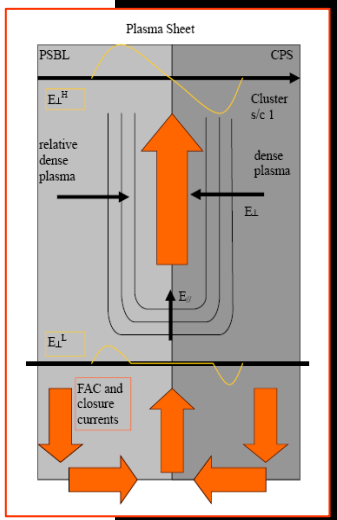

Cluster s/c 2 t = t_0 + 16 min

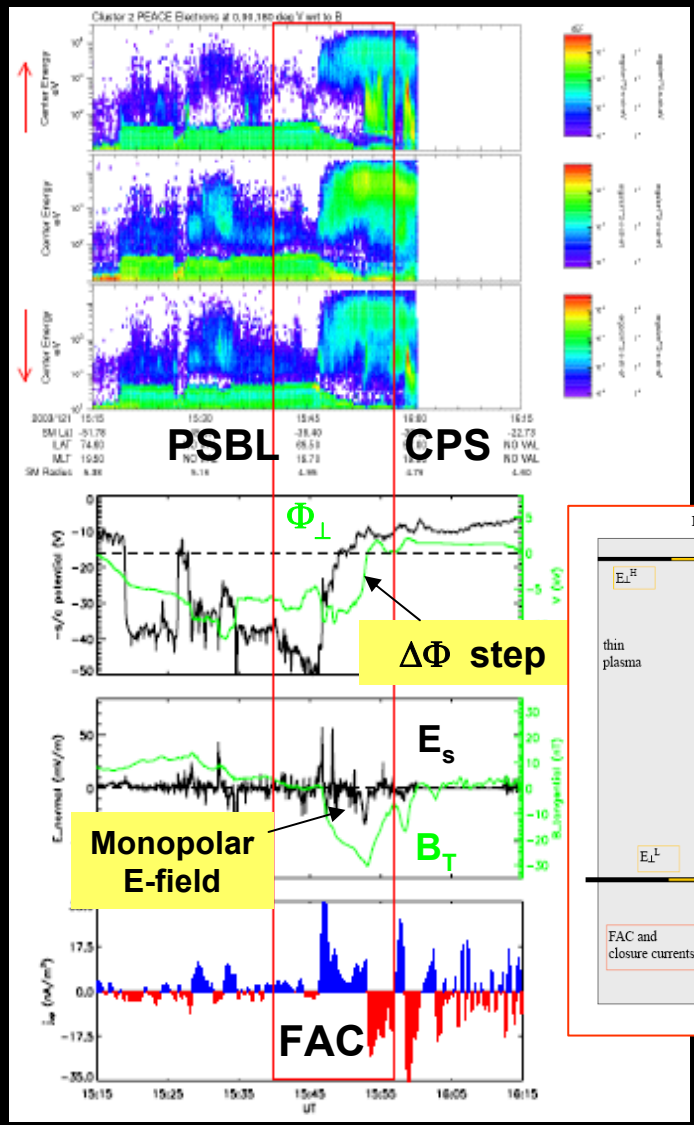

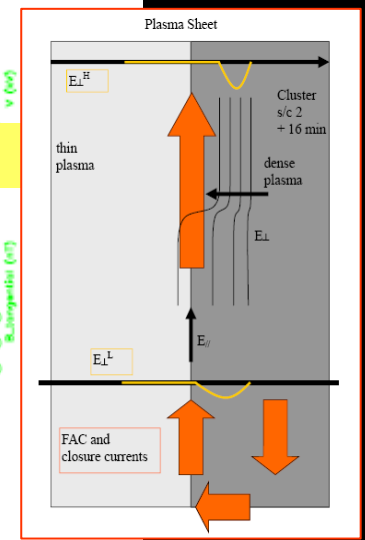

3. Simulation of Cluster 2001-01-14 event

Streltsov and Marklund, JGR, 2006

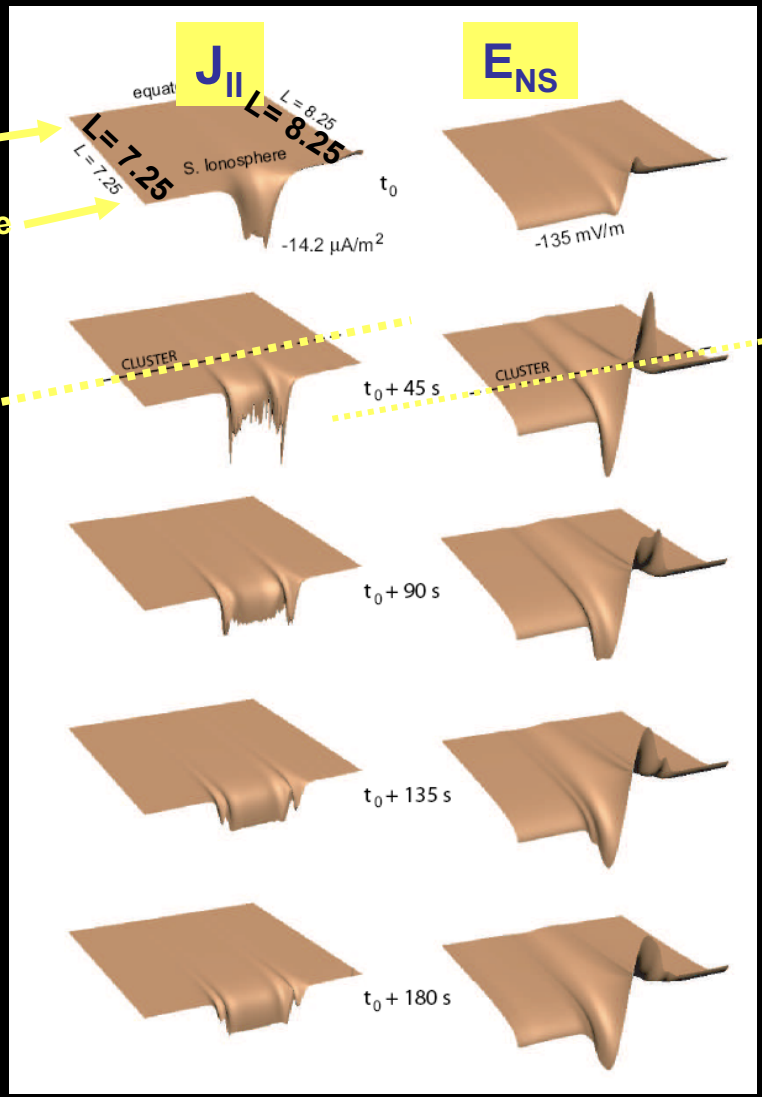

Cut along Cluster track

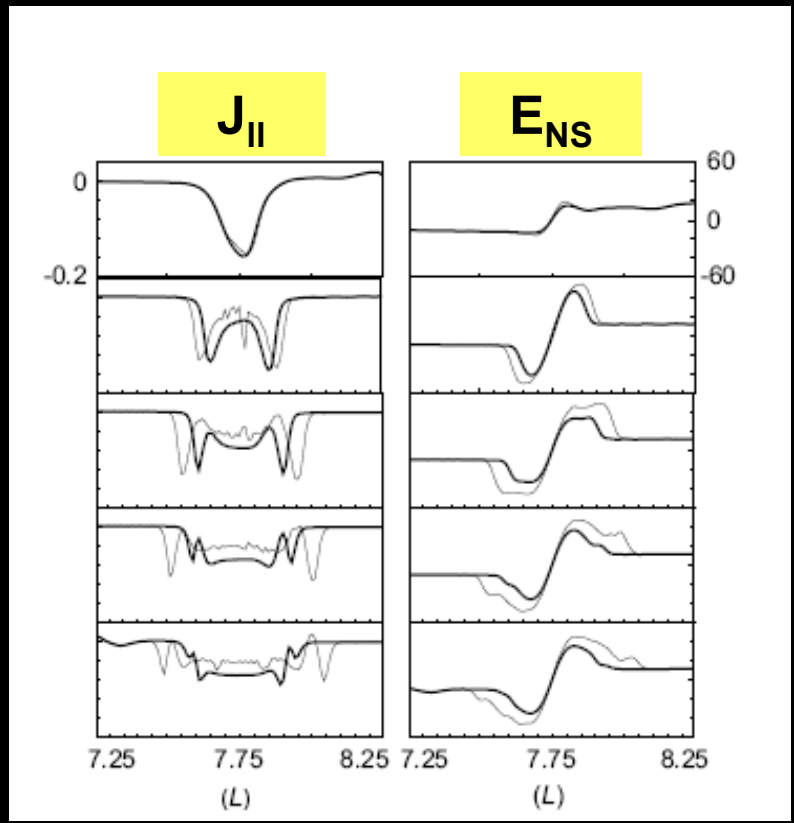

4. On the the degree of ionospheric contribution to high-alt auroral potentials

Compare $\Delta\Phi_{//}$, given by the characteristic energy of the upward acc ions (electrons) with $\Delta\Phi_{\perp} = \int \mathbf{E}_{\perp} \bullet \mathbf{ds}$ in upward (downward) current region.

The ratio $K = \Delta\Phi_{//} / \Delta\Phi$

K = 0	perfect mapping
K = 1	no mapping
0 < k < 1	partly mapping

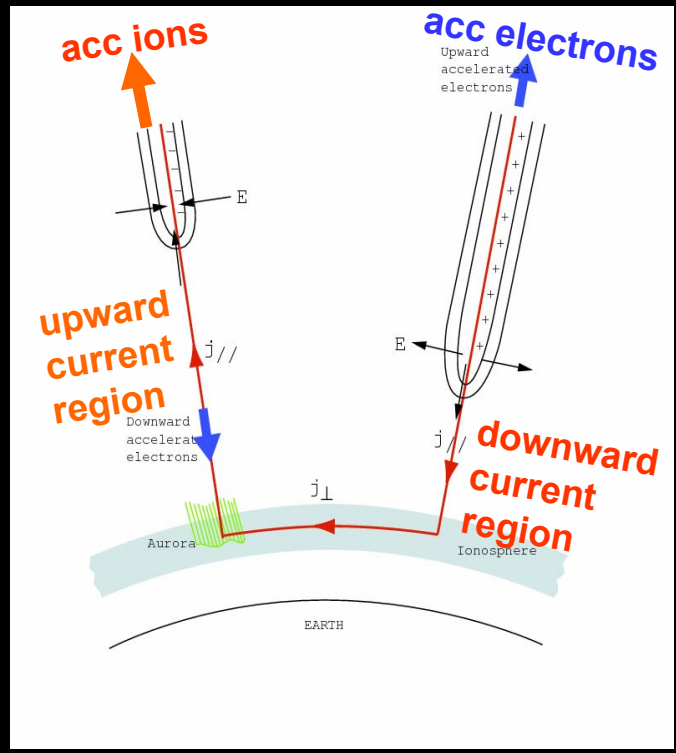

Recently initiated study by Marklund, Johansson, Lynch

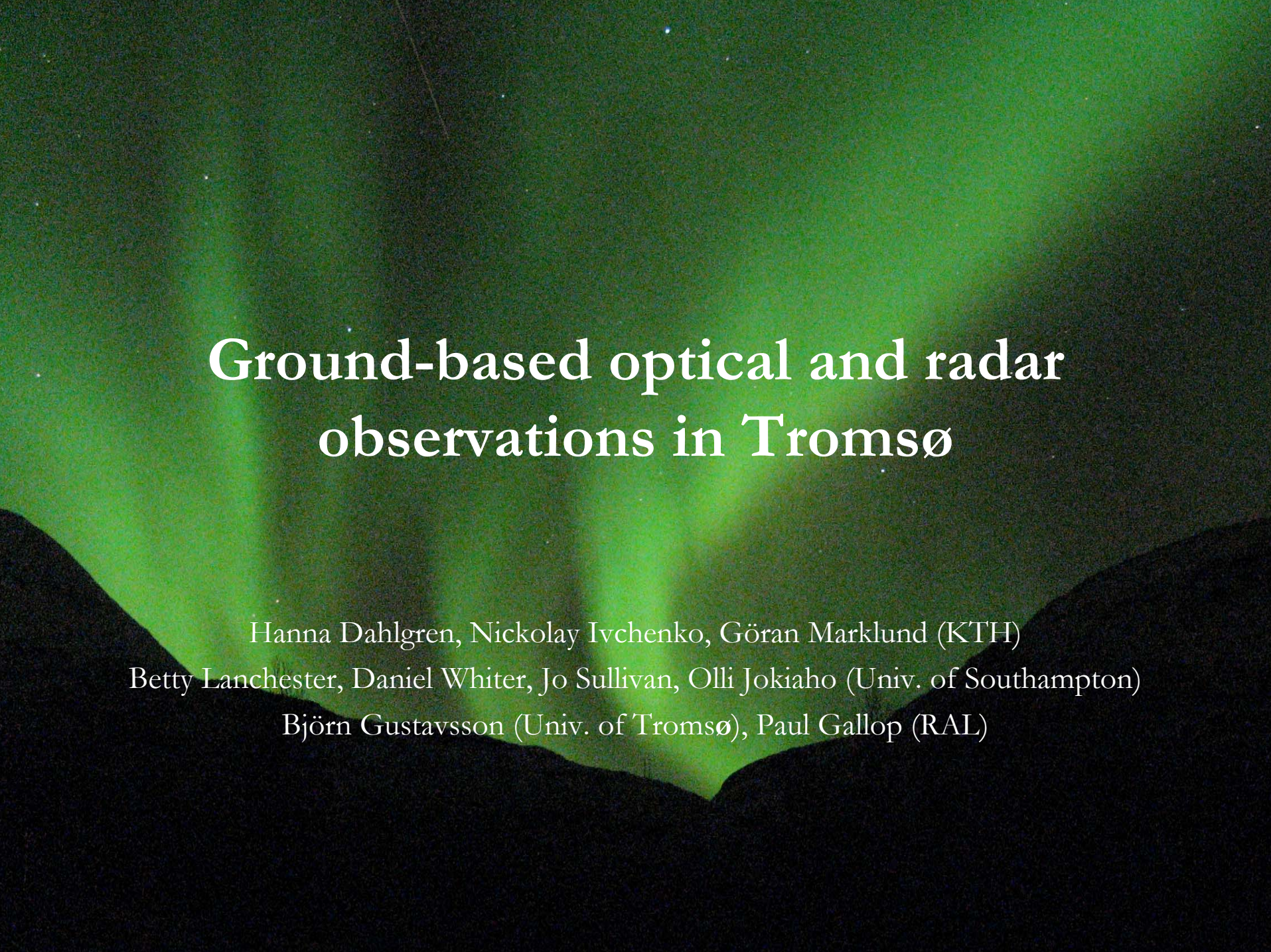

Ground-based optical and radar observations in Tromsø

Hanna Dahlgren, Nickolay Ivchenko, Göran Marklund (KTH)
Betty Lanchester, Daniel Whiter, Jo Sullivan, Olli Jokiaho (Univ. of Southampton)
Björn Gustavsson (Univ. of Tromsø), Paul Gallop (RAL)

ASK – Auroral Structure and Kinetics

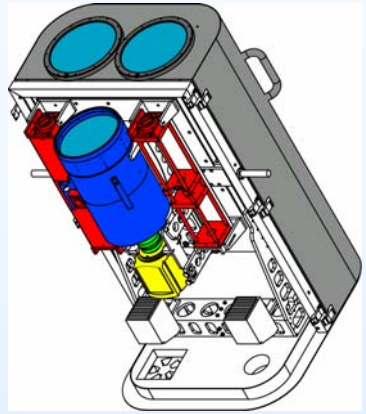

- Instrument to study small scale structure of the aurora, at high temporal and spatial resolution.
- Three narrow (3° × 3°) fov cameras for simultaneous imaging in three spectral bands:

ASK1: 5620 Å → O_2^+ (E-region)
ASK2: 7320 Å → O^+ (F-region)
ASK3: 7774 Å → O (E- & F-region)

ASK + EISCAT SCIENCE

- Imaging with different filters to study the relation between auroral structures and **characteristic energies**, with particular interest in the contribution of **low energy electrons**
- Imaging the aurora in the magnetic zenith in forbidden ion line to measure **plasma drifts** with sub-km and sub-sec resolution. Concurrent imaging in other lines characterises the production of the metastable ions
- Study of the dynamic evolution of **fine structure** in aurora.

- Recent campaign 2006/2007: **ASK in Ramfjordmoen outside Tromsø**

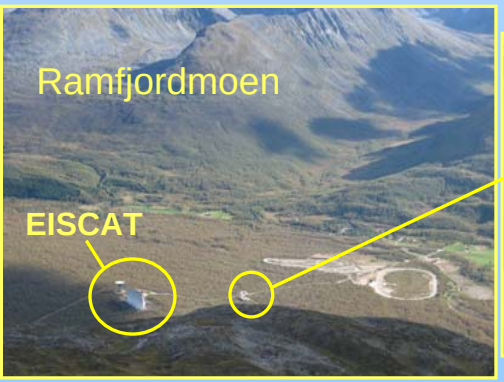

22 October: Data at 32 fps (½ s of data) from ASK1

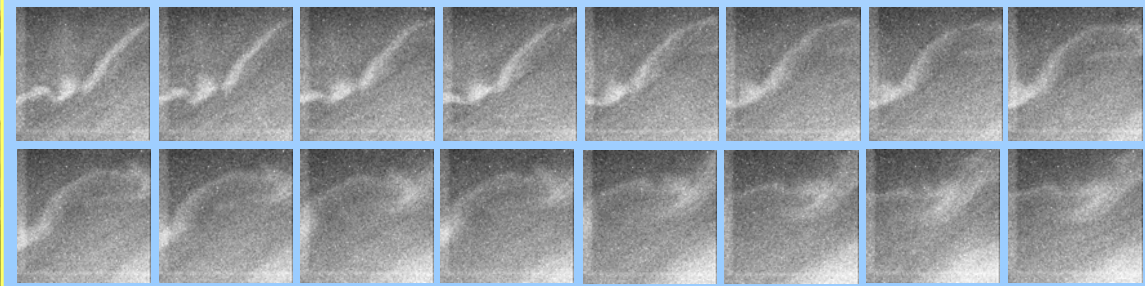

Radar data

Transmitter: EISCAT UHF Antenna

Experiment: **Tristatic arc1, field-aligned**

22 October 2006

Electron density (E region)

Ion temperature

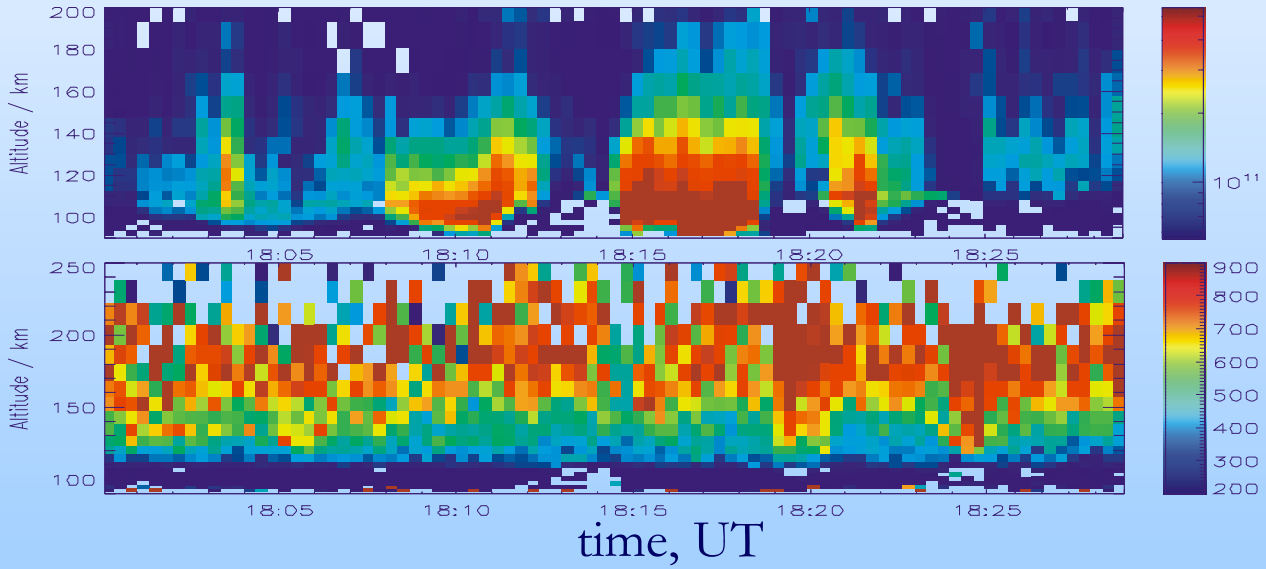

time, UT

Combined optical and radar runs autumn 2006	16 - 23, 30 October 15 – 18 November 9 – 13 December

Ionospheric heating

Heating – High-power transmissions of HF EM waves heating the electrons and thus modifying the plasma state.

RIOE – Radio Induced Optical Emission

High power radio-wave interaction with F-region ionospheric plasma.

Modulation: 2 min on, 2 min off, alternating X- and O-mode, or 10 Hz modulation.

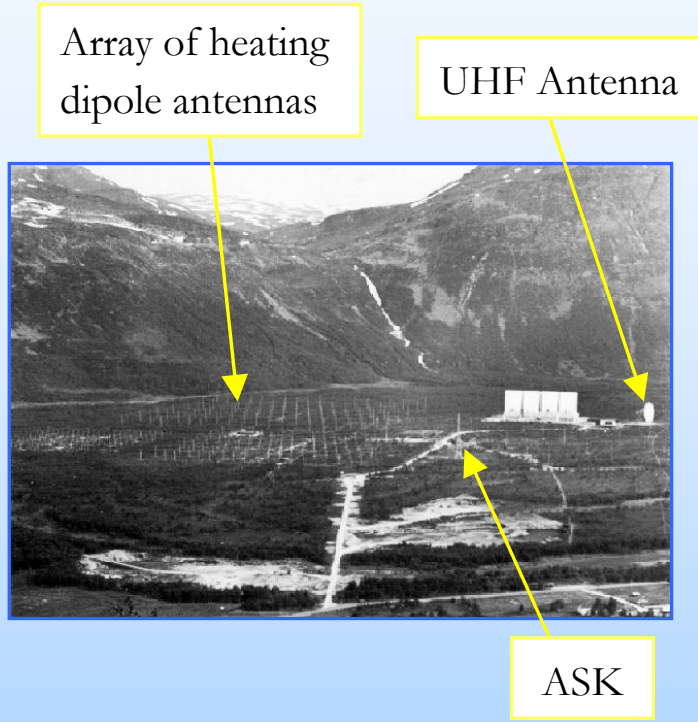

Keogram from ASK1 – pulsations due to heating?

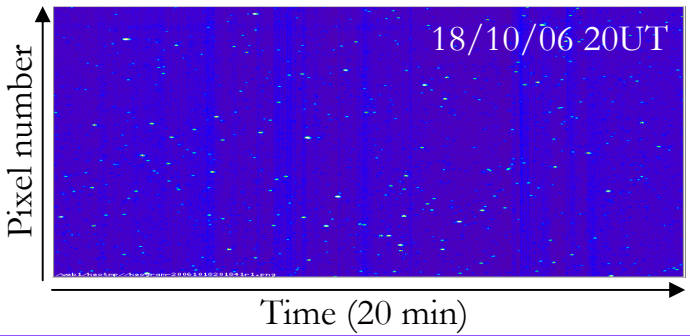

Combined optical and heating runs autumn 2006	16 - 20 October 17 – 18 November 9 – 13 December

Cluster results on auroral scales

Tommy Johansson, KTH, 070201

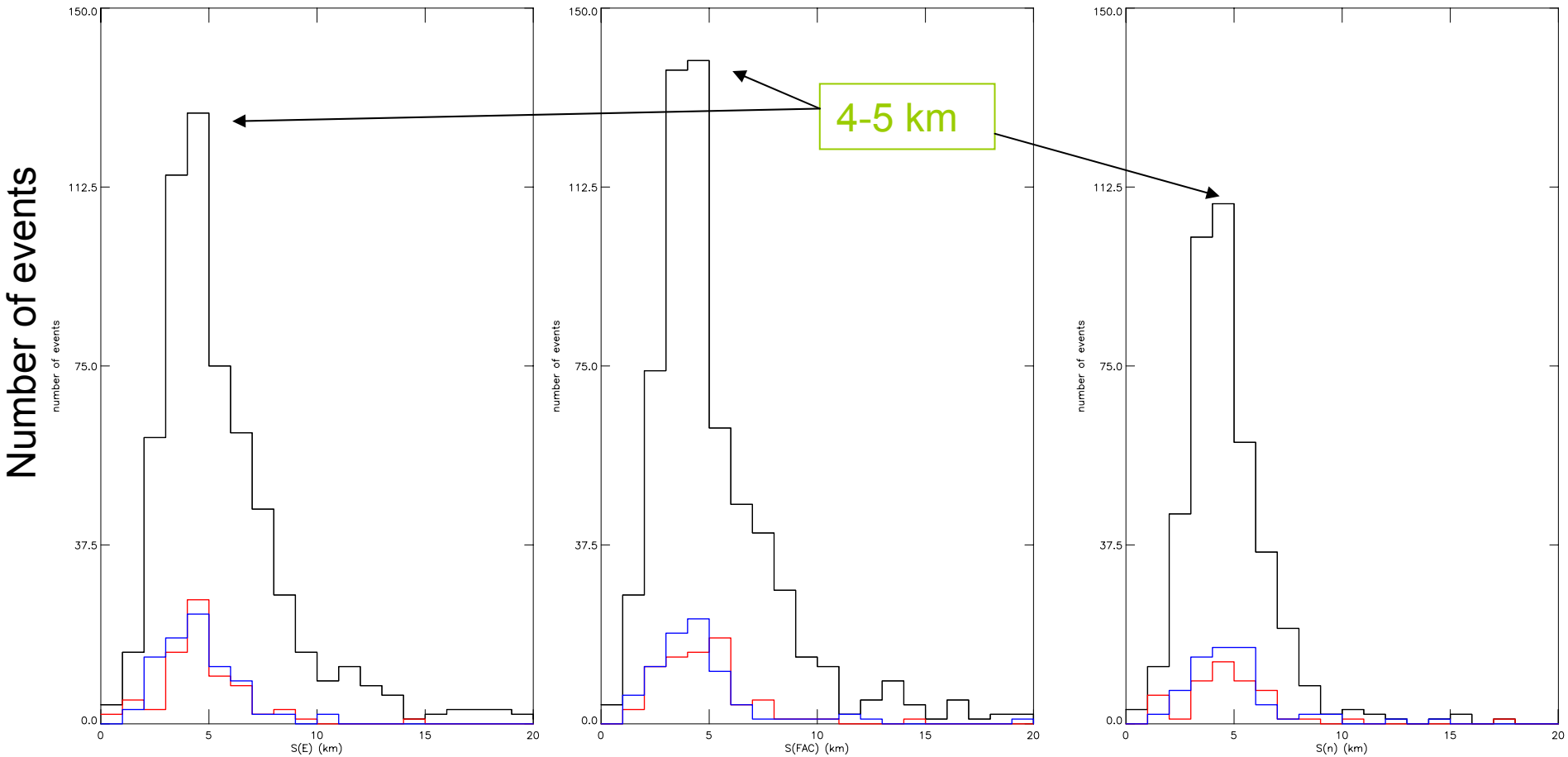

S(E) (km)

S(FAC) (km)

S(dn) (km)

Monopolar, convering bipolar, diverging bipolar E-fields

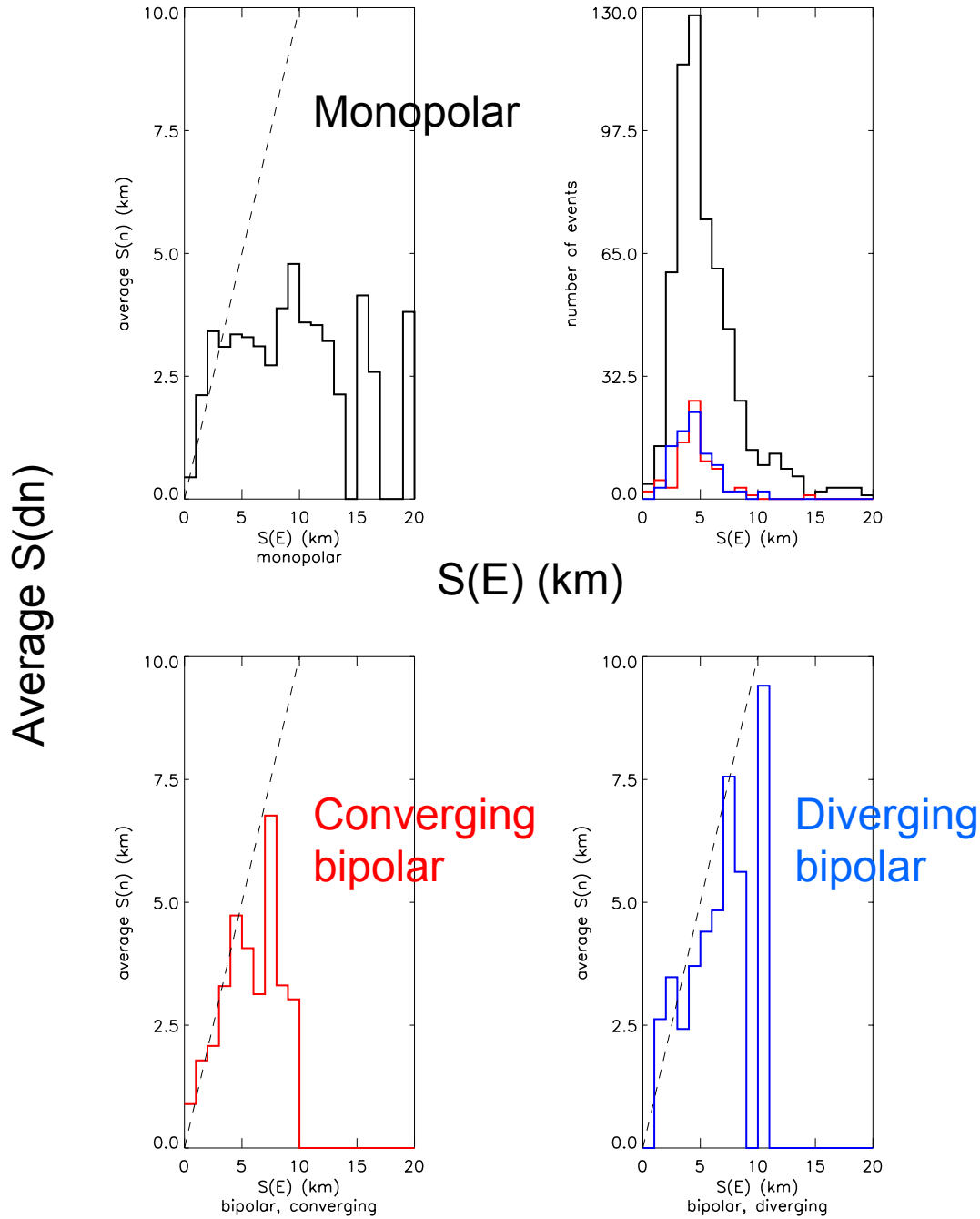
Monopolar
Converging bipolar
Diverging bipolar
Average S(dn)
S(E) (km)
average S(n) (km)
number of events
S(E) (km) monopolar
S(E) (km)
S(E) (km) bipolar, converging
S(E) (km) bipolar, diverging

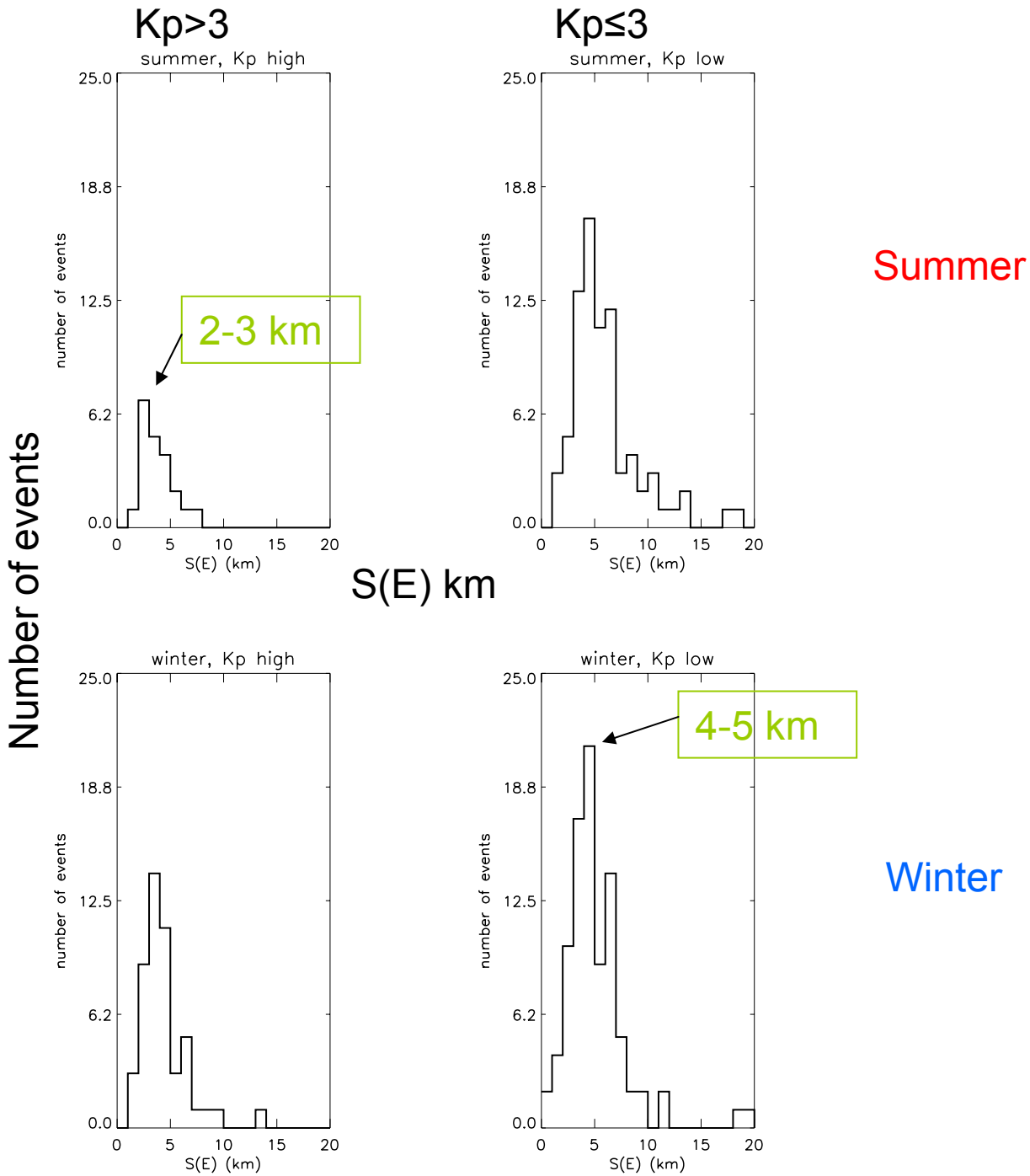
Kp>3
summer, Kp high
Kp≤3
summer, Kp low
2-3 km
Summer
Number of events
S(E) km
winter, Kp high
winter, Kp low
4-5 km
Winter
number of events
S(E) (km)
25.0
18.8
12.5
6.2
0.0
0
5
10
15
20

Cluster position

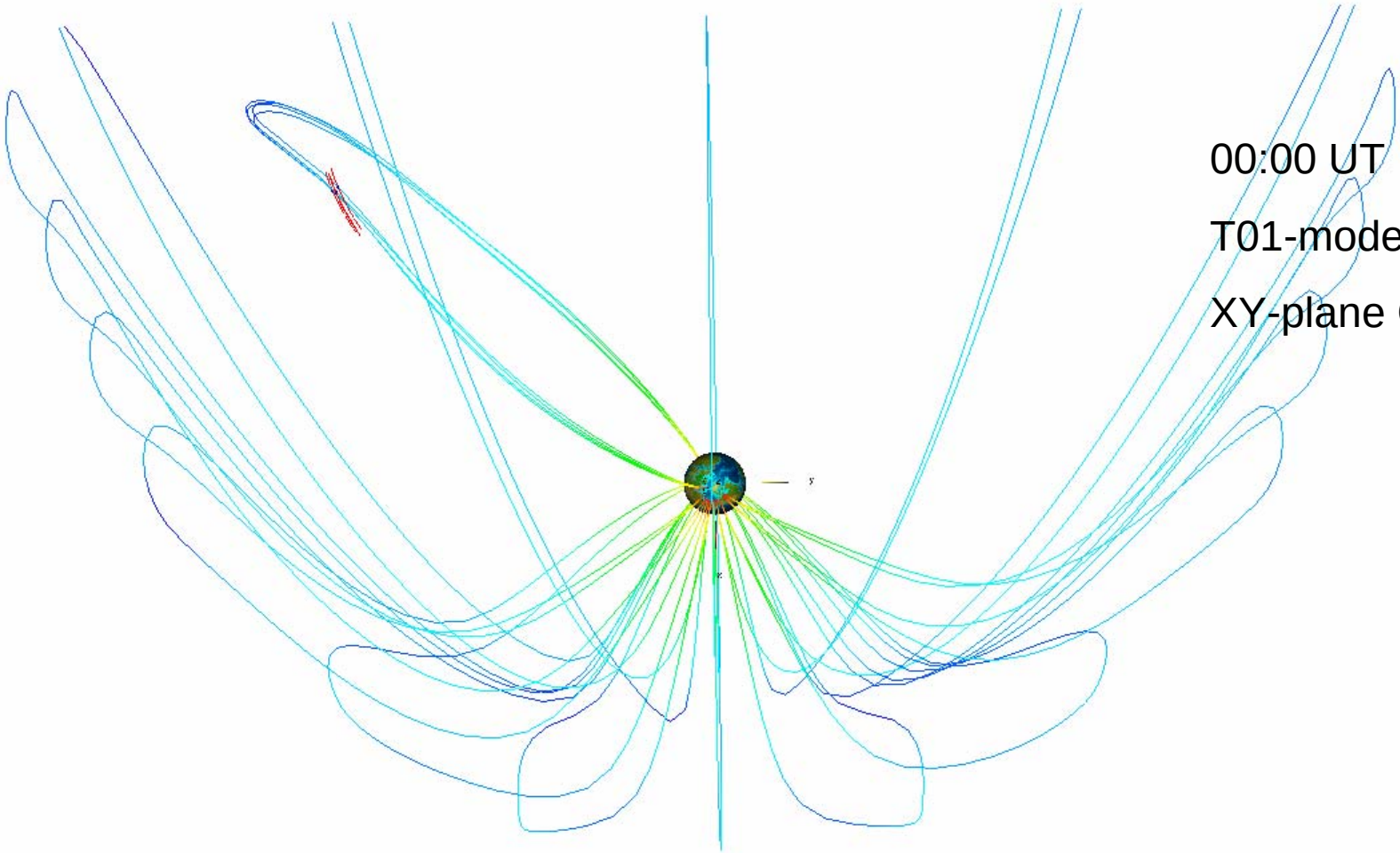

00:00 UT

T01-model

XY-plane GSM

Produced by OVT (http://ovt.irfu.se)

Duskward electric field - Cluster

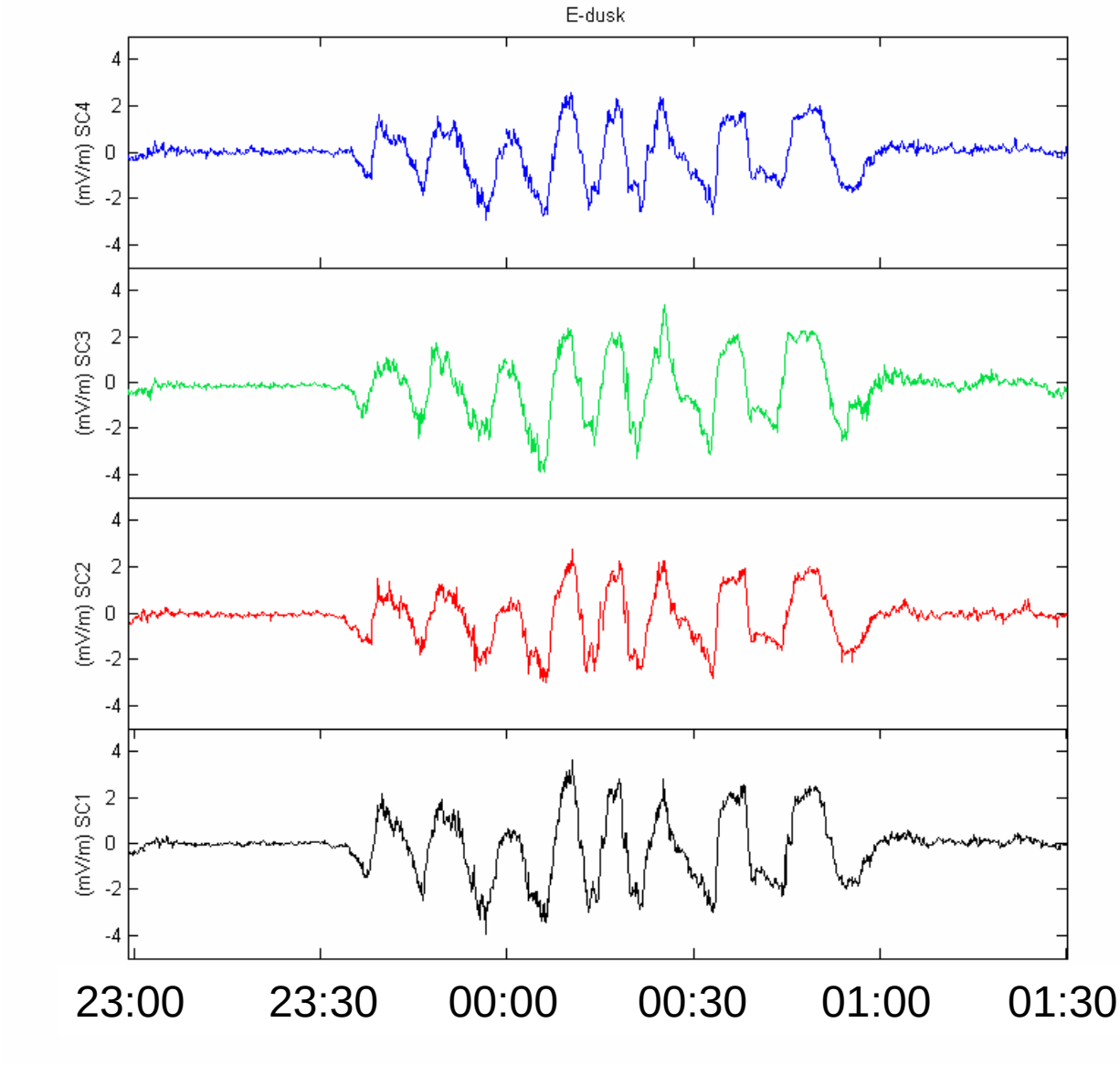

Experimental observation of bursts of whistler waves produced by double layers

N. Brenning[1], M. Koepke[2], I. Axnäs[1], M. A. Raadu[1] , and E. Tennfors[1]

[1]*Royal Institute of Technology (KTH), Stockholm, Sweden*
[2]*West Virginia University, Morgantown, WV, USA*

Work supported by Swedish Research Council and the U.S. NSF.

Schematic of Green Tank at KTH

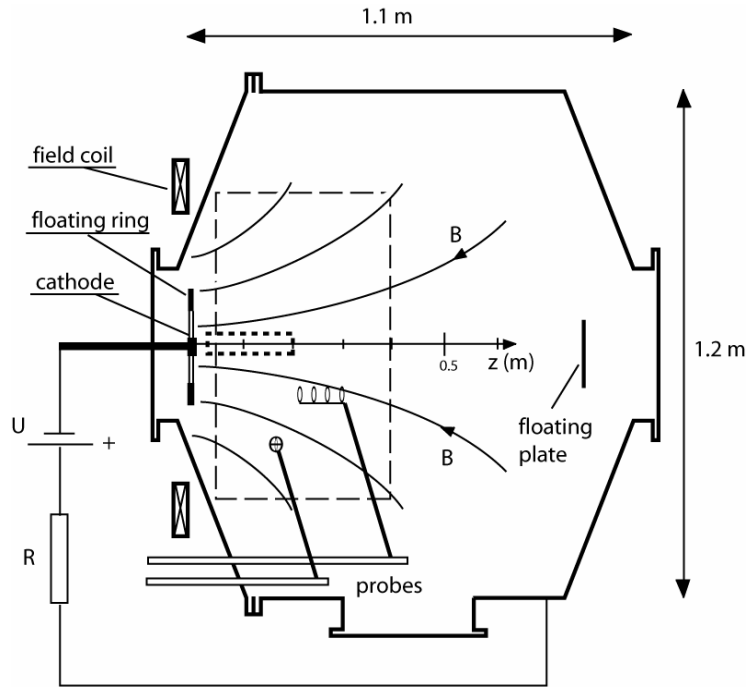

An electron beam from a hot cathode is shot into a plasma along the magnetic field. The magnetic field strength decreases with *z* along the central axis as shown in the lower panel. The small box bordered by thick dashed lines represents a *source region* of radiation. Magnetic-field probes are used to investigate waves that propagate from this source region into the surrounding plasma. There are two types of waves, partly overlapping in space: in the central plasma there are bursts of 7 – 40 MHz whistler mode radiation, while closer to the walls, where the plasma density is lower, there are EM bursts of higher frequency (0.3-0.4 GHz)

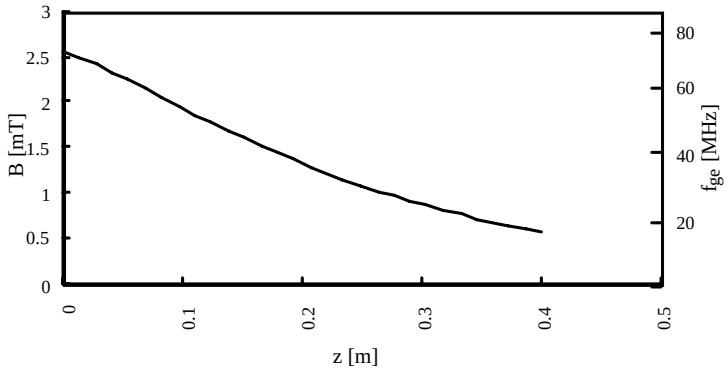

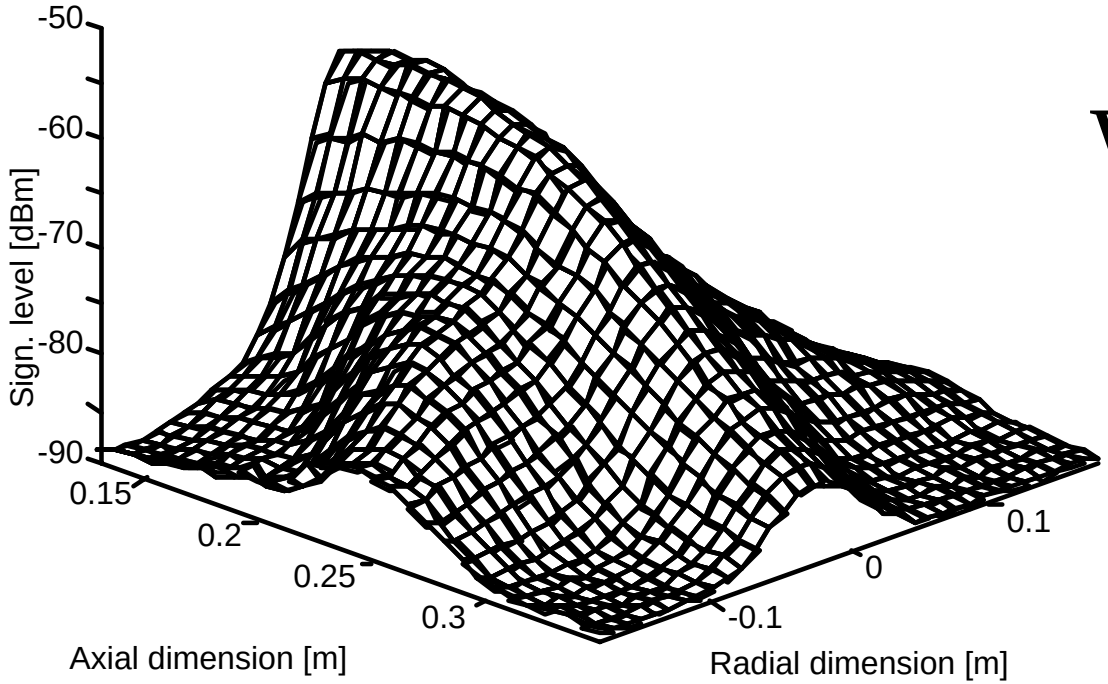

Whistler waves are present

Time-averaged amplitude at 14.5 MHz. The “wings” to the side are consistent with propagation along the group velocity resonance cone angle, $\theta = \sin^{-1}(\omega/\omega_{ce})$, at the selected frequency. There is also a channel with “central waves”. Wing and Center amplitude decrease as *z* increases (and B decreases), presumably because gyro-resonance approaches. The central waves would be good candidates for ducting in a situation with a homogeneous magnetic field.

Whistler waves are driven by electron beam

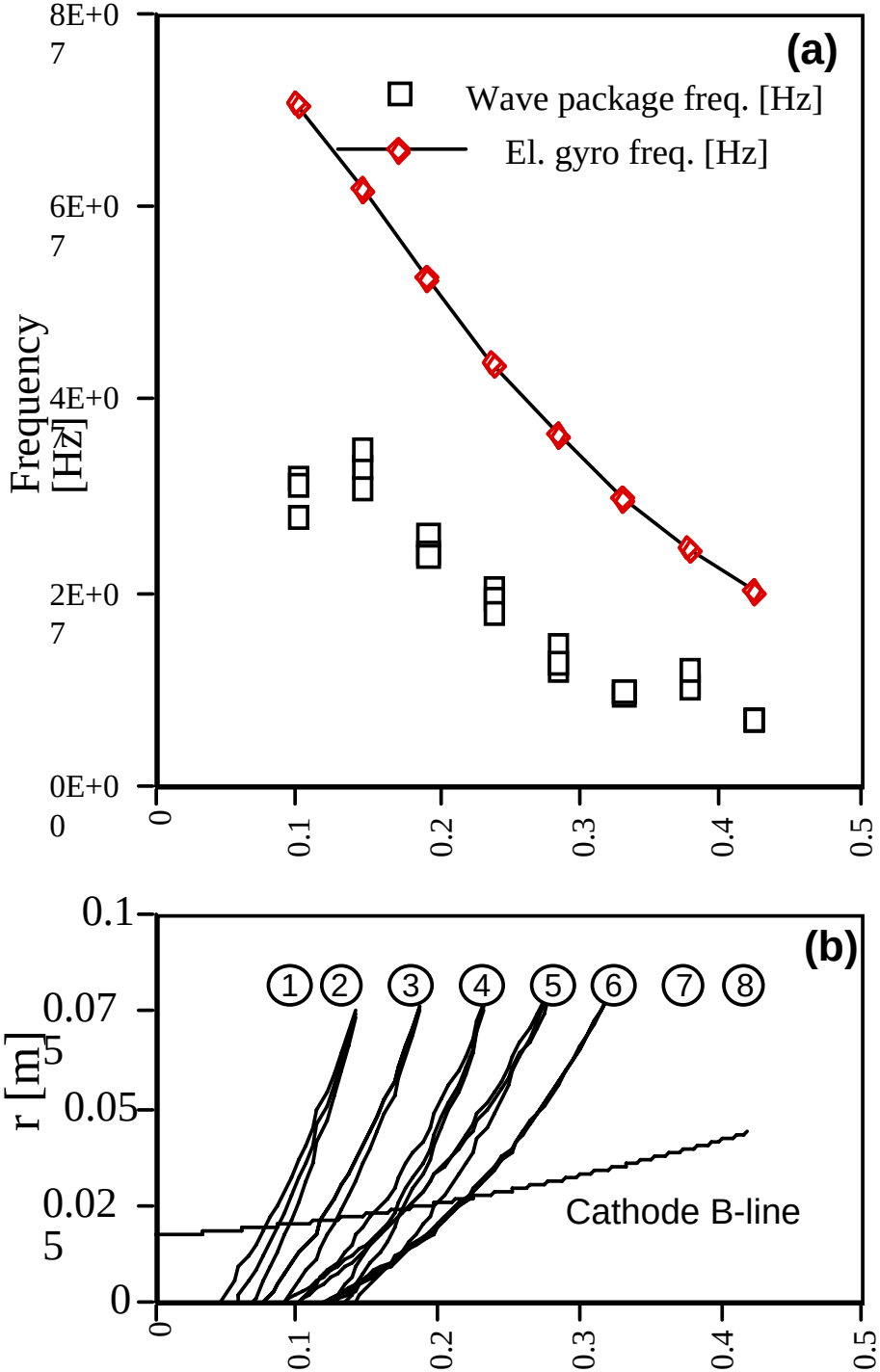

Studies of single wave packets of high amplitude, made with an array of B_z pickup coils, positioned at different z coordinates but at the same radius r = 0.07 m. Panel (a) shows that the frequency, at each probe location, is typically half the local electron gyro frequency. Panel (b) shows ray tracing backwards for individual wave packets towards the axis of the device. The line denoted “cathode B-line” shows the limiting field line that touches the edge of the cathode. The waves are probably driven by a broad electron beam inside this line.

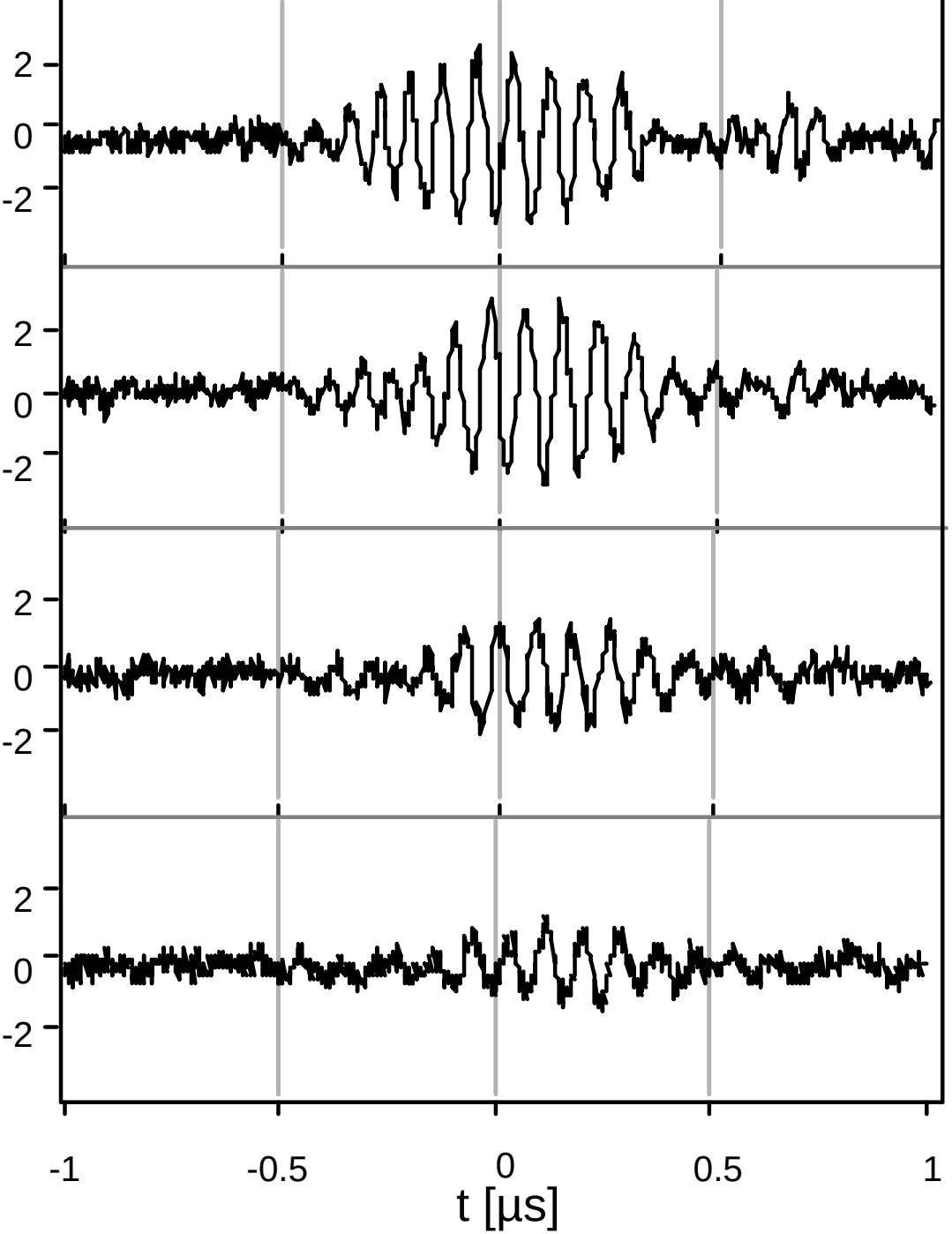

Whistler wave packets have a single frequency

A 12.5 MHz wave packet passes over an array of probes at the same r = 0.7, and spaced 4.5 cm in the z direction

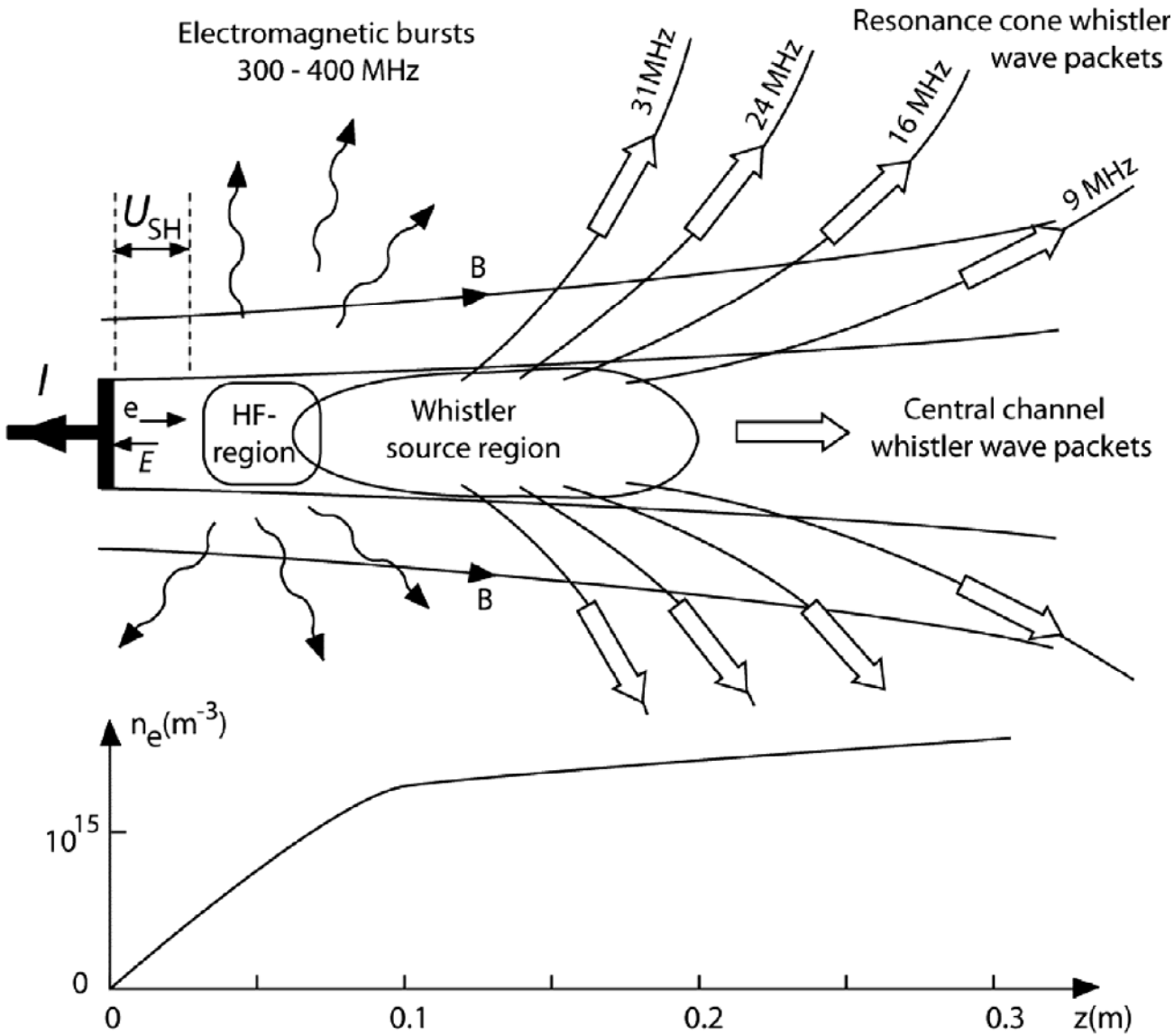
Electromagnetic bursts
300 - 400 MHz
Resonance cone whistler
wave packets
31MHz
24 MHz
16 MHz
9 MHz
U_{SH}
B
I
e
E
HF-
region
Whistler
source region
Central channel
whistler wave packets
B
$n_e(m^{-3})$
10^{15}
0
0
0.1
0.2
0.3
z(m)

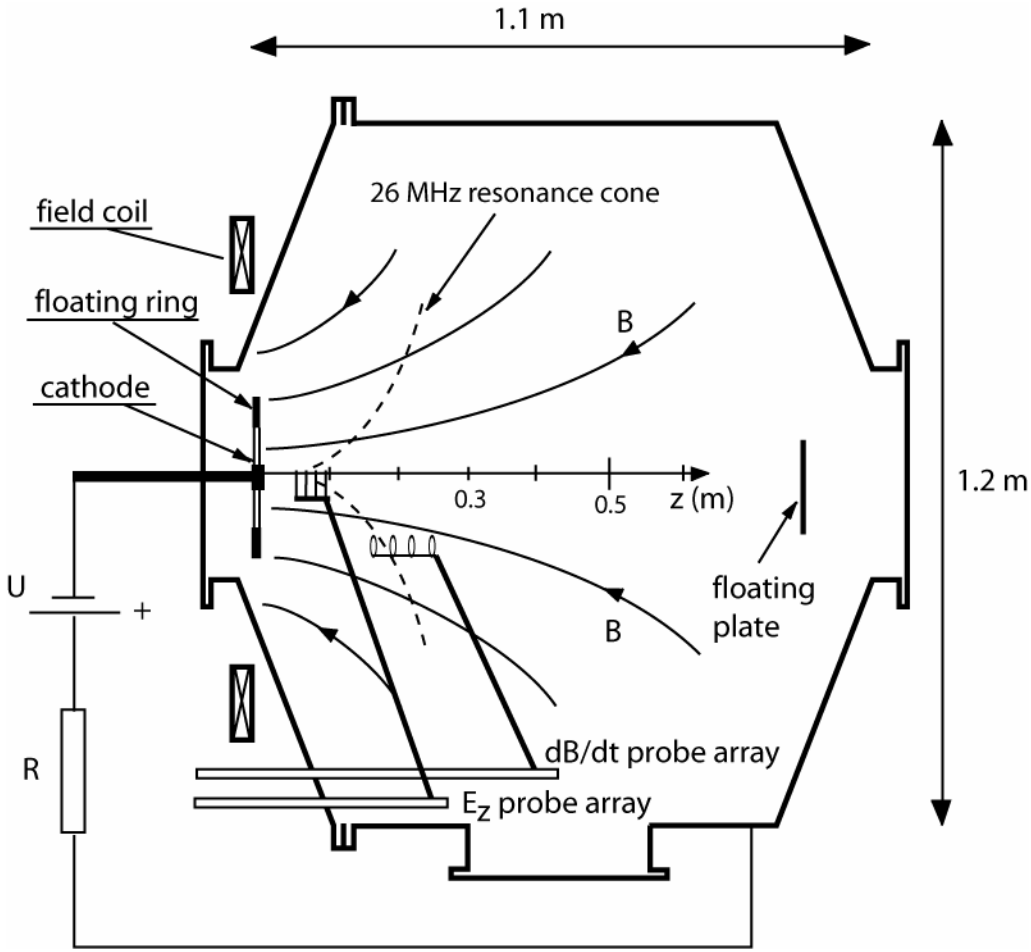
1.1 m
field coil
floating ring
cathode
26 MHz resonance cone
B
0.3
0.5
z (m)
1.2 m
floating
plate
B
U
+
R
dB/dt probe array
E_z probe array

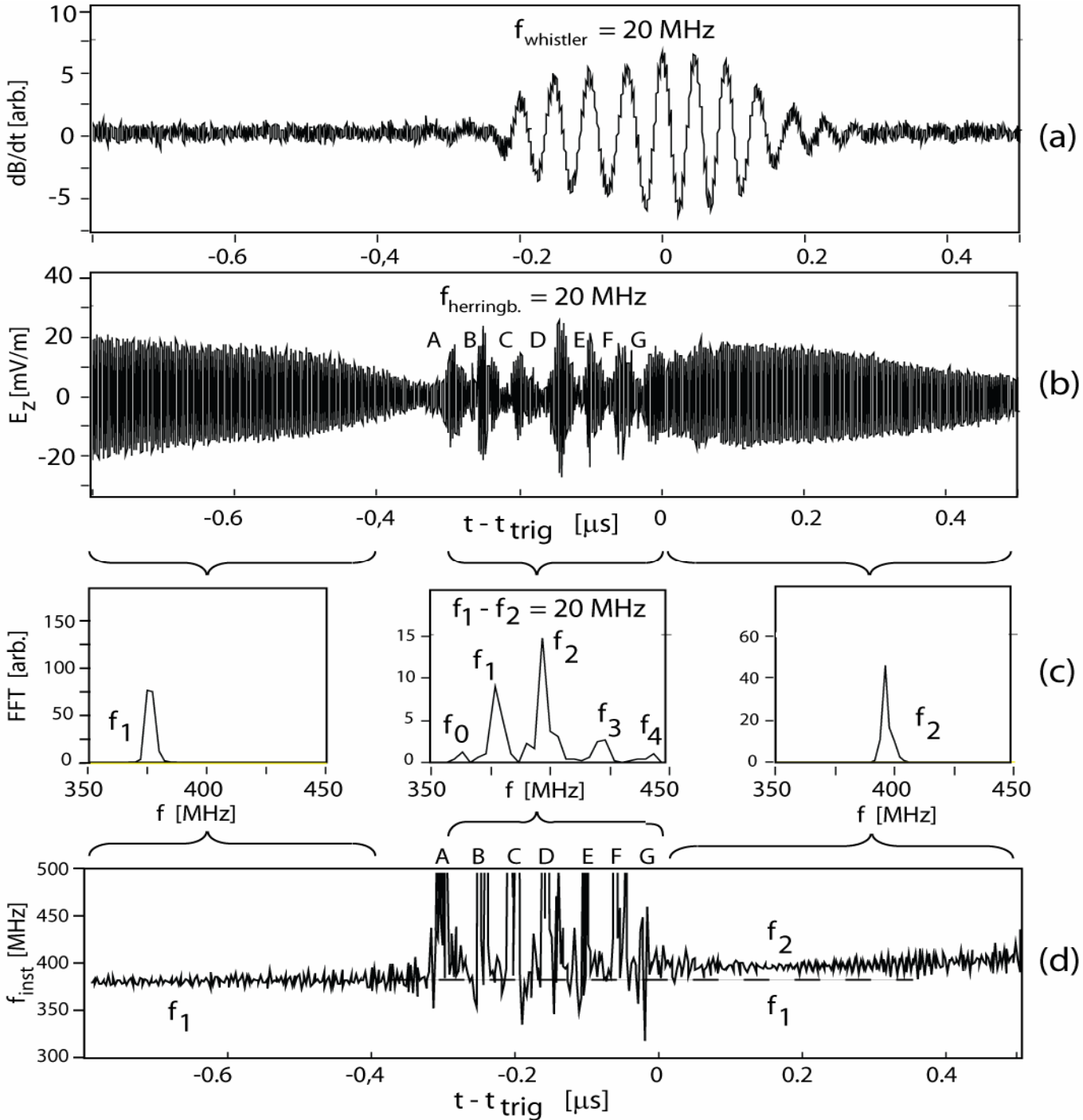
f whistler = 20 MHz
dB/dt [arb.]
(a)
f herringb. = 20 MHz
A B C D E F G
E z [mV/m]
(b)
t - t trig [μs]
FFT [arb.]
f 1
f 1 - f 2 = 20 MHz
f 0
f 2
f 3
f 4
f [MHz]
(c)
f inst [MHz]
(d)

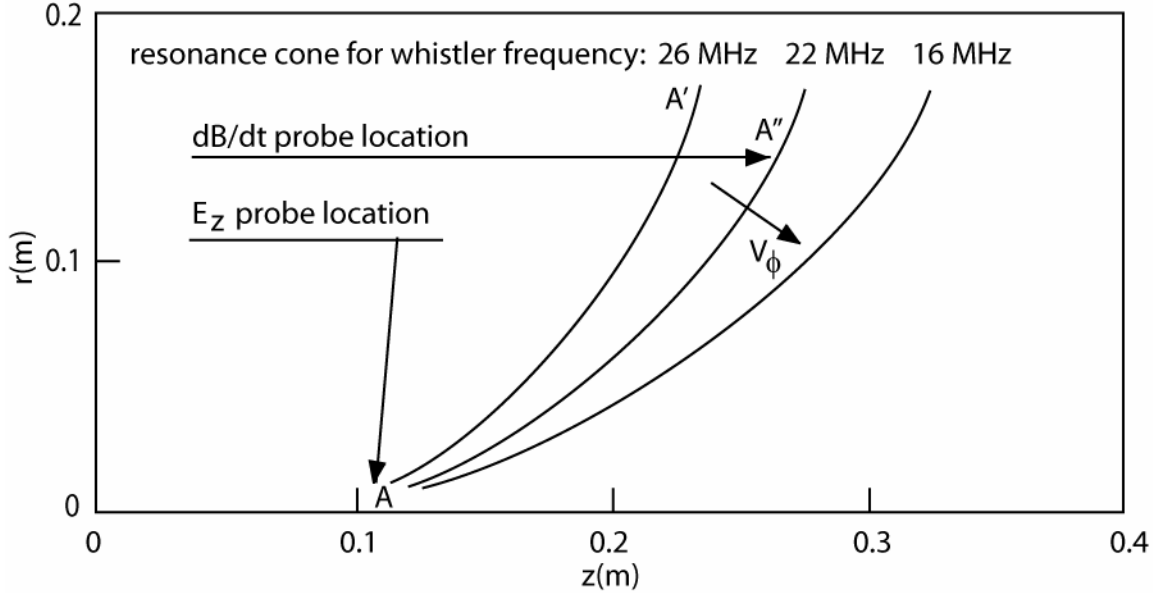
resonance cone for whistler frequency: 26 MHz 22 MHz 16 MHz
A′
A″
dB/dt probe location
E_z probe location
V_ϕ
A
r(m)
z(m)
0
0.1
0.2
0.3
0.4

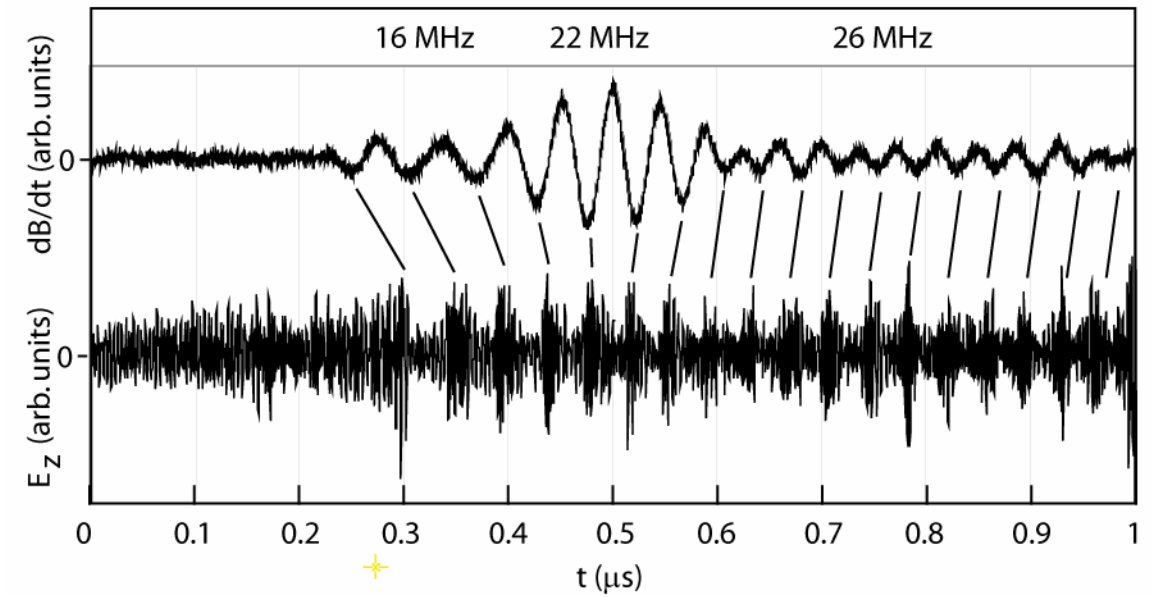
16 MHz
22 MHz
26 MHz
dB/dt (arb. units)
E_z (arb. units)
t (μs)
0
0.1
0.2
0.3
0.4
0.5
0.6
0.7
0.8
0.9
1

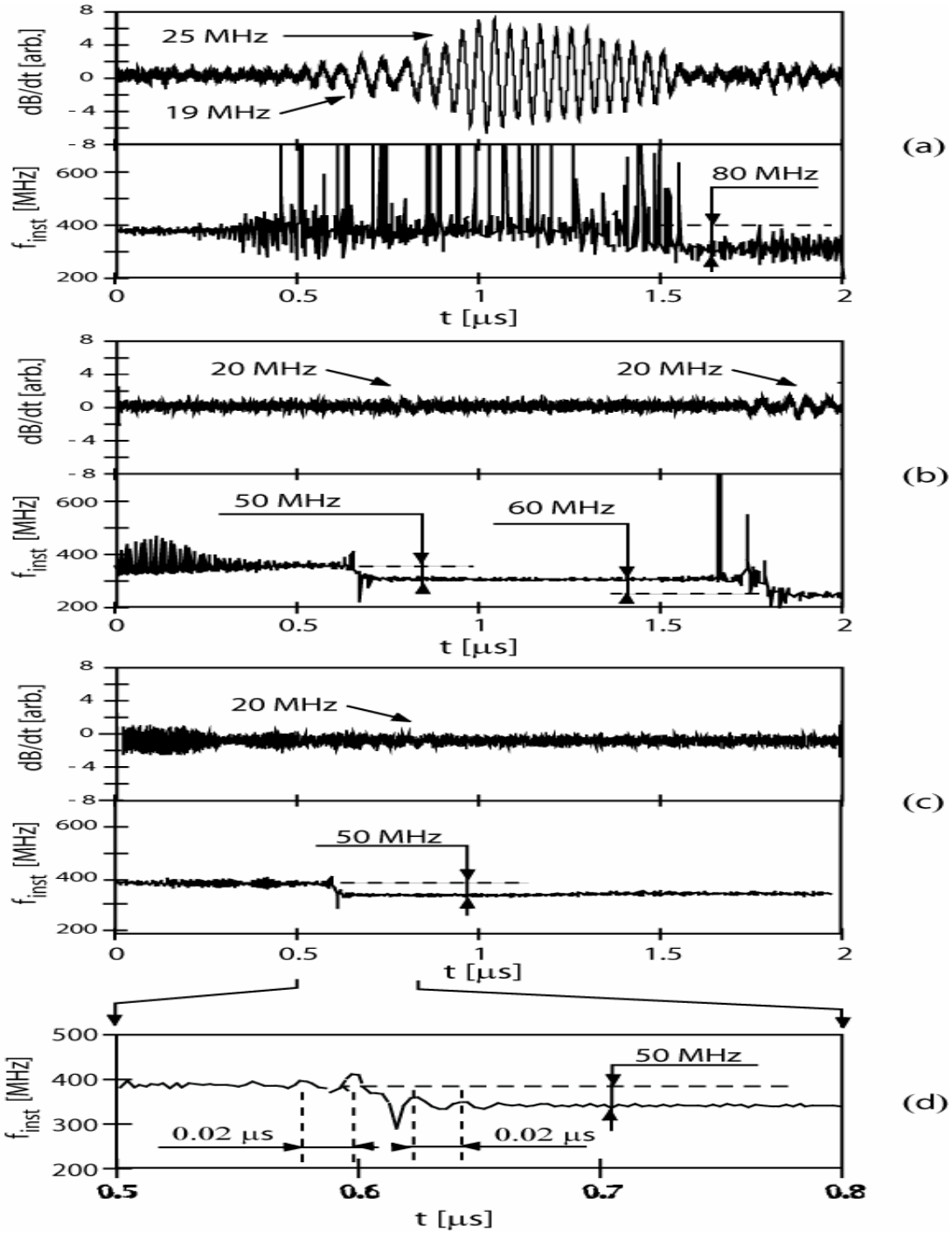
25 MHz
19 MHz
dB/dt [arb.]
80 MHz
f_{inst} [MHz]
t [μs]
(a)
20 MHz
20 MHz
50 MHz
60 MHz
(b)
20 MHz
50 MHz
(c)
50 MHz
0.02 μs
0.02 μs
(d)

Space relevance

Radiation mechanisms associated with the presence of electrostatic double-layers have been proposed for observations of EM radiation in space.

- *Auroral kilometric radiation* is bursty electromagnetic radiation found in high-altitude regions of the terrestrial auroral zone.
    - *Borovsky* [1], proposed that the observed EM radiation is generated by sheet beams of gyrophase-bunched electrons acting as a planar antenna, emitted from oblique auroral double-layers.
- Double layers, formed in *Extragalactic jets* with sufficient parallel current, create field aligned electron beams which are believed to emit polarized radio waves via a collective bremsstrahlung process when scattered off self-generated electrostatic waves [2].
- Intense decimetric spikes observed during *Solar flares* are proposed to be the result of coherent radiation from electrostatic double-layers [3].

Eigenmodes have been observed in space

Jupiter's ionosphere: $f/f_{ce} = 1$, $f_{pe}/f_{ce} << 1$, $\Delta f/f$ = (5 Hz)/(100 Hz)

Ergun, R. E., Y.-J. Su, L. Andersson, F. Bagenal, P. A. Delemere, R. L. Lysak, and R. J. Strangeway (2006), *S* bursts and the Jupiter ionospheric Alfvén resonator, *J. Geophys. Res.*, *111*, A06212, 2006.

Standing inertial Alfvén waves in Jupiter's ionosphere resonate with eigenmodes having frequencies 4 – 400 Hz and are driven by beam electrons which are responsible for upper hybrid waves that mode convert to EM waves. FAST satellite.

Topside auroral ionosphere: $f/f_{pe} > 1$, $f_{pe}/f_{ce} > 1$, $\Delta f/f$ = (500 Hz)/(2 MHz)

HF Chirps: Eigenmode trapping in density depletions, McAdams, K. L., R. E. Ergun, and J. LaBelle, *Geophys. Res. Lett.*, 27, 321, 2000.

B-field-aligned propagation according to Langmuir/upper hybrid wave surface; involve resonance with beam electrons which are responsible for initially generating the waves. PHAZE II rocket.

Eigenmodes have been observed in space

Topside auroral ionosphere: $f/f_{ce} << 1$, $f_{pe}/f_{ce} < 1$, $\Delta f/f$ = (3 kHz)/(8 kHz)

Kintner, Franz, Schuck, and Klatt, (2000), *J. Geophys. Res. 105*, 21237;
Kintner, Schuck, and Franz (2000), *Phys. Plasmas* 7, 2135.

Resonant cavity eigenmodes of lower-hybrid solitary structures lefthand rotate in cylindrical density cavities when below the lower-hybrid frequency and righthand rotate when above the lower-hybrid frequency. TOPAZ 3 and PHAZE 2 sounding rockets.

Topside auroral ionosphere: $f/f_{pe} < 1$, $f_{pe}/f_{ce} < 1$, $\Delta f/f$ = (1 kHz)/(3 kHz)

Statistics of lower hybrid wave cavities detected by the FREJA satellite, Kjus, Pecseli, Lybekk, Holtet, Trulsen, Luhr, and Eriksson, *J. Geophys. Res. 103*, 26633, 1998.

A localized lower hybrid wave packet (“trapped mode”) is noted inside the cavity with frequency 3 kHz. Freja satellite.

Conclusion

Individual whistler wave packet arise from individual cavity-eigenmode HF electrostatic-wave transitions.

Acknowledgements

This work is supported by the Alfvén Centre for Space and Fusion, and by the Swedish Research Council. Participation costs for M. Koepke were supported by the Swedish Research Council and the U.S. National Science Foundation.

Acknowledgements

This work is supported by the Alfvén Centre for Space and Fusion, and by the Swedish Research Council. Participation costs for M. Koepke were supported by the Swedish Research Council and the U.S. National Science Foundation.

Splinter Session II - Aurora & Generator

E- & B-field signatures associated with intense ion acceleration using Cluster EFW / FGM / CIS data

Sónia Liléo - KTH

I will present

- 6 cases showing large electric and magnetic field fluctuations associated with intense ion acceleration
- Occur at the PC/PS boundary during magnetically active periods

Topics for discussion

- Energisation mechanisms

Field-aligned quasi-static acceleration; Magnetic moment pumping; Substorm dipolarisation; Strong transverse E-field gradients; Coherent heating due to electrostatic hydrogen cyclotron waves (EHC)

- Relative contribution of the different energisation mechanisms

Ratio between the estimated perpendicular potential and the measured ion beam peak energy; Mass dependence of the ion flux and energy density

- Coupling of the solar wind plasma dynamo to the acceleration region

Dependence of the ion beam energy on the solar wind velocity

Current closure and generator regions as observed by Cluster in the plasma sheet??

Hamrin & Stenberg

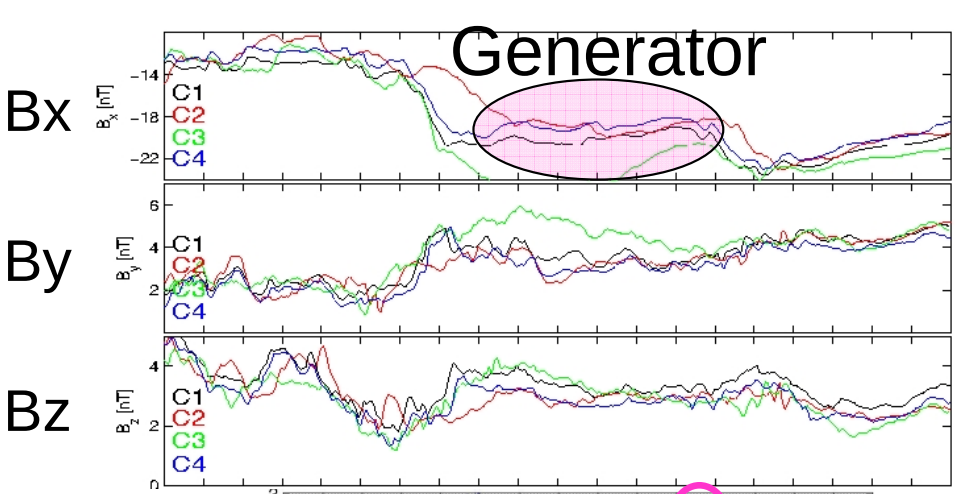

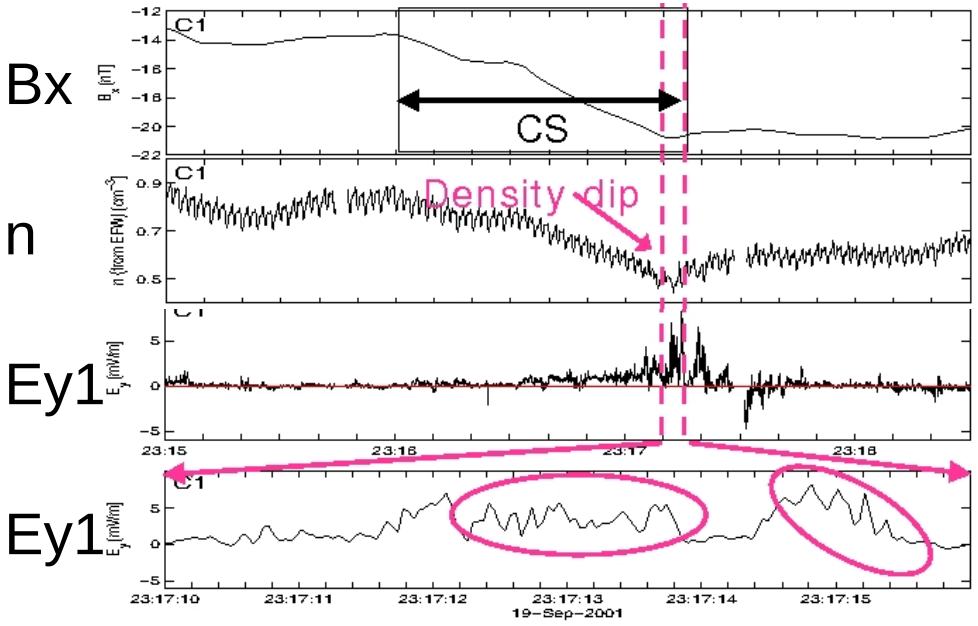

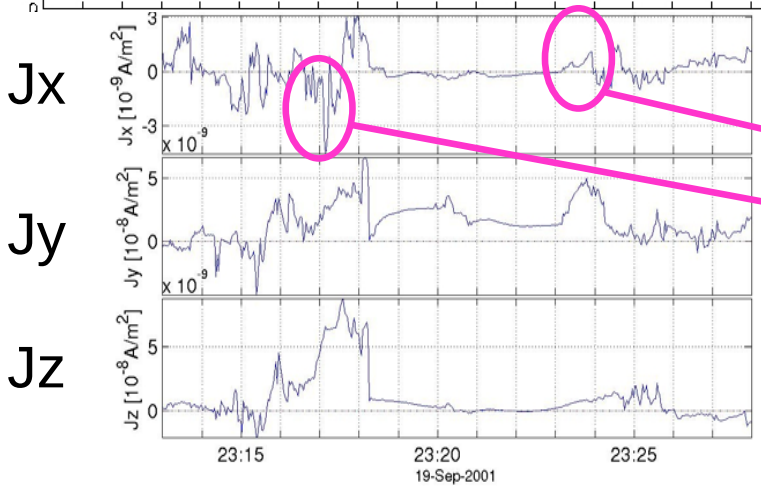

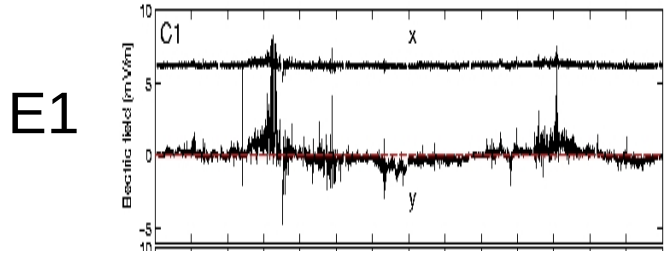

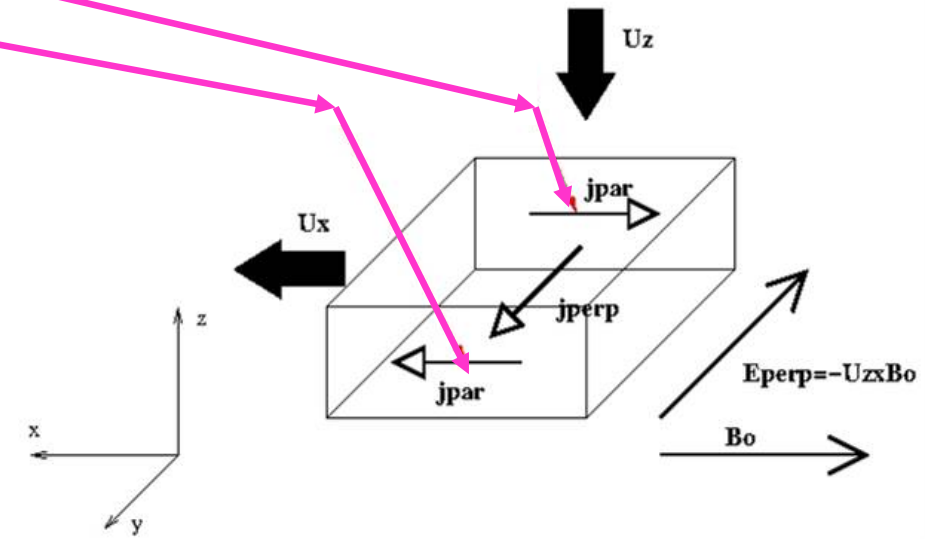

Photo: Y. Ebihara

Optiska mätningar är verkligt viktiga om man vill förstå:

- Norrsken
- Tidsvariationer
- Rumsvariationer

Status för markbaserade optiska norrskensmätningar

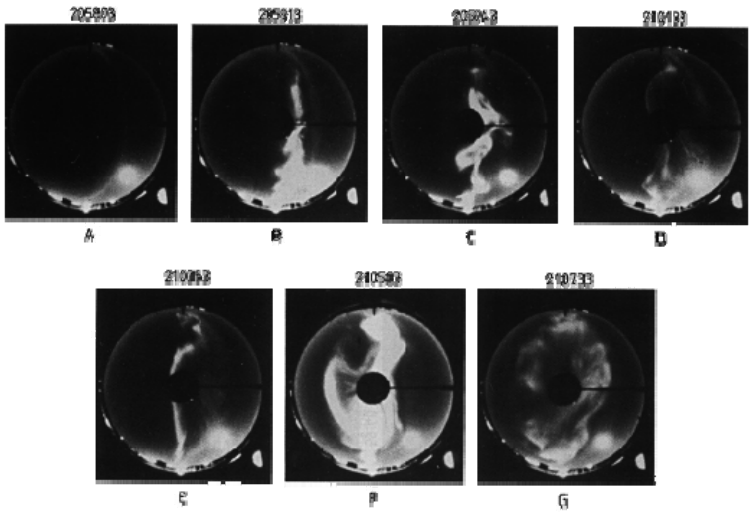

Viktiga resultat från IGY 1957/58
- Norrskensovalen
- Substormar

- Förnyat intresse
- Teknologisk revolution
  - Digitalt
  - CCDs
  - Ej standardisering
- Kvantitativa mätningar
- Bra instrument dyra
- "Vita fläckar"

Auroral imager arrays

THEMIS all-sky imager array

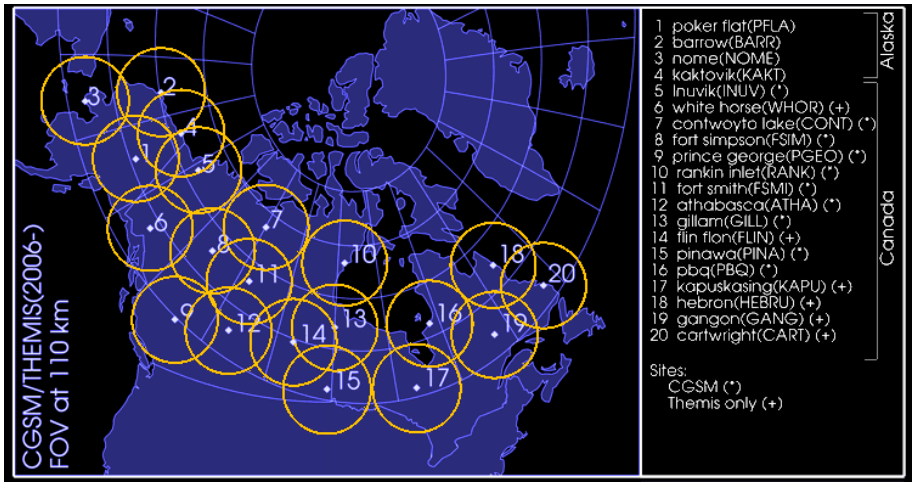

Svalbard

MIRACLE

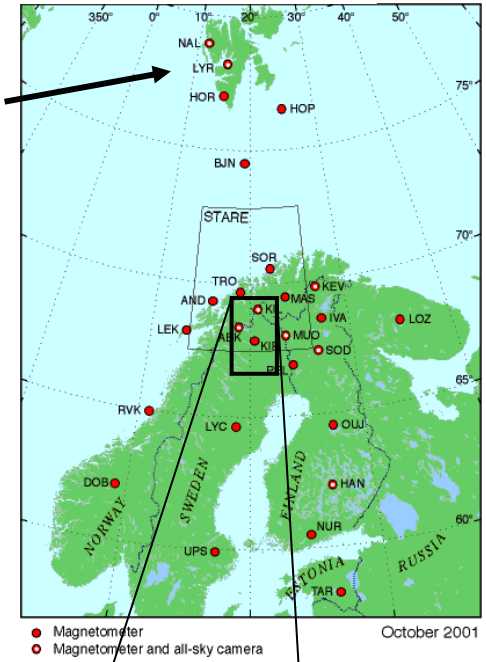

Automatic Geophysical Observatory (AGO) stations

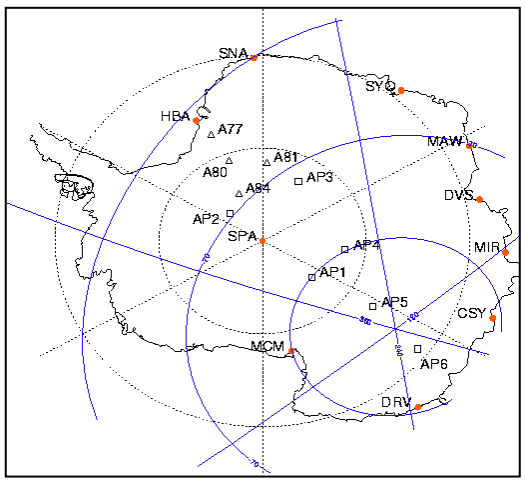

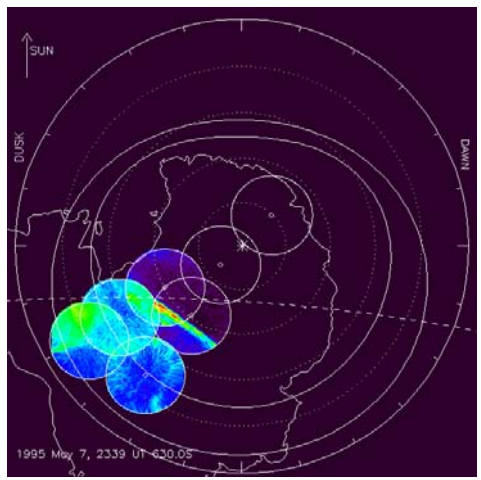

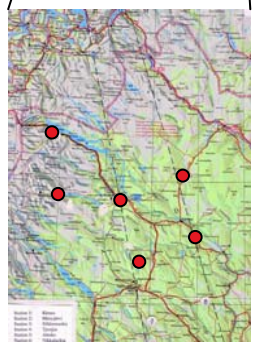

ALIS

Magnetic reconnection in turbulent plasma

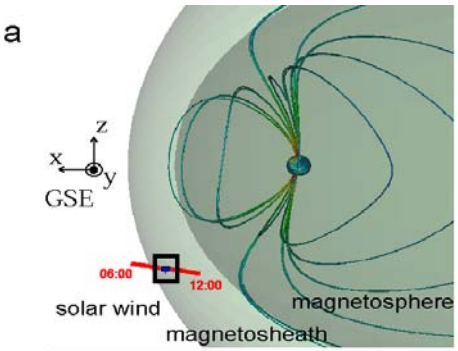

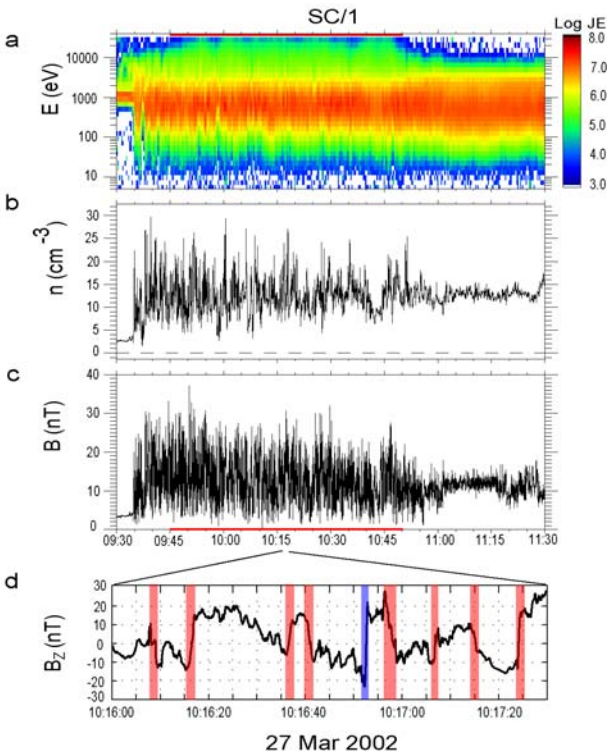

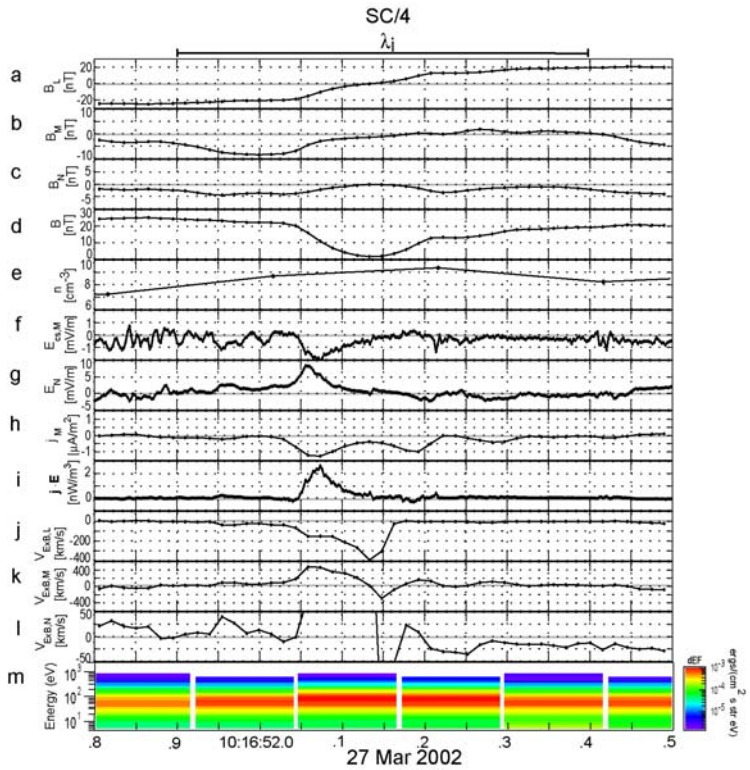

Cluster observations of the local energy transfer at the magnetopause under steady interplanetary magnetic field

Motivation:

- Energy into the magnetosphere ultimately driven by the solar wind
- Observational method
- Investigate variation without influence of varying solar wind

Magnetopause energy transfer

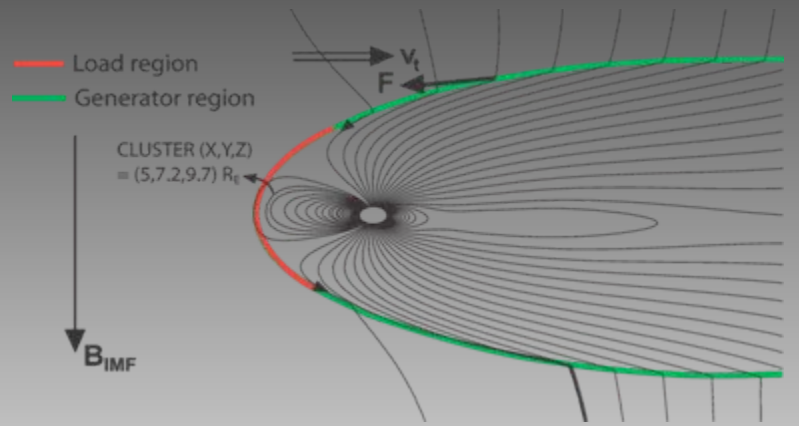

Solar wind conditions (ACE)

Steady!

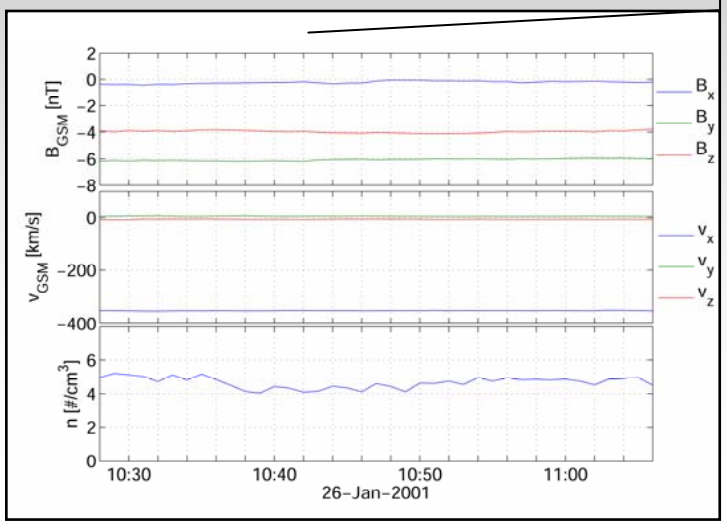

$$U(W) = \int_{A_{mp}} dA \underbrace{\int (\mathbf{j} \times \mathbf{B}) \mathbf{v}_t v_{mp} dt}_{Q_{mp}}$$

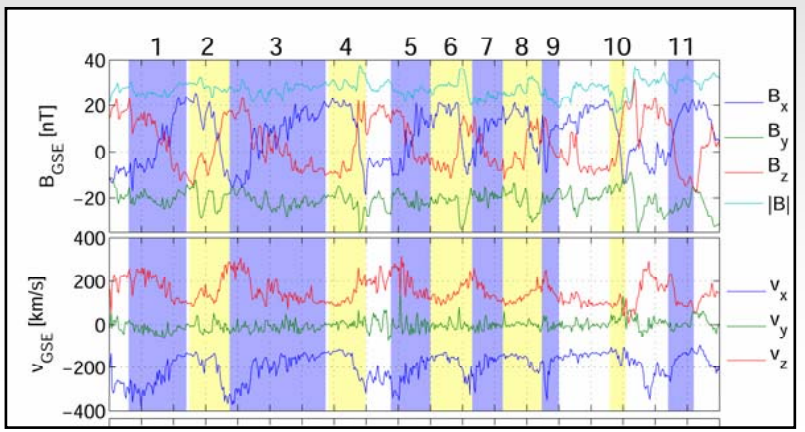

$$Q_{mp,i}$$

$$i = 1, 2, ..11$$

$$R = \frac{1}{2} \frac{Q_{mp}}{\rho v_A^3}$$

Varies!